Spring 5-2017

The Confinement Effects on the Fiber Pullout Response of Ultra-High Performance Concrete (UHPC

Arden McSwain
University of Maine

CONFINEMENT EFFECTS ON THE FIBER PULLOUT RESPONSE OF ULTRA-HIGH PERFORMANCE CONCRETE

By

Arden Caroline McSwain

A Thesis Submitted in Partial Fulfillment

of the Requirements for a Degree with Honors

(Civil Engineering)

The Honors College

University of Maine

May 2017

Advisory Committee:

Eric Landis, Frank M. Taylor Professor of Civil Engineering, Advisor

Edwin Nagy, Lecturer of Civil Engineering,

Roberto Lopez-Anido, Malcolm G. Long Professor of Civil Engineering

Keith Berube, Assistant Professor of Mechanical Engineering Technology

Melissa Ladenheim, Civilizations Preceptor, Associate Dean, Honors College

Abstract

Fiber pullout tests were conducted on more than ninety 10 mm by 10 mm cylindrical concrete specimens with a single, straight steel fiber embedded 10 mm in the center of the concrete specimen. Each specimen was subjected to one of three levels (90 N, 2000 N, 4000 N) of confining force applied by a steel fixture and a servo-hydraulic Instron test frame was used to conduct fiber pullout tests. A previously published fiber pullout model was used to determine the approximate bond strength and frictional stress experienced by the fiber-concrete matrix for each of the three confinement levels. Results show that confinement stresses had a positive correlation with both peak force and work of the pullout force, but the latter was only valid for the first few millimeters of pullout. The correlation with work of pullout disappeared when the entire response was considered. Next an analytical model was used to determine the effects of bond fracture energy and friction. The results of this comparison showed that increased confinement forces caused a measurable increase in frictional stress, but bond energy remained relatively constant. The results of this work can be used to improve future computational model.

Dedication

I would like to dedicate this thesis to my grandmother Carolyn Heveran, or as her many grandchildren call her, “Nanny”. She is one of the most kind, passionate, and inspiring women I have ever had the privilege of knowing and she is truly the backbone of our family. She has never stopped encouraging me to and she taught me to never stop fighting for my hopes and dreams. Thank you Nanny for everything you do for me. I love you so much.

Acknowledgements

The U.S. Army Engineer Research and Development Center (ERDC) funded this thesis project under a subcontract to UMaine from ES3 Inc., San Diego.

I owe special thanks to my advisor, professor, mentor and friend Eric Landis for his unwavering enthusiasm, encouragement and guidance. Without his help, this project would not have been possible. He never failed to answer each of my never-ending questions regarding my research and still found the time to help me figure out what I wanted to do with my future. I'm sorry I won't be here working in the lab for the next two years. He almost convinced me.

I would also like to thank my committee members, Edwin Nagy, Melissa Ladenheim, Roberto Lopez-Anido, and Keith Berube. Each of them spent hours reading my thesis, preparing questions for my defense, and editing my final draft. Their input was extremely valuable to the completion of this work.

Thank you to Taylor Rodrigue for teaching me how to successfully batch Cor Tuf and hanging out with me in the soils lab. Another thanks to Reagan Smith for spending countless hours with me batching and testing specimens in the lab 120. You both made my work much more enjoyable.

And finally, thank you to my friends and family who have supported and encouraged me throughout the last year as I completed this project. Without them this process would have been significantly more difficult. A special shout-out to my mom and dad who have frequently pretended they were interested in the work I was doing when I talked about it nonstop while I was home.

Table of Contents

List of Figures

List of Tables

1. Introduction

Ultra-high performance concrete (UHPC) has recently become popular as a material to provide armor protection to structures so they can resist extreme loading events such as blast or ballistic action. In order for this armor to work, the UHPC must be reinforced with steel fibers to increase the toughness. There are multiple reinforcement schemes that are available, but in all cases the basic micromechanical properties of the system must be known to make high fidelity predictions of the material performance.

Due to the importance of fiber reinforced UHPC in protecting civilian and military structures, significant research efforts have gone into predicting the performance of structures made of this material under blast and ballistic loading. The current performance simulations are based on certain simplified assumptions regarding the behavior of this material such as how energy dissipates due to fibers pulling out of the concrete matrix. One of these assumptions is that the pullout properties of steel fibers embedded in UHPC are not influenced by the stress of the matrix. This assumption may lead to overly conservative performance values for the material. When blast or ballistic loading occurs on a structure, a compression wave propagates away from the center of the blast resulting in confinement stresses in the concrete matrix. This compression wave will likely influence the pullout properties of steel fibers embedded in the concrete. Testing must be completed to fully understand how these properties will change.

The hypothesis in question is how do confining stresses influence the pullout response of steel fibers embedded in UHPC. Traditional fiber pullout laboratory tests were conducted with straight steel fiber reinforcements. The UHPC matrix the fibers

were embedded in were subjected to confining stresses. This simulates the conditions experience for materials in a uniform compression field. An active confining stress was put on an axis normal to the fiber while the orthogonal axis was subjected to passive confinement. These tests resulted in a functional relationship between confining stress and pullout strength.

The research described in this paper investigates the relationship between pullout strength of steel fibers from an UHPC matrix under multi-axial confinement stresses. This information provides the properties required to properly predict the resistance of steel fiber reinforced UHPC to blast/ballistic action. The results from these experiments were used to further develop high fidelity computational tools to simulate the structural response to extreme loading events.

2. Background

Many researchers have worked over the years to analyze fiber pullout behavior from UHPC, and as a result, in the past decade fiber reinforced concrete has advanced from laboratory trials to a full-scale commercial product. These researchers have created and conducted testing procedures and methods, analytical models of bond behavior, energy dissipation, and numerous other characteristics of this composite material, without which, the experiments and analysis necessary to analyze how confining stresses influence the pullout response of steel fibers embedded in UHPC would not be possible.

2.1. Fiber Pullout Characteristics and Modeling

As defined by Naaman and Wille (2012), UPHC is usually distinguished by tensile strengths ranging from 10 to 15 MPa as well as having a strain value at maximum stress of 0.2-0.3 percent. As more information is gathered regarding the interfacial bond between UHPC and steel fibers, the bond itself can be improved leading to the reduction of fiber-volume content as well as smaller crack width and decreased crack spacing. This will allow for a higher resistance to chemical attack and penetration, thus increasing durability.

There are two basic types of bond that are recognized depending on the type of stress being transferred across an interface: the shear bond, and the tensile bond. When a composite is uncracked, the shear bond transfers stresses from the matrix into the reinforcement; then when the matrix cracks, the load is resisted by the fiber bridging the crack and transferred back into the uncracked part of the composite. The shear bond is also responsible for opposing the pullout of the steel fiber from the matrix which makes it

one of the main factors that impacts the failure of steel fiber reinforced UHPC. The tensile bond opposes any displacement that is created by forces acting perpendicular to the bond surface. As noted by Bartos (1981), the tensile bond directly influences the strength of composites reinforced with steel fibers in a random, three-dimensional arrangement or on the transverse strength of a composite with a unidirectional, or random, planar spacing of the fiber reinforcement.

Naaman and Wille (2012) determined from research that straight fibers generally experience a load drop following debonding of the fiber, and steadily decrease for the duration of the test until complete pullout. Based on his microscopic studies, this behavior can be explained by an additional mechanical bond due to fiber end deformation by the cutting of the fiber, abrasion of fine adherent matrix particles and wedge effect caused by these particles being pressed between the surface of the fiber and the tunnel created by the fiber being removed, and the damaging and scratching of the fiber coating which increases the surface roughness and therefore increases the frictional resistance. Naaman and Wille (2012) also found that the post-peak bond stress-slip relationship of straight fibers pulled out from UHPC experience a shear hardening behavior.

Fiber pullout is generally modeled with elastic bond strength as well as frictional bond strength for the fiber-concrete interface. The frictional bond strength usually varies relative to the fiber slippage distance. Wang and Backer (1988) developed a theoretical model for such pullout tests that includes the bond strength variation during pullout, and made predictions of the experimental load versus crack separations relationships from pullout tests with steel fibers. The differences between theoretical predictions and experimental results are assumed to be due to the inclusion of deformations such as the

testing machine or fixture. Wang and Backer (1988) saw similar results as Naaman and Wille (2012) in that surface roughness of the fiber increased the fiber pullout load due to increased friction.

The process of pulling out a straight fiber from UHPC consists of three phases: bonded, debonding, and sliding. Initially the pullout load is not sufficient to separate the fiber from the surrounding matrix and this interface keeps the fiber bonded to the concrete. As slippage increases, the debonding of the fiber begins. The fiber starts to debond and stretch slightly at the surface of the concrete, and as this happens, the fiber begins to slide along the matrix channel while the lower part remains bonded. When the fiber is fully debonded, the fiber enters the sliding phase and the matrix deteriorates due to abrasion and particle compaction, or hardens due to jamming effect (Naaman and Wille, 2012).

Schauffert and Cusatis (2012) modeled pullout resistance through combining the effects of debonding of the fiber with the concrete matrix and the fiber matrix friction forces. Fiber-matrix interaction occurs on a sub-millimeter scale. The overall pullout behavior is typically characterized by the relationship between the pullout load, P, and the relative displacement or slippage, v, between the fiber and the matrix at the point where the fiber exits the matrix. This debonding stage is characterized by two parameters: (1) the bond fracture energy G_d, and (2) a constant value of frictional stress τ_0 for the portion of the embedded segment that has debonded. The slippage has a critical value, v_d, that represents full debonding as shown in eq. (1). Eq. (2) presents the relationship between the load and slippage during the debonding stage. After full debonding, the

resistance is entirely frictional and the fiber load is given as shown below in eq. (3). Figure 1 illustrates the interaction of the various parameters.

$$v_d = \frac{2\tau_0 {L_e}^2}{E_f d_f} + \left(\frac{8G_d {L_e}^2}{E_f d_f}\right)^{1/2} \quad (1)$$

$$P(v) = \left[\frac{\pi^2 E_f {d_f}^3}{2}(\tau_0 v + G_d)\right]^{1/2} \quad (2)$$

$$P(v) = P_0\left(1 - \frac{v - v_d}{L_e}\right)\left[1 + \frac{\beta(v - v_d)}{d_f}\right] \quad (3)$$

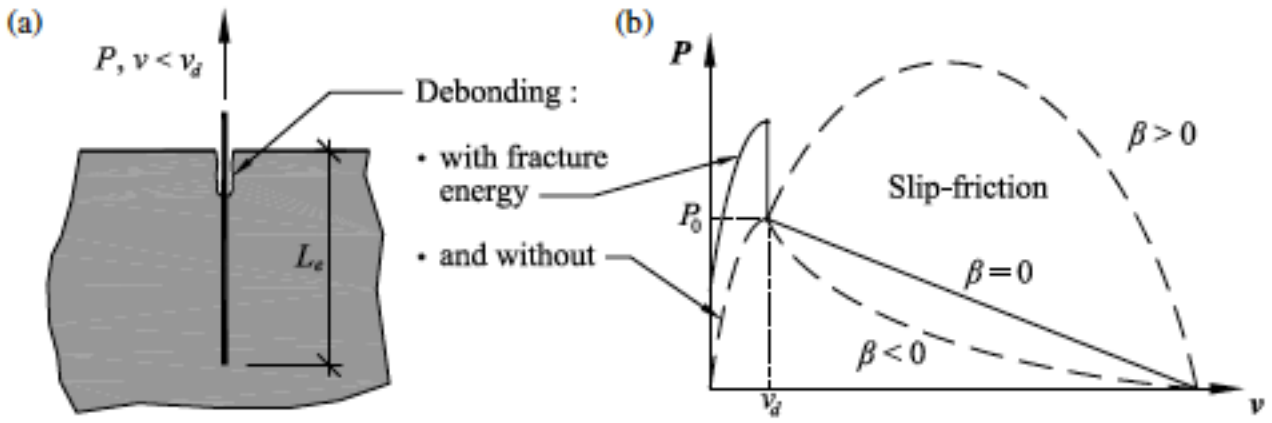

Figure 1. (a) Debonding; (b) typical load versus slippage relationships (From Schauffert 2012)

2.2. Fiber Pullout Testing Procedures

Many different testing procedures have been used throughout the study of fiber reinforced UHPC. Many researchers tested multiple fiber types such as straight, brass-coated, and hooked fibers. Bentur's pull out testing rig used the aid of a motor driven grip which was connected to a ball joint such that the rate of its movement could be controlled

by adjusting the input voltage to the motor. The loading rate was maintained at 0.3 mm/min with the fiber initially embedded 10 mm into the matrix. (Bentur *et al.* 1985)

Naaman's testing procedure started with positioning and centering the fiber. The specimens that were used were half dog-boned shaped. Once this was complete, the fiber was tightly gripped within the fixture, which was attached to a load cell with a maximum of 500lbs (2224 N) of MTS deformation-controlled servo-hydraulic testing machine. The vertical movement of the grip system was measured with an attached linear variable differential transformer (LVDT). This was used to determine the slip of the fiber. Naaman decided to ignore the elastic deformations of the fiber and specimen in his results. The pullout load speed was set to 1.1 mm/min, approximately three times the speed of Bentur's experiments. The fiber embedment length was targeted at 6.5mm, approximately half the length of each fiber.

Flanders's (2012) conducted testing using half dog-bones for the fiber pullout specimens, which was similar to Naaman. These tests were conducted using a 5 kN servo hydraulic Instron test frame fitted with tension grips. The crosshead was set at a loading rate of 0.5 mm/min with a 5 mm LVDT used to measure the displacement of the specimen relative to the grip, also known as slip. The load dropping to below 5 N dictated complete pullout (Flanders 2012).

Extensive research has been conducted on fiber reinforced UHPC over the past decades as this material has gained momentum as a structural armor material. The research herein adds to the known properties of this material, but contrasts to previous work in that the tests completed include confinement, which has not yet been studied.

3. Materials and Methods

3.1. Batching:

The specimens tested in this study were batched according to the Army Corps of Engineers' ultra high performance composite (Cor tuf) concrete mix-design. This mix design is extensively described in Williams *et al.* (2009). To summarize, Cor tuf is an ultra high performance concrete with a compressive strength of approximately 200 MPa. It gains the majority of its strength from its low water/cement ratio and small particle sizes (<0.6mm). Half batches were mixed for this project due to the small volume required to fill the mold (see Table 1). The dry ingredients were combined in the motorized baker-mixing bowl, then after 5 minutes the wet ingredients were added while the mixer continued to run. At approximately 10 minutes, the mixer was stopped so the sides of the bowl and the mixing paddle could be scraped off with a metal spoon to ensure that all of the ingredients were fully combined. The mixer was then started up again until the concrete mixture "kicked over," or became fully mixed together. After kick-over the concrete mixture changes from a wet looking sand mixture, to a cookie dough like consistency. The concrete was then put in the specimen molds.

Table 1. Cor tuf Mix Constituents

Material	**Mass (grams)**
Silica Fume	241.4
Silica Flour	171.9
Class H Cement	620.5
Silica Sand	600.0
Water	129.1
Super Plasticizer (ADVA 190)	10.6

The specimen mold (See Figure 2) was made out of a 10 cm x 10 cm x 1 cm thick Teflon mold with 49, 1 cm holes drilled through it. This mold was clamped to a second piece of Teflon, used for the base. Once mixing was complete, the concrete was put into a cake icing bag and squeezed into the mold while in the wet room. A metal spatula was used to flatten out the surfaces of each specimen and remove any excess concrete. Next a single, straight, steel fiber was positioned in the center of each concrete specimen, pushed to the bottom of the mold to ensure 10 mm of embedment. The mold was held on a vibration table for 30 seconds to ensure the concrete was completely consolidated around the fiber so there would be full fiber-matrix bond development. After casting, the specimens cured in a wet room for a week before they were moved to an 85 degree Celsius water bath for another week.

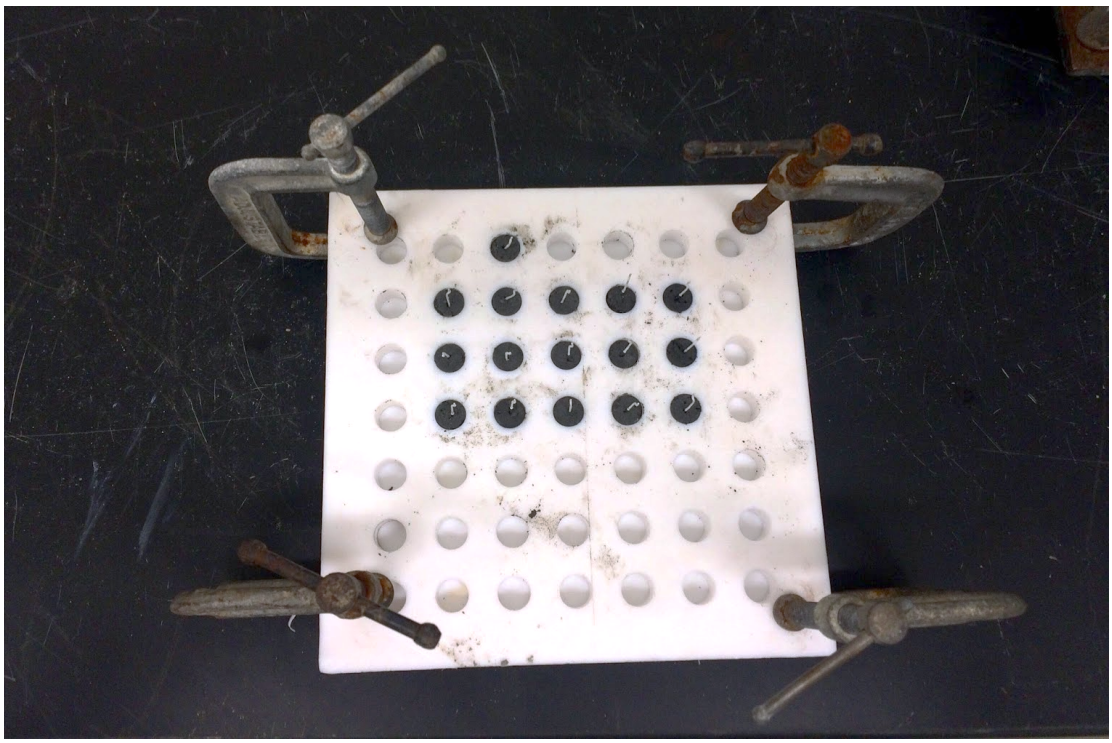

Figure 2. Teflon Specimen Mold (Capacity: 49 specimens)

The fibers used in this study were Dramix ZP 305 hooked steel with a manufacturer specified elastic modulus of 200 GPa and a tensile strength of 1100 MPa. The fibers were initially 30 mm in length, with a diameter of 0.55 mm. In order to eliminate pullout variability introduced by the hooked ends, fibers were clipped on one end so that only straight segments were embedded in the UHPC matrix.

Casting the specimens proved to be more difficult than originally expected due to their small size and the concrete's sensitivity to batching environment. Batching started in early January 2016 when the humidity was around 20 percent, which often prevented the concrete from kicking-over, and the batch would have to be thrown out. As the temperature and relative humidity increased as the year progressed, the concrete batches became more predictable and the Cor tuf that was produced could be cut into half dogbone molds.

Each specimen was only 1 cm in diameter and 1 cm high, with 49 specimens fitting approximately 1cm apart on the mold. This made it nearly impossible to do multiple rodded lifts or layers to create the specimens. It was extremely difficult to seat the fiber in the concrete such that it would not shift or rotate during the consolidation process, which consisted of using a secondary fiber to rod or consolidate the specimen to ensure that the concrete was fully mixed between layers. The early batches resulted in specimens with accidentally inclined fibers that were often not centered in the specimen. After multiple batching trials over two semesters, the final batching procedure using a cake icing bag and the vibration table, was finalized that produced consistent, high strength specimens. The three batches that were used for testing were batches 15, 16, and 17. Batches 16 and 17 were completed using the finalized successful batching procedure.

Batch 15 was completed using a slightly different batching procedure, but it was included in testing for comparison.

3.2. Testing

All of the specimens were tested in simple single, straight, steel fiber pullout tests using a 5 kN servo hydraulic Instron test frame fitted with a specialty fixture (See Figure 3) designed by Keith Berube to hold each specimen and apply variable confining stresses. A second fixture was attached to the crosshead to grip the steel fiber. The specialty fixture consisted of a large cylindrical piece of steel that could be bolted to the base of the Instron test frame. It had a hole in the center large enough to fit a 4.5 kN load cell, shims, and the 1 cm diameter by 1 cm tall specimen. A hex head screw (lateral) was located on either side of the confining fixture to passively confine the specimen, and a third hex head screw was located perpendicular to the load cell to be used for active confinement.

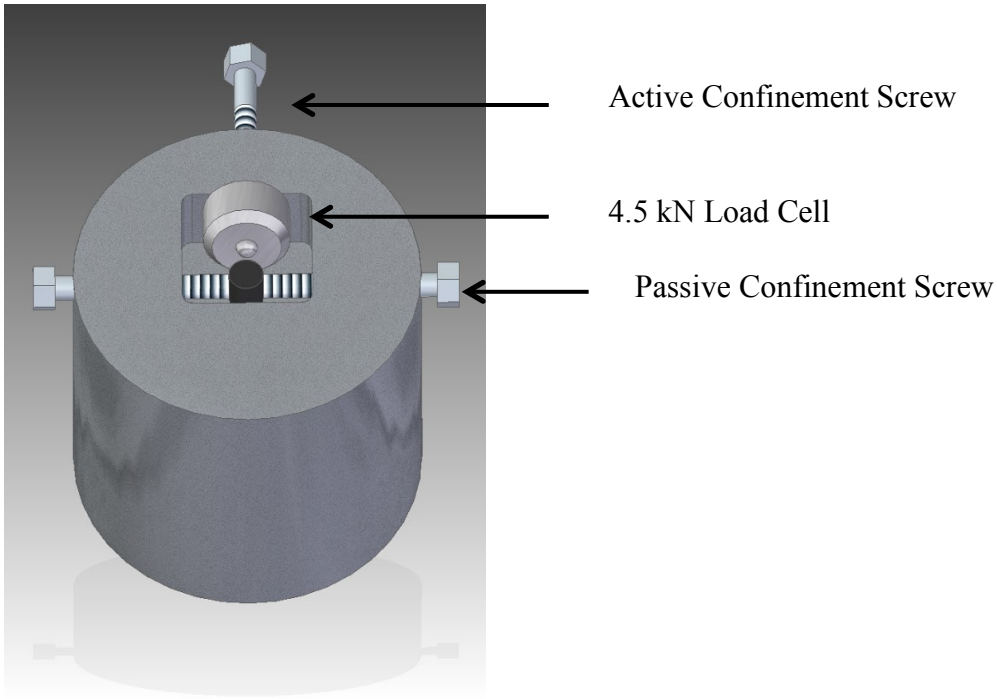

Figure 3. Steel Specimen Confinement Fixture (Image by Keith Berube)

Figure 4, shows the Instron test frame setup with the confining fixture. Each specimen was put into the confining fixture and aligned with the lateral screws such that the steel fiber was located in the center of the overhead fixture and could be gripped without any torque being applied to the fiber. The crosshead was then lowered so the overhead fixture was approximately 3 mm above the concrete surface of the specimen. Next the passive lateral screws were hand tightened to approximately 90 N (1.7 MPa) of confining force to hold the specimen in place. This procedure was practiced many times beforehand using a load cell to determine the required tightness of the screws. After this, the active force (90 N, 2000 N, 4000 N) was applied using the third screw. The required force was purposely overshot by about 5-10 percent because creep would balance it out before the test began. The last step before the test was initiated was to add a shim to the overhead fixture and tighten bolt to grip the steel fiber. The test was then initiated, and the fiber was pulled out of the specimen at a rate of 1mm/min. The data acquisition rate of the test was 10 samples/second. The test was continued until the load dropped below 1 N. The specimen was then inspected to determine if it had cracked or not due to the confining force.

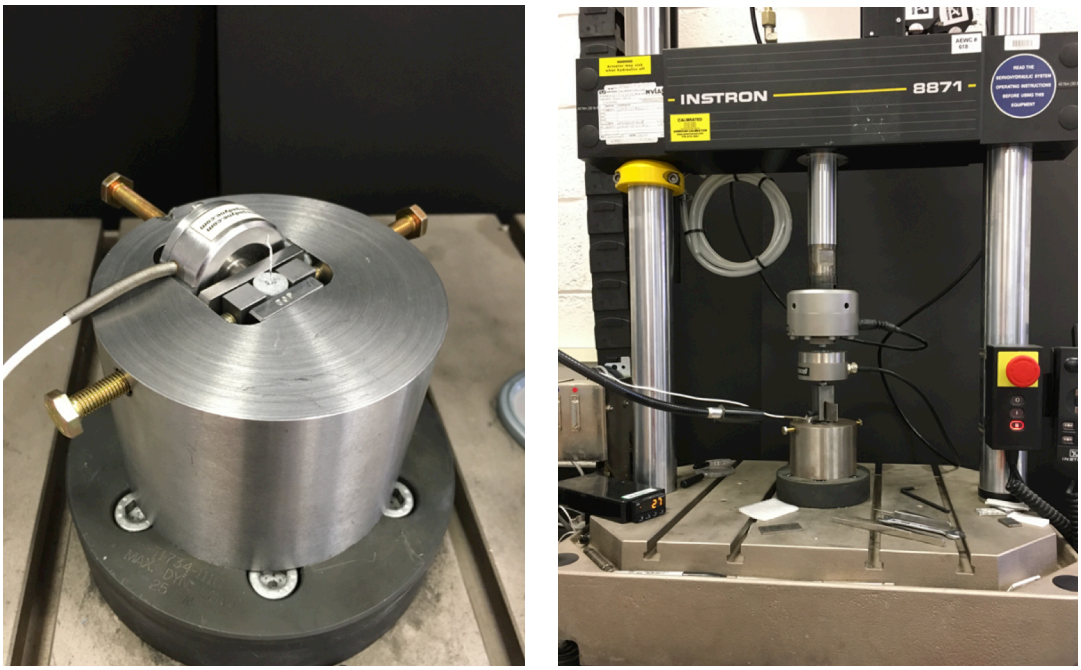

Figure 4. Photographs of 5kN Servo hydraulic Instron test frame with Confining Fixture (Right) and Specimen in Confining Fixture (Left)

The accuracy of the 250 N load cell was within 1 percent of full scale. The same was true for the 4.45 kN (1000 lb.) load cell that was used for later testing. No LVDT was used for testing. Instead, the Instron crosshead position was used to calculate displacement. The forces the Instron test frame experienced during testing were less than 5 percent of its capacity; therefore, an assumption was made that the entire Instron test frame setup could be assumed rigid for this testing application.

4. Results

4.1. Experimental Results

A total of 93 specimens were tested, each at one of the three different levels of confinement. As stated in the testing section, the confinement was applied with the active screw to a single axis of the specimen. On occasion, the specimen would crack if the confining force was too high. Testing was continued with the cracked specimen and the data was included, but a note was made. After analyzing batches 15, 16, and 17, it became clear that the specimens from batch 15 had a weaker fiber-concrete bond most likely due to a difference in batching procedure. These specimens were not consistent with the results gathered from batches 16 an 17 and the results were therefore removed from final analysis.

A load slip curve was plotted and analyzed for each specimen tested. (A complete catalog of load-slip curves is shown in Appendix C). The recorded data was analyzed using Matlab code (Appendix B) that extracted peak load and work-of-load for each test. Work-of-load is defined as the area under the load-slip curve and was calculated using a trapezoidal-based numerical integration. Figure 5 shows a characteristic curve for each of the three levels of confinement as well as the work or energy dissipation. Each curve consists of two major parts: the breaking of the relatively weak chemical bond between the fiber and the matrix, called debonding, and then the subsequent pullout of the fiber which is characterized by the friction experienced between the fiber and the matrix. During the steep portion of the graph leading up to the peak the loading is elastic and the fiber is undergoing pre debonding and then debonding. After the peak, the fiber begins to

pull out and the rest of the interaction is purely frictional and the load slowly decreases until the load dips below 1 N.

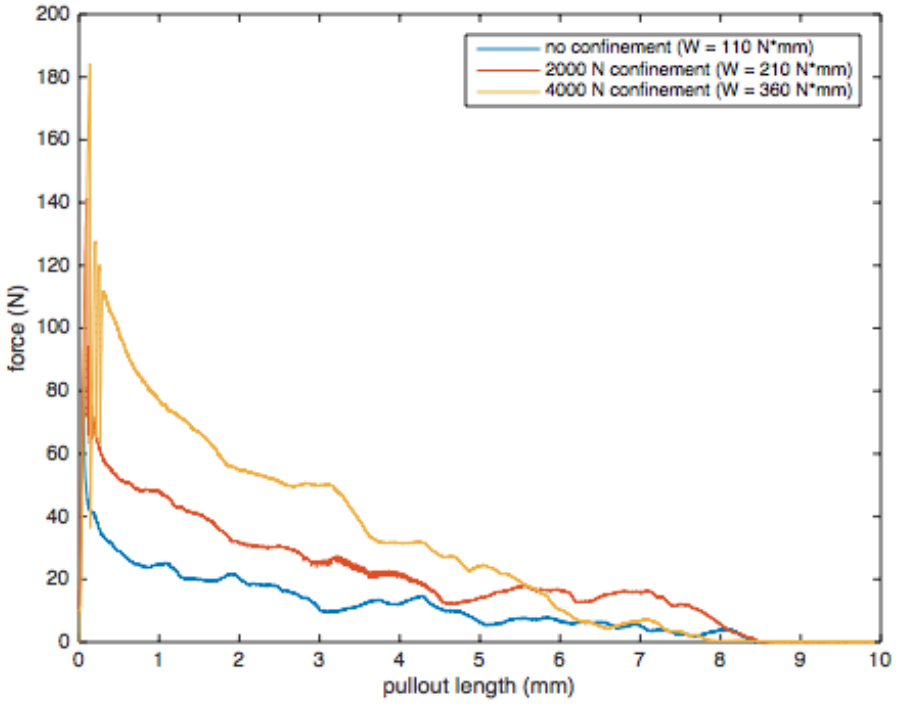

Figure 5. Characteristic Load-Slip Curves and Calculated Work (Unconfined, 2000N, 4000N)

The mean peak load for unconfined specimens (90 N) from batches 16 and 17 was 90 N, it was 137 N for 2000 N of confinement, and 144 N for 4000 N of confinement. Figure 6 shows the peak load values for the specimens from batches 16 and 17. Qualitatively, one can observe that confining stress has a positive effect on peak pullout force. The average work for batches 16 and 17 was 200 N-mm, 229 N-mm, and 231 N-mm, for unconfined, 2000 N, and 4000 N, respectively. Figure 7 shows the work or energy dissipation values for all of the specimens from batches 16 and 17. The experimental scatter is such that it is not clear there are significant differences in work. The average displacement was approximately 8.4 mm. Total embedment depth for each

steel fiber was 10mm, but since the tests were stopped when the load dipped below 1 N, the last 1.6 mm of the fiber was pulled out manually. The exact peak load, work, and displacement values are shown in Tables A-1, 2, and 3, respectively in Appendix A. Individual load-slip curves for each specimen can be found in Appendix C.

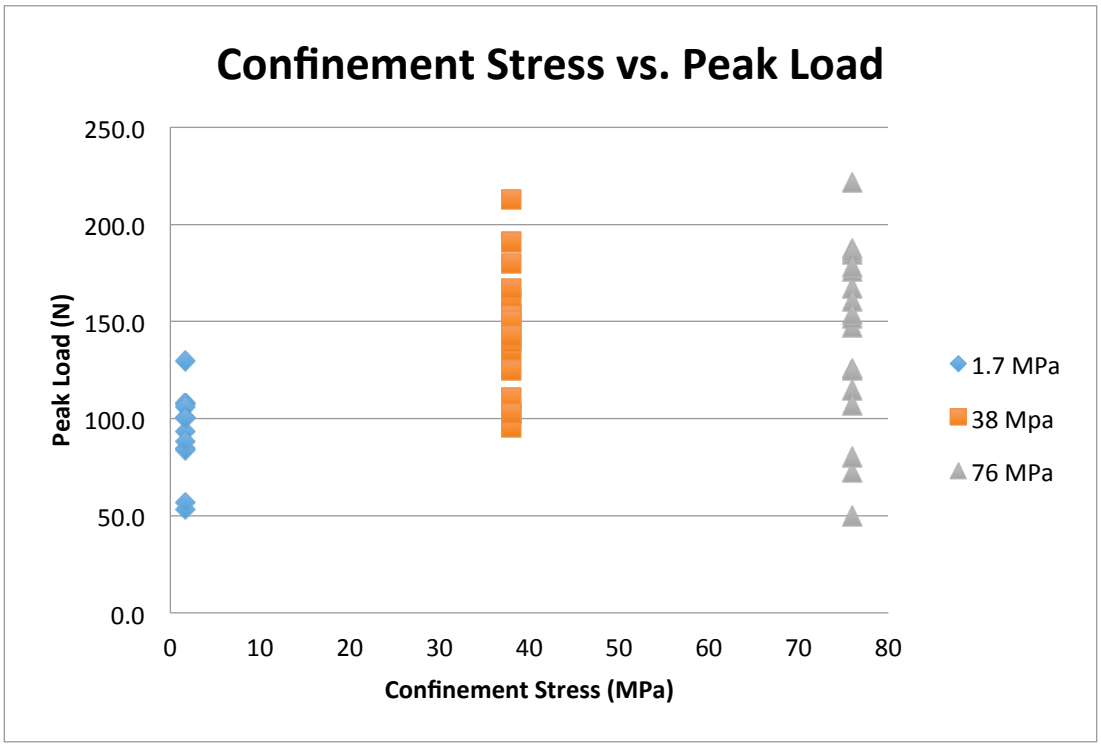

Figure 6. Average Confining Stress vs. Peak Pullout Load

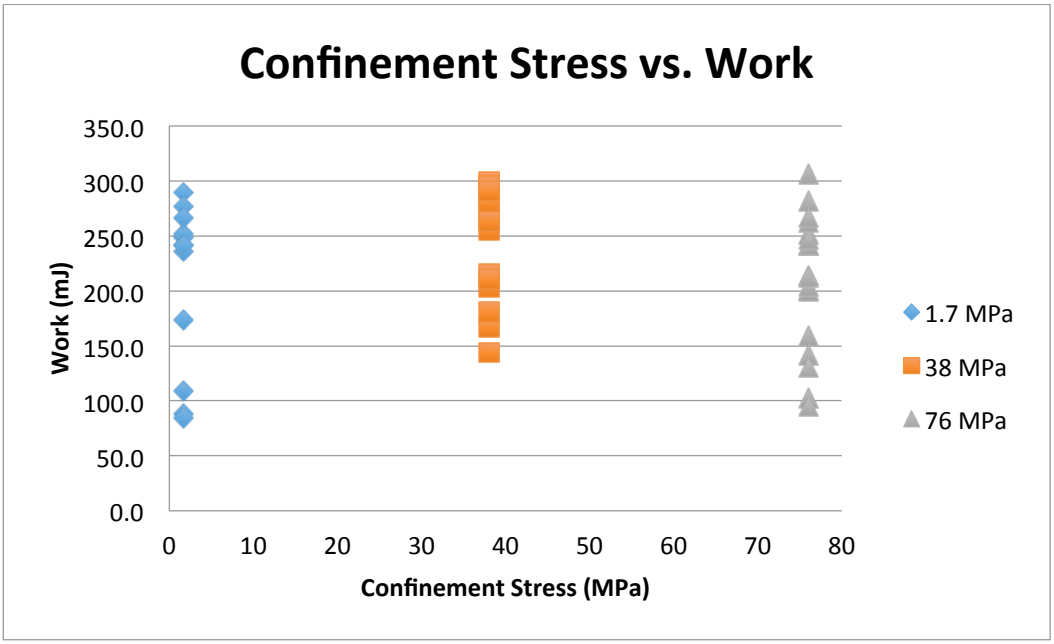

Figure 7. Average Confining Stress vs. Work

There were some interesting features that occurred on many of the graphs, and some anomalies that only occurred once or twice. Approximately half of the specimens tested presented a load-slip graph with a saw tooth pattern starting after the peak load, similar to that of Figures 8 and 9. The pullout load would increase with no fiber displacement until the load was high enough to cause a small displacement of the fiber and the load would drop. This process repeated until the pullout load was approximately 20 N and then the response would become relatively smooth for the remainder of the test as the fiber was continuously pulled out of the matrix. The saw tooth pattern was always accompanied by quick clicking sounds during testing. A possible explanation of this phenomenon is that debonding starts at the surface of the concrete, and slowly works its way down along the fiber. When the current load is not high enough to displace the fiber, the load increases until the current debonding section releases and then immediately drops and begins to increase again, repeating until debonding is complete. The smooth

part of the graph after the saw tooth pattern represents the final stage of testing where the interaction is purely frictional. When the higher confining stresses of 2000 N and 4000 N were applied to the specimens, the saw tooth pattern became more apparent with a larger amplitude. This comparison can be seen in Figures 8 and 9 (scale is different). This was most likely due to the higher frictional values caused by increased normal stress from the confining fixture.

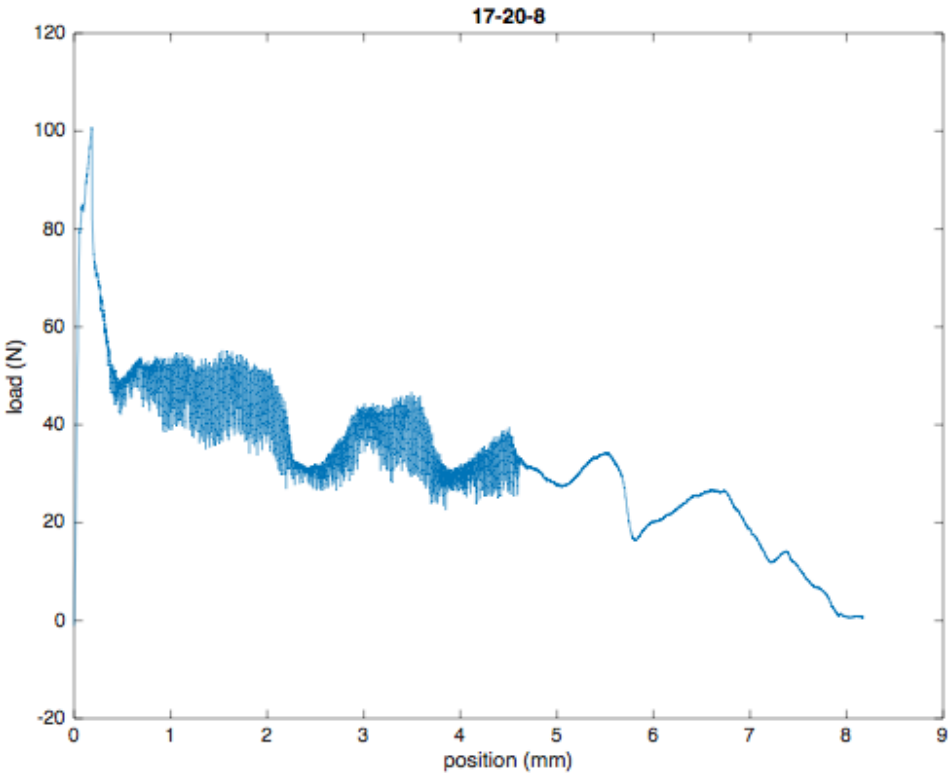

Figure 8. Saw Tooth Pattern for Unconfined Specimen 17-20-8

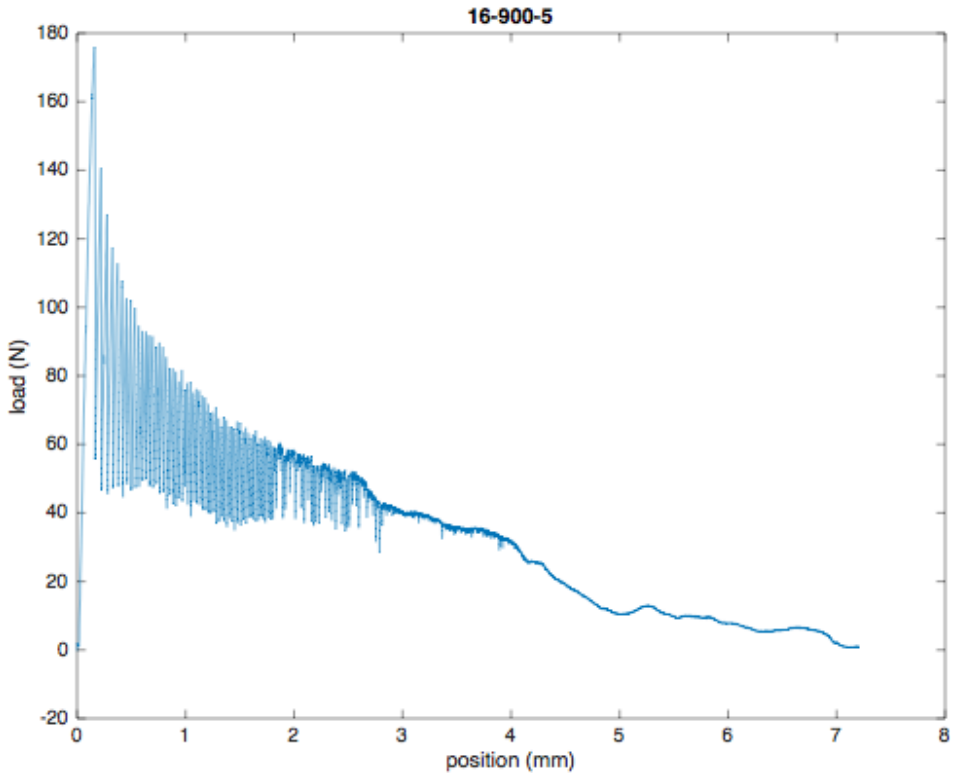

Figure 9. Saw Tooth Pattern for Specimen 16-900-5 Subject to 4000 N of Confinement

Another graph feature that occurred a limited number of times during testing was a secondary peak after the initial load peak followed by the characteristic feature of a slow load decrease until the end of the test (See Figure 10). After the initial peak load was reached and the load was beginning to slowly decrease, a few specimens experienced a secondary steep increase in load. This was unusual and only occurred approximately 10 percent of the time. This is most likely due to the fiber not completely debonding at the initial peak, leading to a load increase until the fiber is fully debonded. Once the fiber is fully debonded the load slowly decreases until the conclusion of the test. This anomaly may also be a magnified variation of the saw tooth pattern mentioned previously.

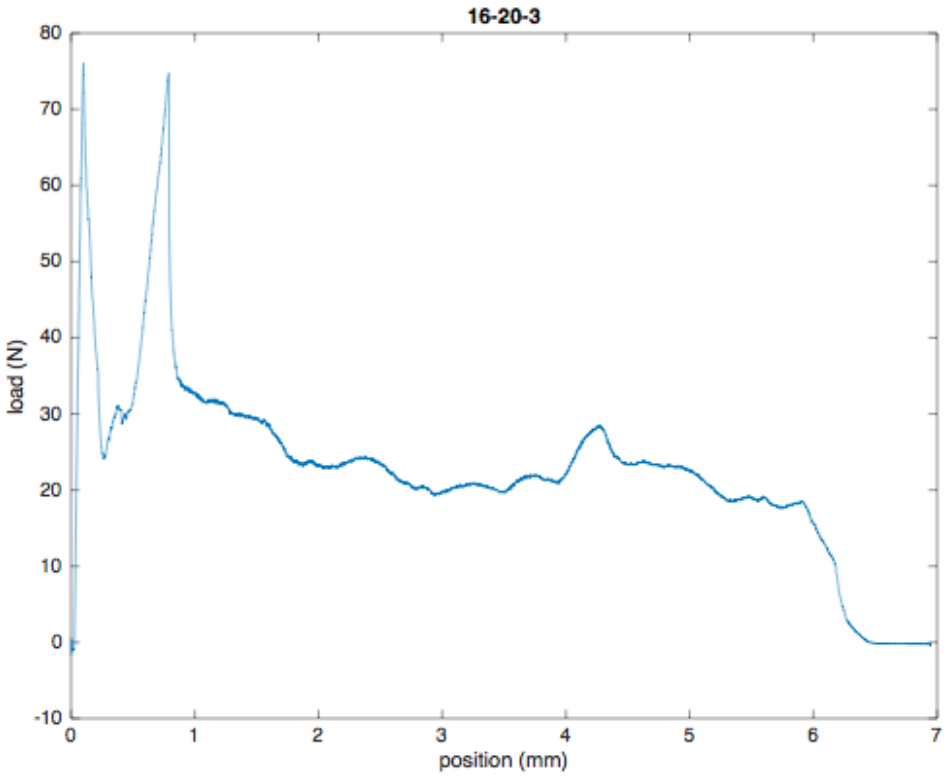

Figure 10. Secondary Load Peak for Unconfined Specimen 16-20-3

Some specimens were outliers for multiple reasons. If a specimen cracked under the applied confinement pressure, the resulting peak load would be lower than average due to the majority of the chemical bond having been broken before the test started. The work required to pull fibers out of these specimens was similar to that of the non-cracked specimens. This is likely a result of the higher confinement forces leading to increased frictional forces, which overcame the reduced bond strength. Specimen 16-900-1, tested under 4000 N of confinement required 781 N-mm of work to be removed from the concrete matrix. This was an anomaly, which was almost four standard deviations above the mean. The peak load for this specimen was 244 N, which was also significantly higher than the average of 144 N. It is unclear exactly why this test resulted in such high values, but it could have been caused by the fiber being accidently inclined during

batching, causing additional frictional resistance, or human error during the specimen setup procedure that caused friction between the Instron crosshead and the specimen fixture.

4.2. Model Parameters

Matlab was used to write a code that replicated Schauffert's model and plotted a graph of pullout length versus pullout force (Appendix B). The code calculated the work for each graph by integrating and calculating the area under the curve using a trapezoidal-based numerical integration. This value, along with the peak of each Schauffert model, was used to determine the values for the parameters bond strength, G_d, and frictional stress, τ, that best represents the data compiled from this research. Figure 11 shows plots of equations 2 and 3 and illustrates how changing the bond fracture energy G_d and the frictional stress τ influences the load-slip curve.

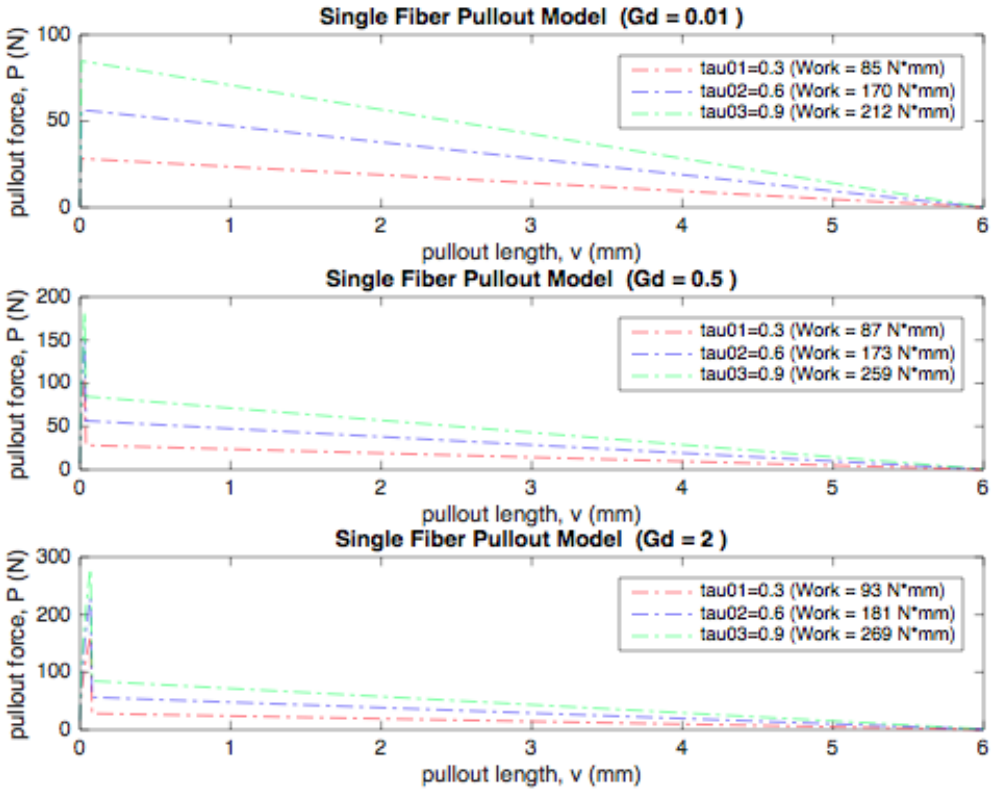

Figure 11. Illustration of Schauffert Model Parameters and their Effect on Load-Slip Curves

Test data was used to establish the model parameters. Fiber properties were obtained from the manufacturer's specification. Next, for each group of confinement tests, the values for G_d and τ_0 were determined by minimizing the squared difference between the model output and the measured data over the complete pullout response curve. Figure 12 below shows an example of the model fit overlaid on the pullout response curve. Table 2 below presents the results of the model parameter analysis. Fitting the data to a fiber pullout model made it possible to isolate the effects of bond strength and pullout friction. Based on these results it is clear that confinement stresses have little to no affect on bond strength (G_d), however does have an effect on bond

friction (τ_0). It can also be concluded that the bond friction increases approximately 20 to 60% when the confining stresses increase from 38 to 76 MPa.

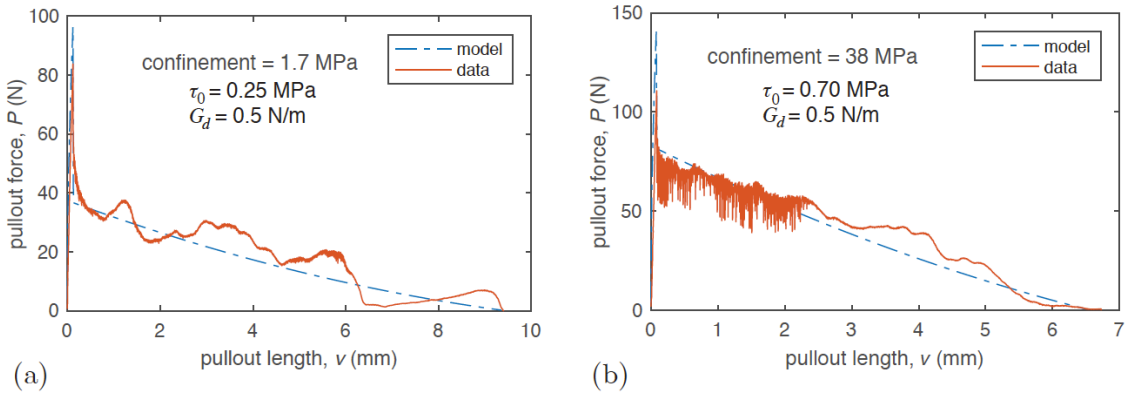

Figure 12. Data Comparison to Schauffert Fiber Pullout Model for (a) no confinement and (b) intermediate confinement.

Table 2. Table of Pullout Mean Model Parameters

Confinement	G_d **(N/mm)**	τ_0 **(N/mm^2)**
90 N (1.7 MPa)	0.52	0.40
2000N (38 MPa)	0.54	0.51
4000 N (76 MPa)	0.49	0.65

Applying the pullout model made it possible to isolate the bond strength and pullout friction, however it did not explain the poor correlation between confinement stress and total work. All of the pullout specimens were cast with a fiber embedment length of 10mm but after inspecting the pullout curve, it appeared that many of the specimens ceased to resist pullout after much less than 10mm, which implies that, the effective embedment length was in fact less than 10mm. Here the effective embedment depth is defined as the distance to which the pullout force drops to zero. Figure 12 above shows a contrast in effective embedment depths between (a) and (b). After investigating the load-pullout distances for all of the load-slip curves, there appeared to be no

correlation between confinement stress and effective embedment length, which is likely due to the influence of microstructural behavior that occurs after the fiber, is totally debonded. This behavior was tested by evaluating the work that was required to pull out only the first 2 mm of the steel fibers. The results of this analysis are shown in Figure 13 below.

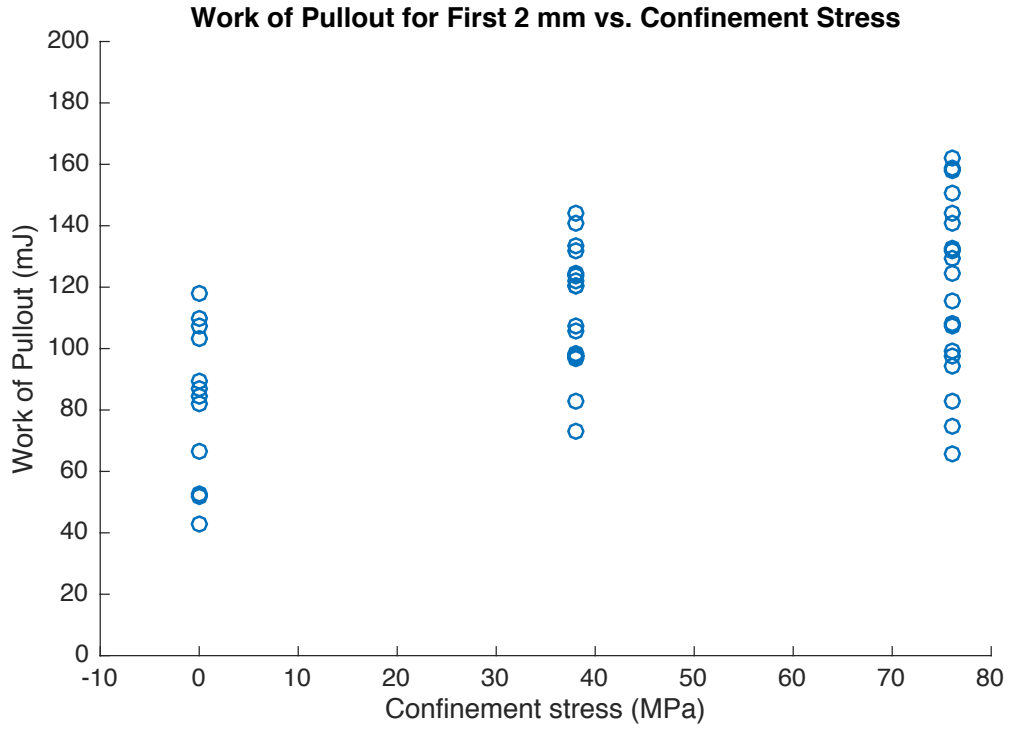

Figure 13. Work of Pullout for the First 2mm of Steel Fiber vs. Confinement Stress

The data shows significant scatter but quantitatively one can observed that there is a positive correlation between confining stress and the work required to pull the fiber out 2 mm. The mean values for no confinement, 38 MPa, and 76 MPa of confinement, were 83 J, 113 J, and 120 J respectively. It is not clear why the increase in pullout work disappears when the entire pullout curve is considered. The damage zone between the fiber and the concrete matrix may cause the variability. The result of this secondary

analysis is that an increase in confinement has a stronger influence on the initial pullout response than it does on final stages of pullout.

5. Summary and Conclusions

The initial hypothesis under investigation was how will confining stresses influence the pullout response of steel fibers embedded in UHPC. In order to answer this question new experimental protocol and testing procedure were developed. Cylindrical UHPC specimens were made with a single, straight steel fiber embedded 10 mm in the center of each specimen. Each specimen was then subjected to a confining stress (90 N, 2000 N, 4000 N) using a specialty confinement fixture and an Instron test frame was used to pull the steel fiber out of the concrete matrix. More than 90 specimens were tested and analyzed.

The results of the experiments along with Schauffert ‘s fiber pullout model were used to estimate values of bond strength and frictional stress that account for each of the three levels of confining forces. The results of this investigation led to a functional relationship between confining stress and pullout strength. Although there was significant experimental scatter, the results of this work conclude that the peak force had a positive correlation with confinement stress, but the total work of the pullout force did not. The analysis also showed that the work of pullout force only correlated positively for the first few millimeters of the steel fiber pullout. Parameters of an analytical fiber pullout model were set based on the data that was collected. The results showed that confinement stress had no affect on the bond fracture energy, however there was an influence to the friction stress. The friction stress increased approximately 20 to 60%.

The results of this work shows that applying confinement forces to fiber reinforced UHPC will increase the peak load required to pull a steel fiber out of the matrix. These tests were used to simulate the conditions for fiber reinforced UHPC subjected to a uniform compression field. This research has led to additional known properties regarding this material's performance under extreme loading events. The results herein allow us to have improved predictive capabilities through the incorporation of these findings into high fidelity, computational models for blast and ballistic structure performance.

Fiber reinforced UHPC is of extreme importance due to its recent popularity as a material to provide armor protection to military and civilian structures to protect them against blast or ballistic action. This research is a continuation of the efforts of professionals all over the world to learn more about this material. These findings demonstrate that the assumption that the pullout properties of steel fibers embedded in UHPC are not influenced by the stress of the matrix which is used for current computational models is inaccurate and leads to overly conservative values for the material. The implications of this is that these models will need to be updated to properly reflect the properties of fiber reinforced UHPC. The confinement waves that result from blast or ballistic action have a positive influence on the energy dissipation mechanisms of the fiber reinforced UHPC. The confinement waves that propagate out from the center of blast or ballistic action increase the overall toughness of the reinforced concrete.

6. References

Bartos, Peter (1981). "Review paper: Bond in Fibre Reinforced Cements and Concretes." *The Int. J. of Cement Composites and Lightweight Concrete.,* 3(3), 159-177

Bentur, A., Mindess, S. Diamond, S. (1985). "Pull-out processes in steel fiber reinforced cement." *The Int. J. of Cement Composites and Lightweight Concrete.,* 7(1), 29-37

Flanders, L. (2012). "A 3D Image Analysis of Energy Dissipation Mechanisms in Ultra High Performance Fiber Reinforced Concrete Subject to High Loading Rates." M.S. thesis, Univ. of ME, Orono, ME.

Mathworks. (2013). MATLAB [computer software]. Natick, MA.

Naaman, A. E. and Wille, K. (2012). "Pullout Behavior of High-Strength Steel Fibers Embedded in Ultra-High-Performance Concrete." *ACI Mat J.,* 109(4), 479-487

Schauffert, E.A. and Cusatis, G. (2012). "Lattice Discrete Particle Model for Fiber-Reinforced Concrete. I:Theory" *Journal of Engineering Mechanics American Society of Civil Engineers, 138(7), 826-833.*

Wang, Y., Li, V. C., and Backer, S. (1988). "Modeling of Fibre Pull-out from a Cement Matrix." *The Int. J. of Cement Composites and Lightweight Concrete,* 10(3), 143-149

Williams, E.M., Graham, S.S., Reed, P.A., and Rushing, T.S. (2009). "Laboratory Characterization of Cor-Tur Concrete with and Without Steel Fibers (ERDC/GSL TR-09-22)." *US Army Corps of Engineers Engineer Research and Development Center (ERDC).*

Appendix A - Peak Load, Work, Displacement Values for Batches 15, 16, &17

Table A- 1. Unconfined Specimen (90 N) - Work, Peak and Displacement for Batches 15, 16, & 17

Batch	Specimen	Peak(N)	Work (N*mm)	Displacement (mm)
15_20	1	29.25	33.93	3.80
15_20	2	89.21	432.33	8.81
15_20	3	54.24	229.29	9.48
15_20	4	35.65	93.34	6.89
15_20	5	72.49	210.30	7.46
15_20	6	48.65	60.60	4.66
15_20	7	69.11	150.90	7.40
15_20	8	64.37	161.62	8.02
15_20	9	59.66	248.51	9.64
15_20	10	27.39	49.67	6.23
Average		**52.08**	**163.66**	**6.86**
16_20	1	53.14	88.34	5.55
16_20	2	108.02	241.60	9.47
16_20	3	76.04	157.55	6.95
16_20	4	81.77	151.92	5.57
16_20	5	84.51	248.98	9.10
16_20	6	68.91	130.48	6.41
16_20	7	83.79	173.78	9.49
16_20	8	107.73	235.72	7.87
16_20	9	130.46	492.65	10.86
16_20	10	93.41	289.30	9.95
Average		**88.78**	**221.03**	**8.12**
17_20	1	82.78	125.91	6.78
17_20	2	129.77	276.50	9.01
17_20	3	88.13	108.85	8.43
17_20	4	56.86	84.80	6.87
17_20	5	94.25	12.50	0.25
17_20	6	105.89	251.53	9.78
17_20	7	68.82	177.60	9.34
17_20	8	100.81	266.21	8.17
17_20	9	100.04	241.40	11.04
17_20	10	55.44	195.31	5.95
17_20	11	117.66	220.78	8.89
Average		**90.95**	**178.31**	**7.68**
Average of 16 &17		**89.86**	**199.67**	**7.90**

Table A- 2. 2000 N Confinement - Work, Peak and Displacement for Batches 15, 16, & 17

Batch	Specimen	Peak (N)	Work (N*mm)	Displacement (mm)
15_450	1	26.44	31.51	5.36
15_450	2	81.96	77.56	6.33
15_450	3	78.64	153.68	7.04
15_450	4	81.80	109.10	7.76
15_450	5	77.14	252.33	8.10
15_450	6	57.69	137.46	6.54
15_450	7	82.79	222.89	9.14
15_450	8	115.12	243.03	7.70
15_450	9	54.42	266.01	10.20
15_450	10	60.21	94.00	6.51
Average		**71.62**	**158.76**	**7.47**
16_450	1	153.58	296.41	10.86
16_450	2	135.45	170.64	5.47
16_450	3	135.45	286.45	15.52
16_450	4	161.51	299.47	11.56
16_450	5	96.32	173.22	4.73
16_450	6	110.72	255.24	6.73
16_450	7	101.90	215.75	7.99
16_450	8	212.64	281.11	9.38
16_450	9	152.99	266.12	9.35
16_450	10	139.72	203.20	8.61
16_450	**11**	**137.32**	**230.52**	**8.00**
16_450	12	147.49	147.89	7.73
Average		**140.42**	**235.50**	**8.83**
17_450	1	179.66	291.01	8.58
17_450	2	141.34	210.28	9.69
17_450	3	95.58	143.92	10.01
17_450	4	124.70	166.55	7.86
17_450	5	150.35	280.69	10.12
17_450	6	102.52	295.29	10.10
17_450	7	167.09	263.44	10.57
17_450	8	46.05	99.80	7.72
17_450	9	142.66	180.56	7.64
17_450	10	191.09	290.91	8.93
Average		**134.10**	**222.24**	**9.12**
Average of 16 &17		**137.26**	**228.87**	**8.97**

Table A- 3. 4000 N Confinement - Work, Peak and Displacement for Batches 15, 16, &

Batch	specimen	Peak (N)	Work (N*mm)	Displacement (mm)
15_900	1	122.71	131.53	6.48
15_900	2	90.92	60.62	5.66
15_900	3	183.43	177.14	7.31
15_900	4	167.47	285.06	7.56
15_900	5	129.48	206.51	6.59
15_900	6	202.90	345.28	7.41
15_900	7	141.27	200.28	8.34
15_900	8	41.50	69.27	6.14
15_900	9	98.17	221.16	6.28
15_900	10	125.11	94.86	7.34
Average		**130.30**	**179.17**	**6.91**
16_900	1	243.67	780.79	20.89
16_900	2	167.41	158.95	5.34
16_900	3	147.04	241.71	8.00
16_900	4	187.67	200.16	6.69
16_900	5	175.96	251.71	7.20
16_900	6	151.63	241.78	8.33
16_900	**7**	**160.81**	**281.91**	**8.22**
16_900	8	72.21	199.86	7.55
16_900	9	114.95	246.93	9.23
16_900	10	125.72	262.00	7.71
Average		**154.71**	**286.58**	**8.91**
17_900	1	184.36	306.43	9.92
17_900	2	185.99	204.18	6.84
17_900	3	49.87	82.01	6.65
17_900	4	221.50	266.73	9.37
17_900	5	107.01	102.40	8.10
17_900	6	124.90	213.83	7.58
17_900	7	80.11	212.43	6.54
17_900	8	49.98	95.13	7.97
17_900	9	178.06	141.46	6.59
17_900	10	153.87	130.54	8.42
Average		**133.57**	**175.51**	**7.80**
Average of 16 &17		**144.14**	**231.05**	**8.36**

17

Appendix B - Matlab Scripts and Functions

Fiber Specimen Analysis Function

```
function [ work,peak,max_displ ] = PulloutAnalysis( filename,specimen_no )
 percentThis function plots and analyzes the graph for each specimen and creates a  percentmatrix with
peak load, total fiber displacement, and work. The function then
 percentsaves the graph of each individual test into the appropriate folder.


[time,position,load]=importfile(filename);

position=position-position(1);
figure,plot(position,load)
title(specimen_no),xlabel('position (mm)'),ylabel('load (N)');
saveas(gcf,[specimen_no '.eps'],'epsc')

peak=max(load);
max_displ=max(position);

m=length(load);
work=0;
for i=1:m-1
work=work+0.5*(position(i+1)-position(i))*(load(i)+load(i+1));
end

save([specimen_no '.mat'])
end
```

Specimen Analysis

```
 percentThis script compiles the data from the pullout analysis function into a
 percentsingle matrix.

N=10;

batch='16-900-';
results=zeros(N,4);

for i=1:10
   No=num2str(i);
   folder=['Test' No];
   file=['./' folder '/Test' No '.Stop.csv'];
   specimen_no=[batch No];
   [ work,peak,max_displ ] = PulloutAnalysis( file,specimen_no );
   results(i,1)=i;
   results(i,2)=peak;
   results(i,3)=work;
   results(i,4)=max_displ;

end
```

Schauffert Model Force Calculation

```
function [P] = pullout(v,tau0,Gd,Le,beta)
 percent P = pullout(v,tau0,Gd,Le)
 percent
 percent  Function returns force, P, the pullout force (in N) of an embedded fiber
 percent
 percent  Input arguments:
 percent     v = pullout distance (mm)
 percent     tau0 = friction stress (MPa)
 percent     Gd = fracture energy of bond (N/m)
 percent     Le = fiber embedment length
 percent     beta = model parameter (see paper)
 percent
 percent  Function uses units Newtons and mm

 percent fiber parameters
Ef=200000;   percent N/mm^2
df=0.5;      percent mm

 percent Bond Length
vd=(2*tau0*Le^2)/(Ef*df) + ((8*Gd*Le^2)/(Ef*df))^.5;

 percent Unit conversions (to be consistent with N & mm)
Gd=Gd/1000;   percent convert from N/m to N/mm
tau0=tau0*10;   percent convert MPa to

P0=pi*Le*df*tau0;

if v < vd
   P=(pi^2*Ef*df^3*(tau0*v+Gd)/2)^.5;
else
   P=P0*(1-((v-vd)/Le))*(1+(beta*(v-vd)/df));
end

end
```

Shauffert Model Comparison Script

```
 percentThis script uses the pullout function used to plot Shauffert's fiber pullout model with multiple
 percentvalues for the parameters Gd, and tau. The work is also calculated for
 percenteach graph.
Gd1=.01;
Gd2=0.5;
Gd3=2;
tau01=.3;
tau02=.6;
tau03=.9;
Le=6;
beta = 0;

v=0:.01:Le;
z=length(v);
P1=zeros(z,1);
for i=1:z
```

```
    P1(i)=pullout(v(i),tau01,Gd1,Le,beta);
    P2(i)=pullout(v(i),tau02,Gd1,Le,beta);
    P3(i)=pullout(v(i),tau03,Gd1,Le,beta);
    P4(i)=pullout(v(i),tau01,Gd2,Le,beta);
    P5(i)=pullout(v(i),tau02,Gd2,Le,beta);
    P6(i)=pullout(v(i),tau03,Gd2,Le,beta);
    P7(i)=pullout(v(i),tau01,Gd3,Le,beta);
    P8(i)=pullout(v(i),tau02,Gd3,Le,beta);
    P9(i)=pullout(v(i),tau03,Gd3,Le,beta);
end

m=length(v);

work1=0;
for i=1:m-1
work1=work1+0.5*(v(i+1)-v(i))*(P1(i)+P1(i+1));
end

work2=0;
for i=1:m-1
work2=work2+0.5*(v(i+1)-v(i))*(P2(i)+P2(i+1));
end

work3=0;
for i=1:m-1
work3=work3+0.5*(v(i+1)-v(i))*(P3(i)+P1(3+1));
end

work4=0;
for i=1:m-1
work4=work4+0.5*(v(i+1)-v(i))*(P4(i)+P4(i+1));
end

work5=0;
for i=1:m-1
work5=work5+0.5*(v(i+1)-v(i))*(P5(i)+P5(i+1));
end

work6=0;
for i=1:m-1
work6=work6+0.5*(v(i+1)-v(i))*(P6(i)+P6(i+1));
end

work7=0;
for i=1:m-1
work7=work7+0.5*(v(i+1)-v(i))*(P7(i)+P7(i+1));
end

work8=0;
for i=1:m-1
work8=work8+0.5*(v(i+1)-v(i))*(P8(i)+P8(i+1));
end

work9=0;
```

```
for i=1:m-1
work9=work9+0.5*(v(i+1)-v(i))*(P9(i)+P9(i+1));
end
work=[work1,work2,work3,work4,work5,work6,work7, work8, work9];

subplot(3,1,1)
plot(v,P1,'-.r',v,P2,'-.b',v,P3,'-.g')
tau1label=num2str(tau01);
tau2label=num2str(tau02);
tau3label=num2str(tau03);
str1 = ['tau01=' num2str(tau1label) ' (Work = ' num2str(work1,2) ' N*mm)'];
str2 = ['tau02=' num2str(tau2label) ' (Work = ' num2str(work2,3) ' N*mm)'];
str3 = ['tau03=' num2str(tau3label) ' (Work = ' num2str(work3,3) ' N*mm)'];
legend(str1, str2, str3);
xlabel('pullout length, v (mm)')
ylabel('pullout force, P (N)')
G1label=num2str(Gd1);
 percenttaulabel=num2str(tau01);
title(['Single Fiber Pullout Model  (Gd = ' G1label ' )' ])

subplot(3,1,2)
plot(v,P4,'-.r',v,P5,'-.b',v,P6,'-.g')
tau1label=num2str(tau01);
tau2label=num2str(tau02);
tau3label=num2str(tau03);
str1 = ['tau01=' num2str(tau1label) ' (Work = ' num2str(work4,2) ' N*mm)'];
str2 = ['tau02=' num2str(tau2label) ' (Work = ' num2str(work5,3) ' N*mm)'];
str3 = ['tau03=' num2str(tau3label) ' (Work = ' num2str(work6,3) ' N*mm)'];
legend(str1, str2, str3);
xlabel('pullout length, v (mm)')
ylabel('pullout force, P (N)')
G2label=num2str(Gd2);
 percenttaulabel=num2str(tau01);
title(['Single Fiber Pullout Model  (Gd = ' G2label ' )' ])

subplot(3,1,3)
plot(v,P7,'-.r',v,P8,'-.b',v,P9,'-.g')
tau1label=num2str(tau01);
tau2label=num2str(tau02);
tau3label=num2str(tau03);
str1 = ['tau01=' num2str(tau1label) ' (Work = ' num2str(work7,2) ' N*mm)'];
str2 = ['tau02=' num2str(tau2label) ' (Work = ' num2str(work8,3) ' N*mm)'];
str3 = ['tau03=' num2str(tau3label) ' (Work = ' num2str(work9,3) ' N*mm)'];
legend(str1, str2, str3);
xlabel('pullout length, v (mm)')
ylabel('pullout force, P (N)')
G3label=num2str(Gd3);
 percenttaulabel=num2str(tau01);
title(['Single Fiber Pullout Model  (Gd = ' G3label ' )' ])
```

Appendix C - Load-Slip Curves for Batches 15, 16, & 17 (90 N, 2000 N, 4000 N)

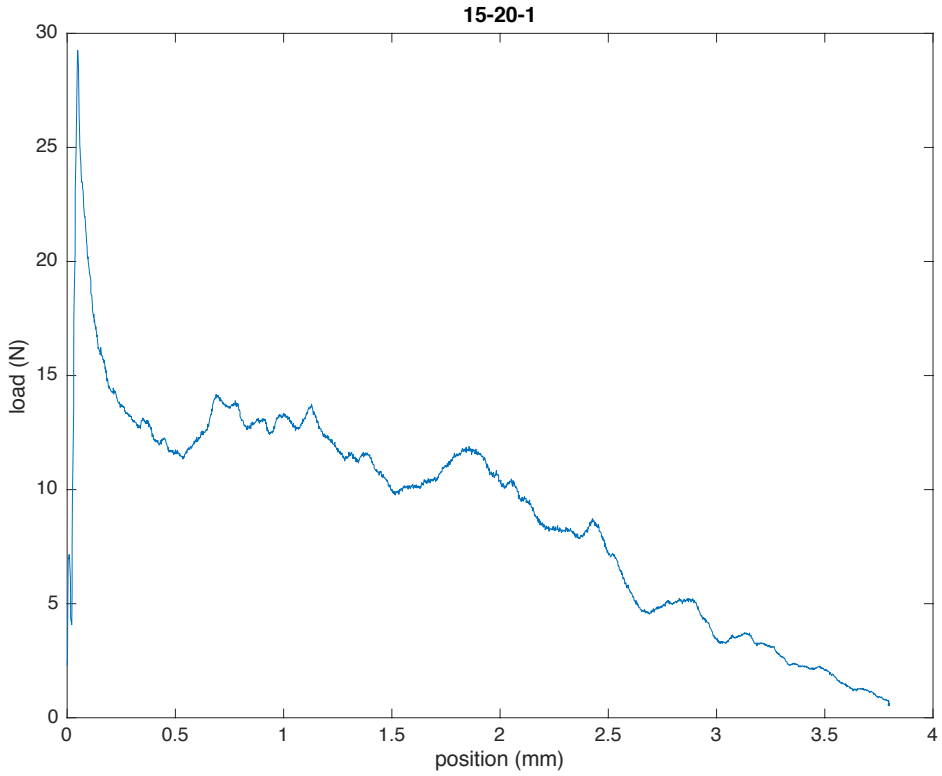

Figure 14. Specimen 15-20-1

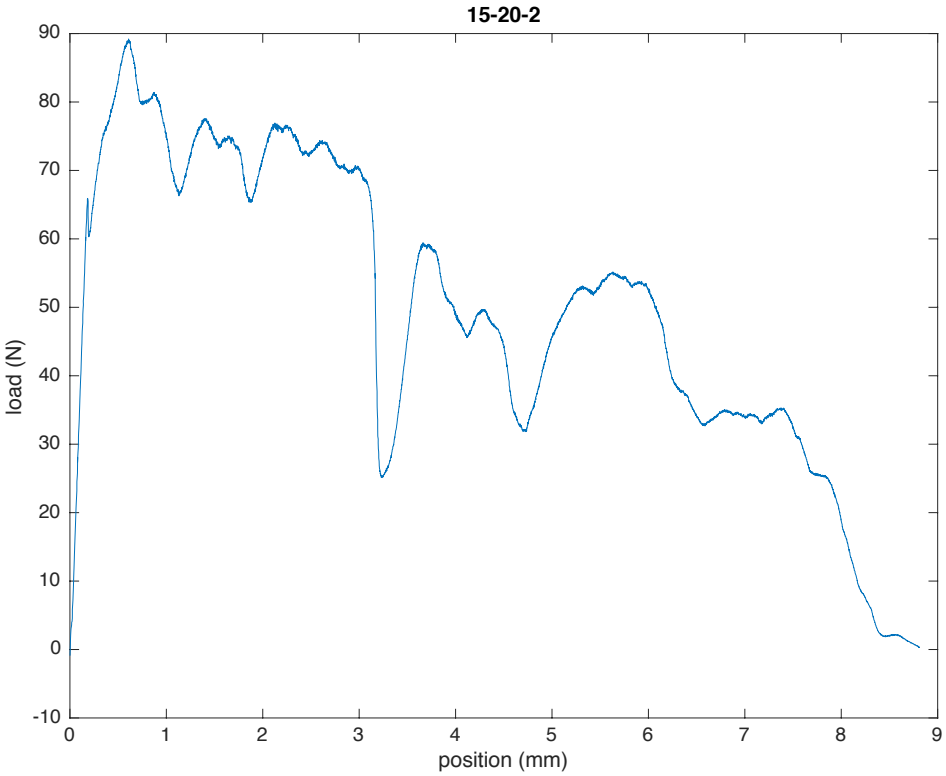

Figure 15. Specimen 15-20-2

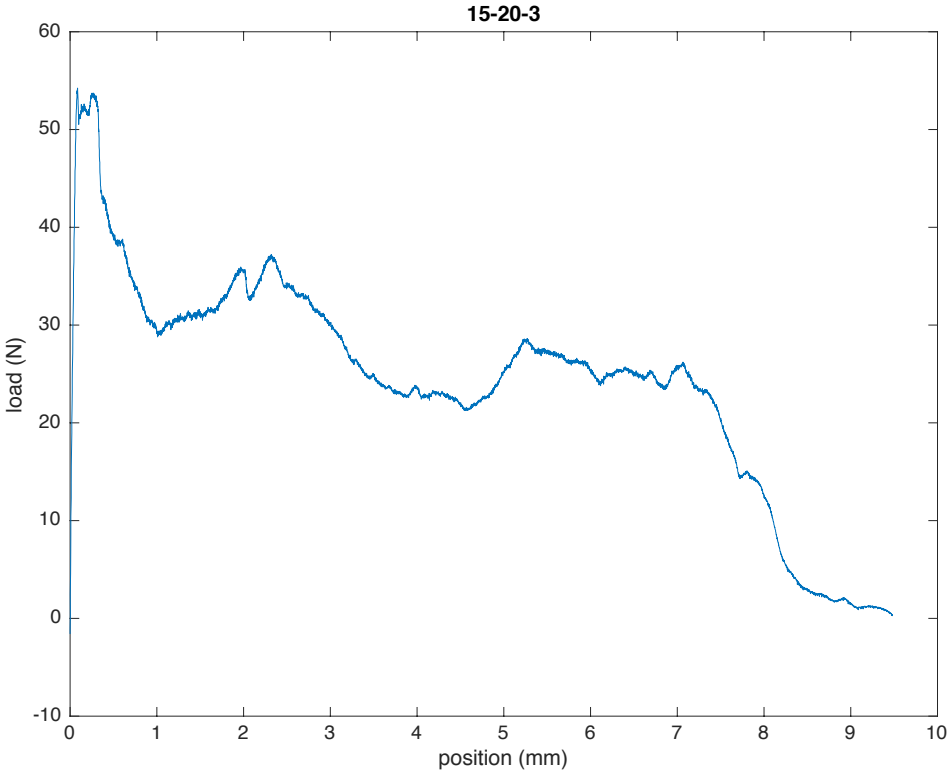

Figure 16. Specimen 15-20-3

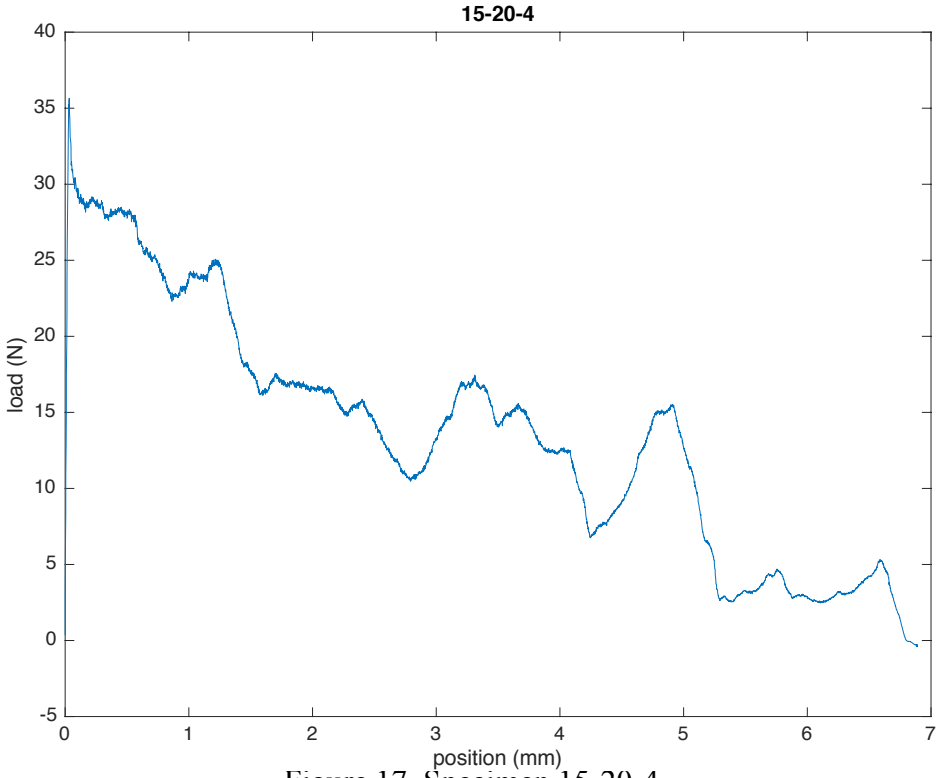

Figure 17. Specimen 15-20-4

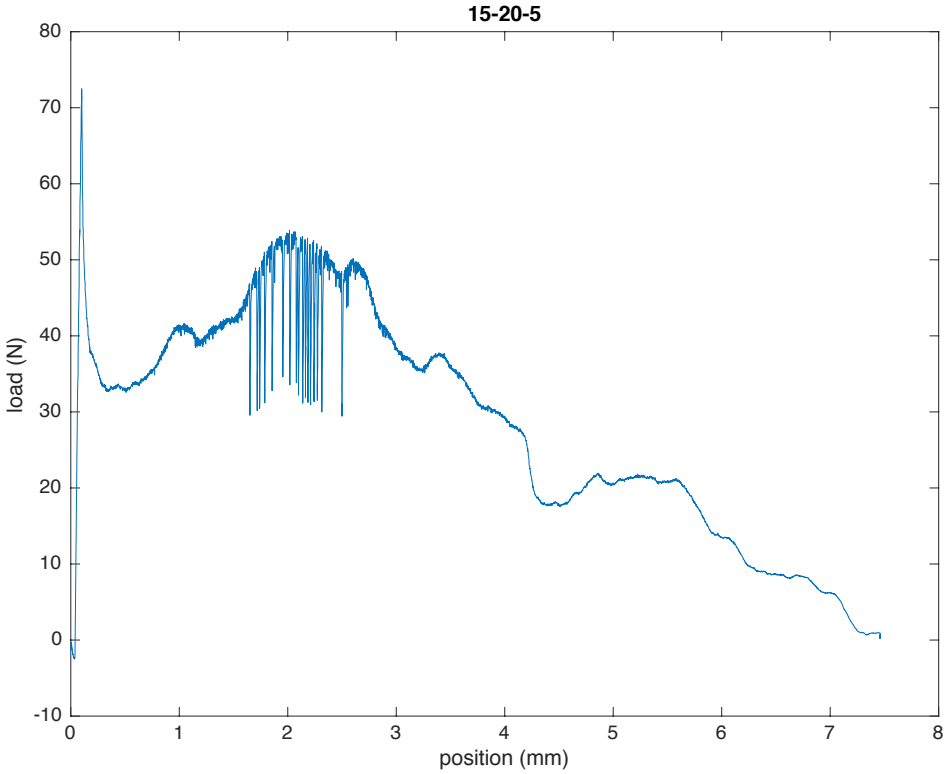

Figure 18. Specimen 15-20-5

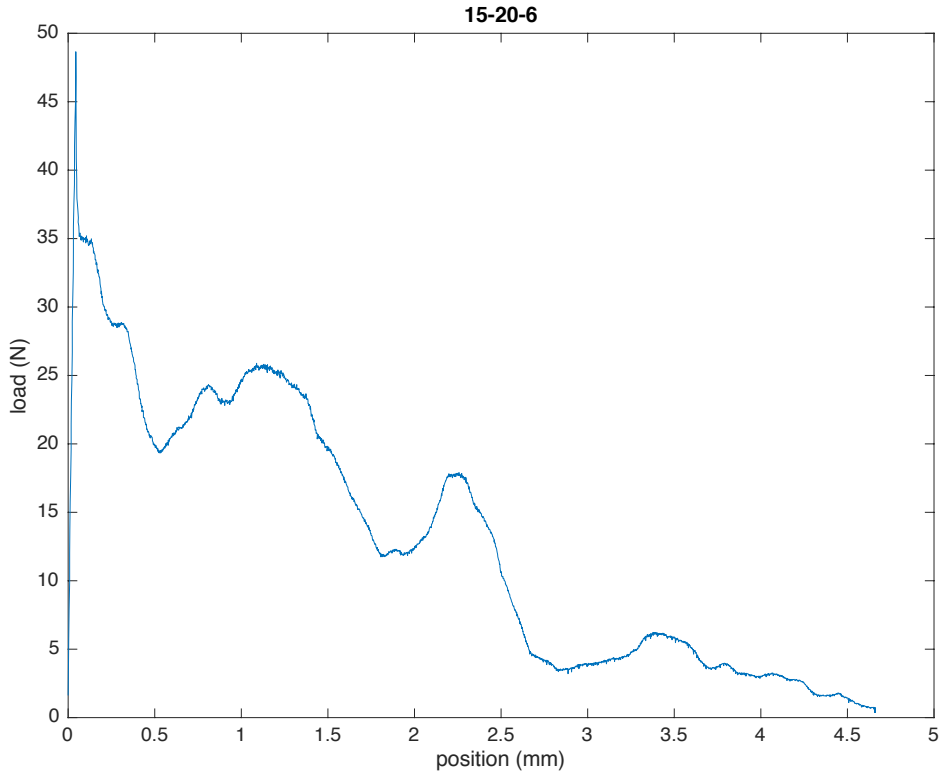

Figure 19. Specimen 15-20-6

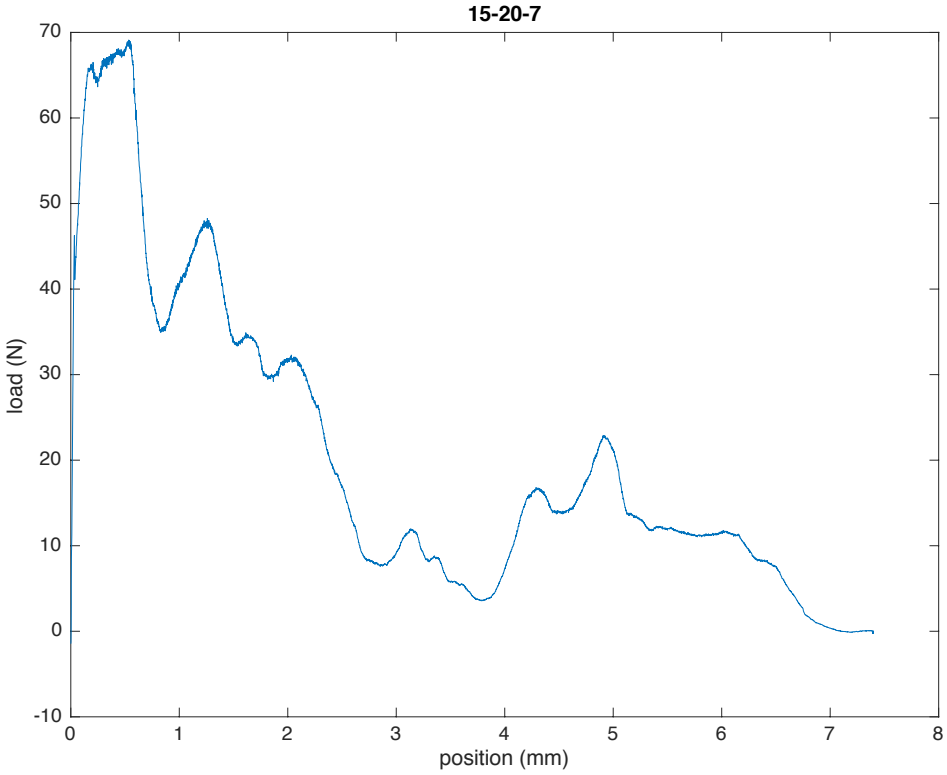

Figure 20. Specimen 15-20-7

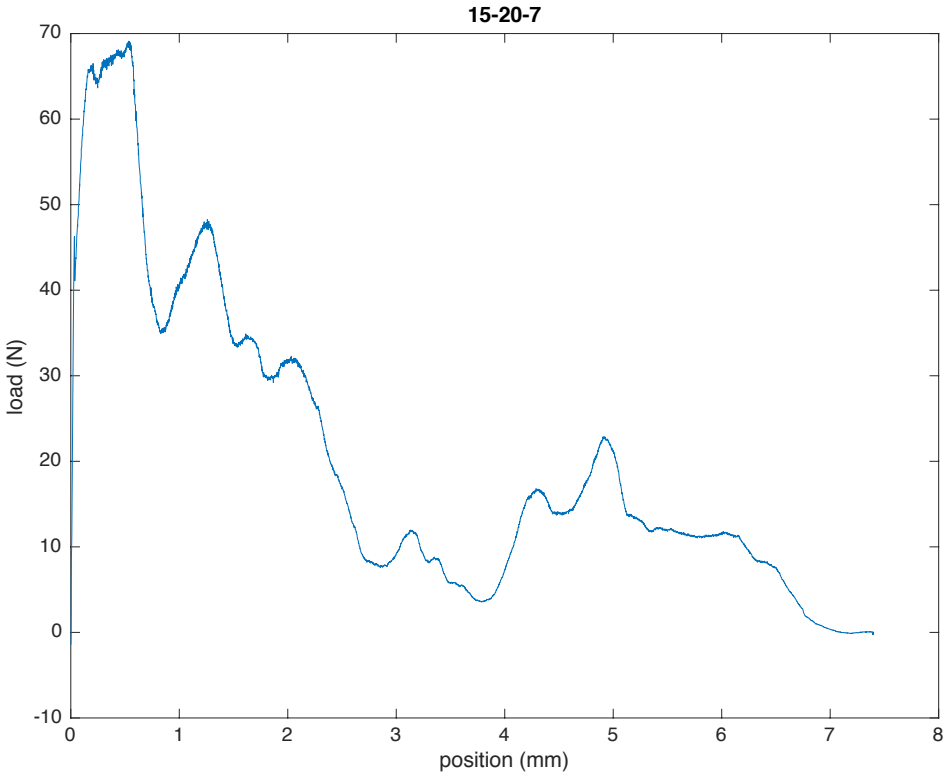

Figure 21. Specimen 15-20-8

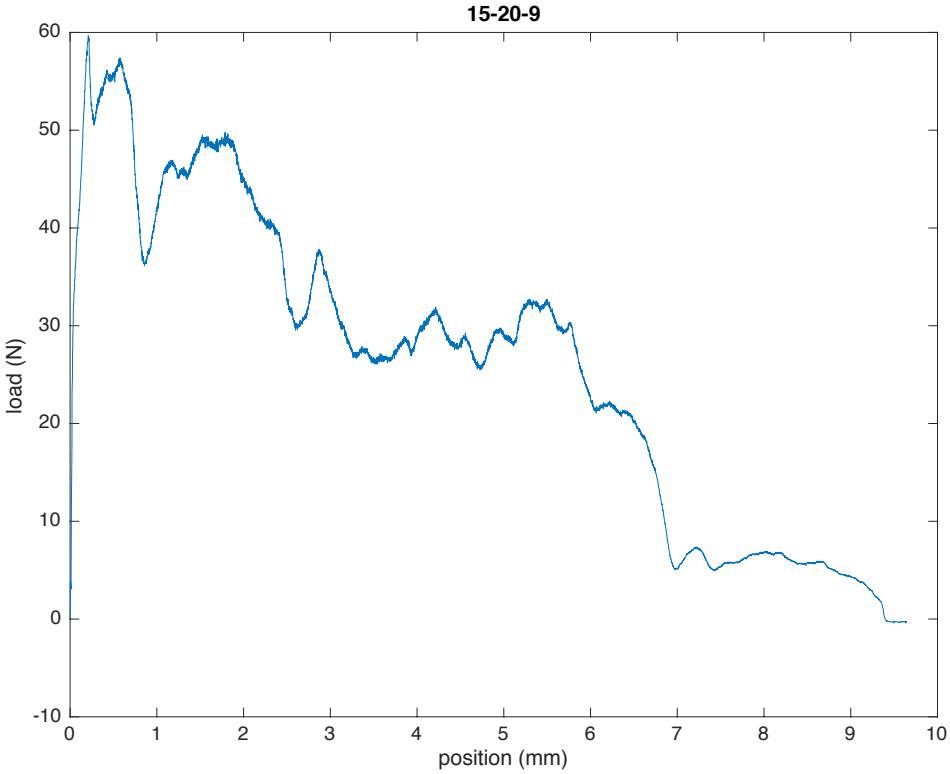

Figure 22. Specimen 15-20-9

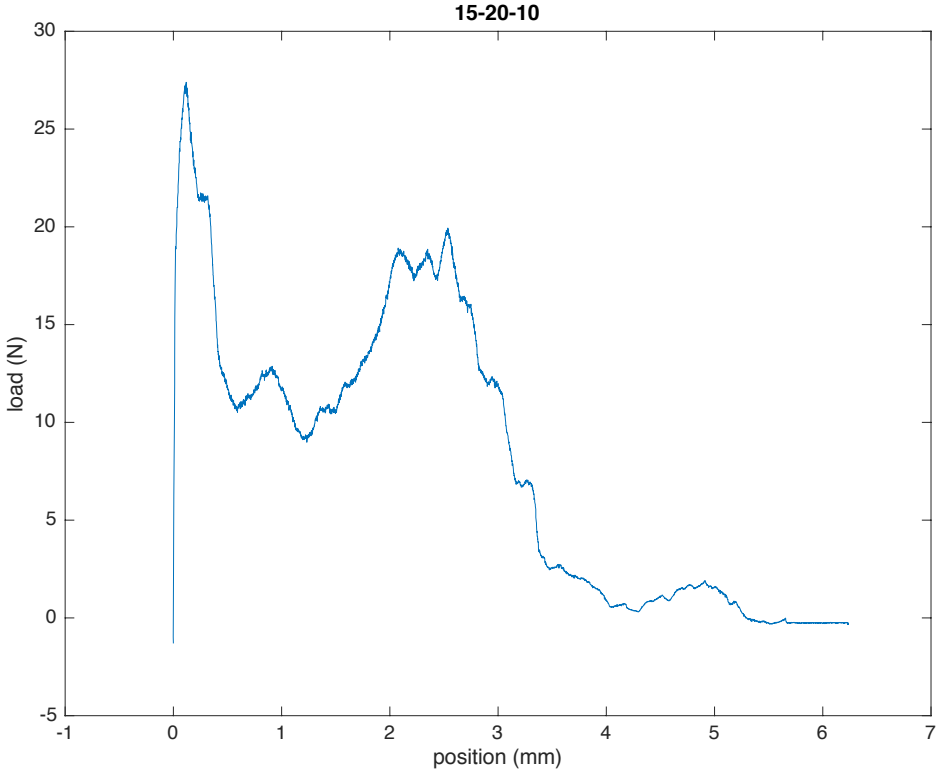

Figure 23. Specimen 15-20-10

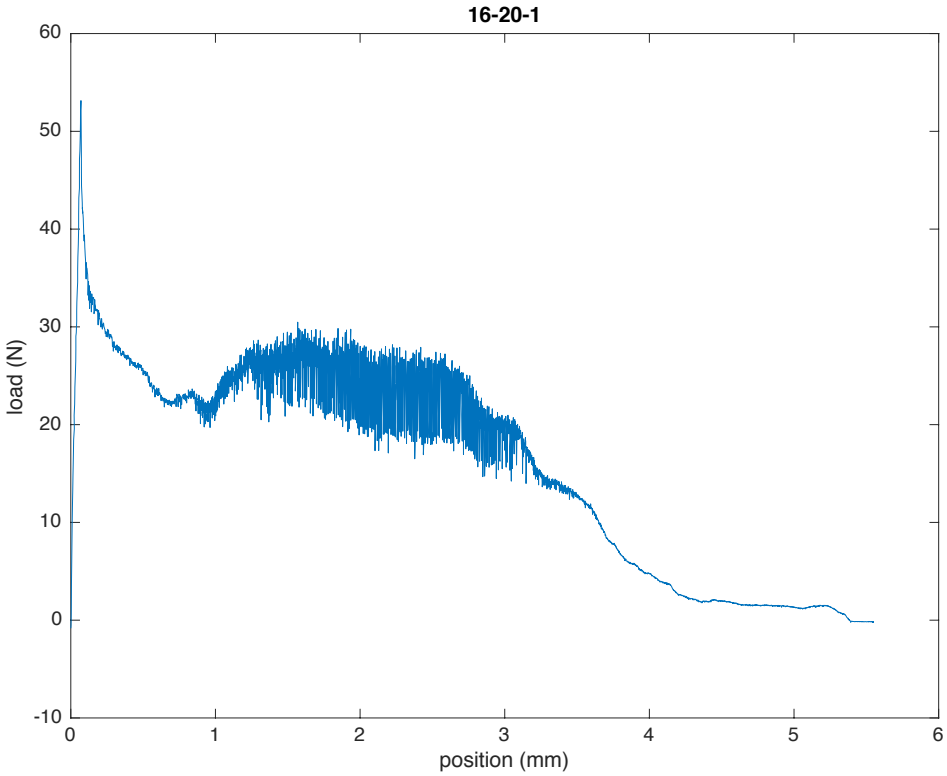

Figure 24. Specimen 16-20-1

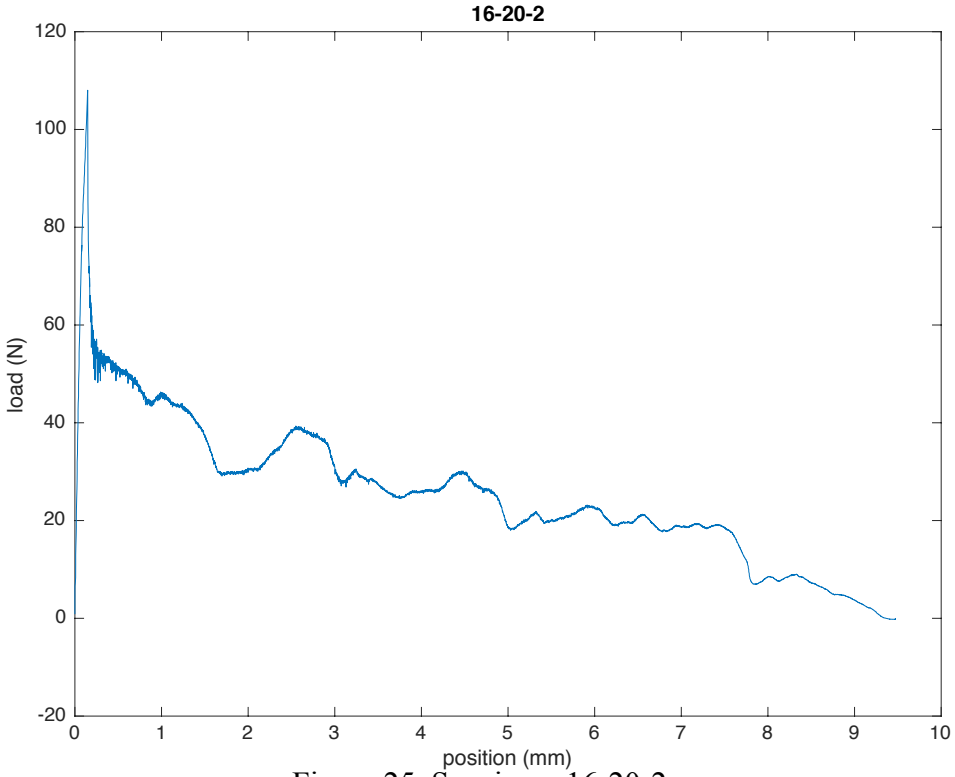

Figure 25. Specimen 16-20-2

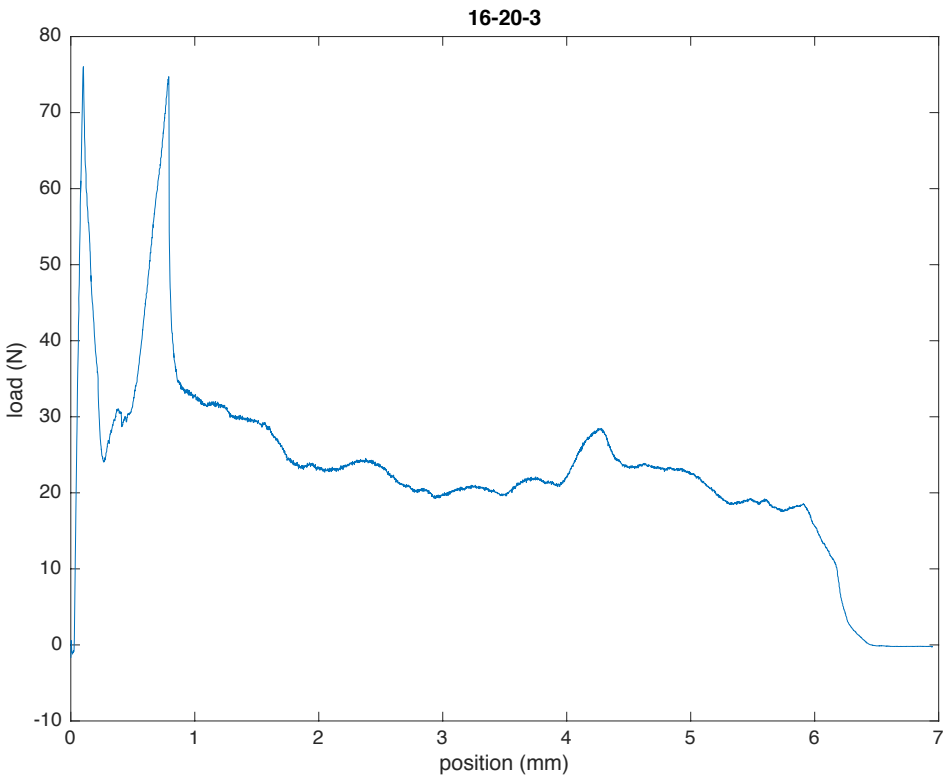

Figure 26. Specimen 16-20-3

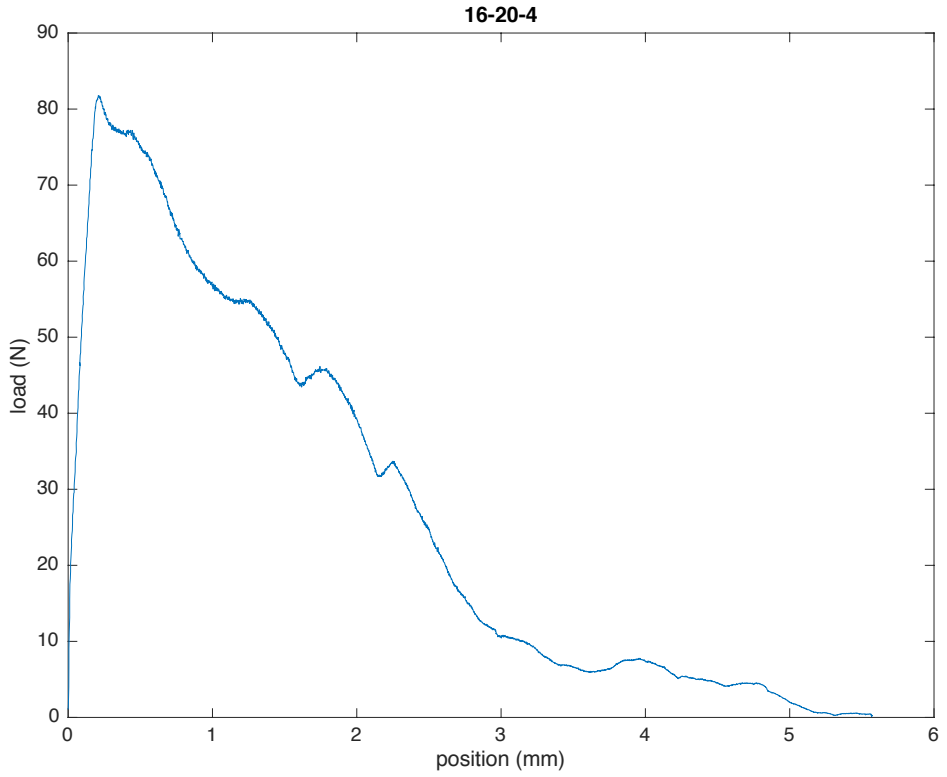

Figure 27. Specimen 16-20-4

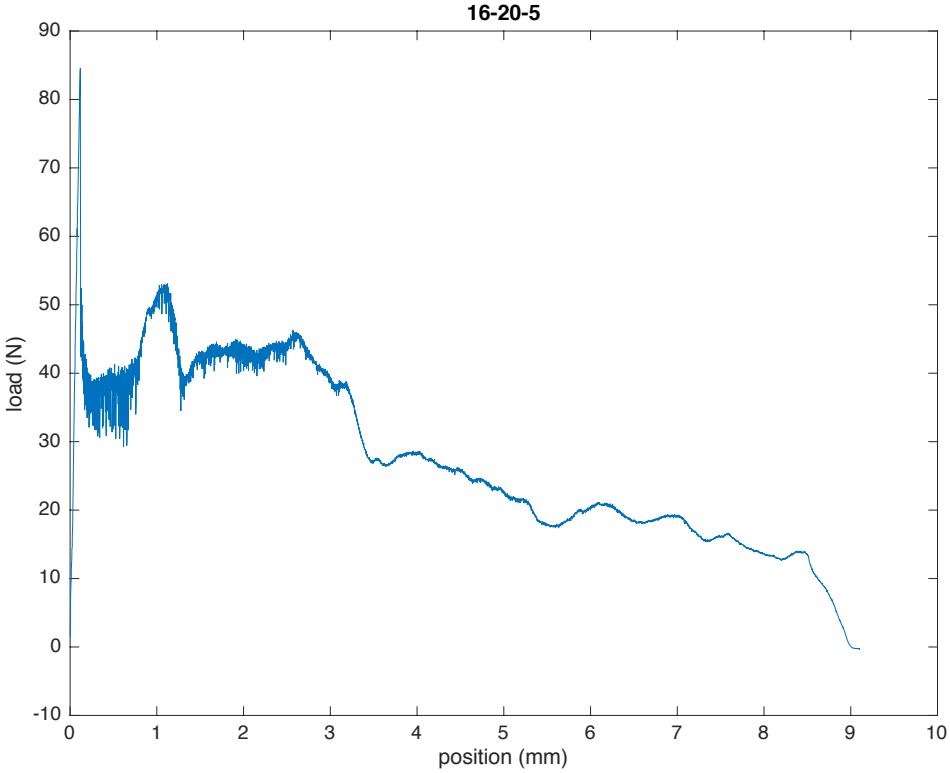

Figure 28. Specimen 16-20-5

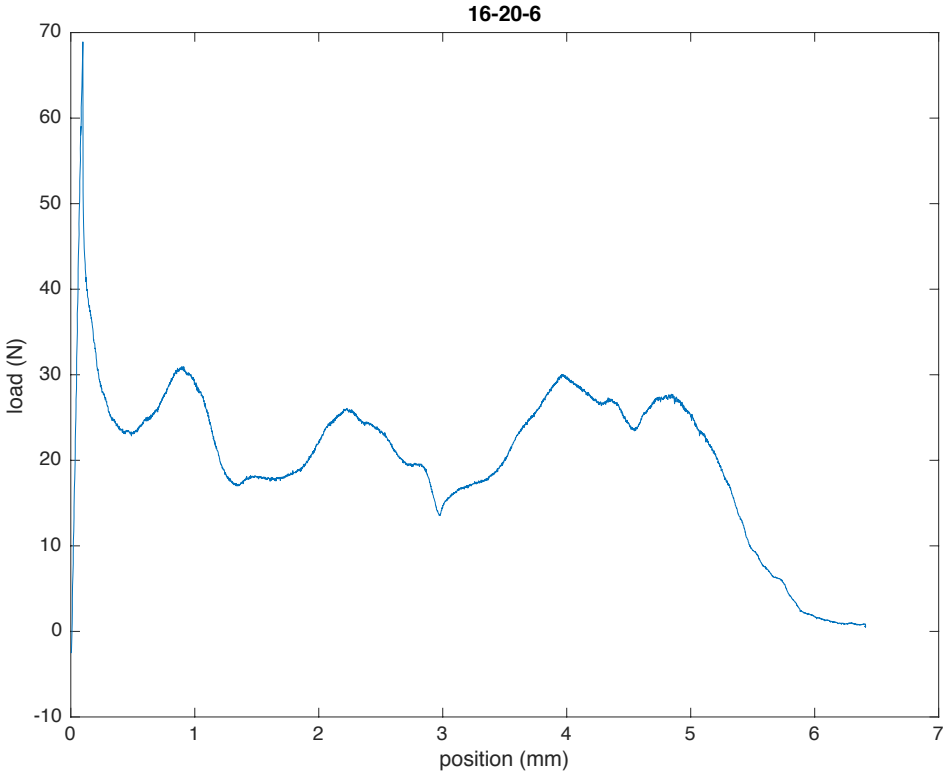

Figure 29. Specimen 16-20-6

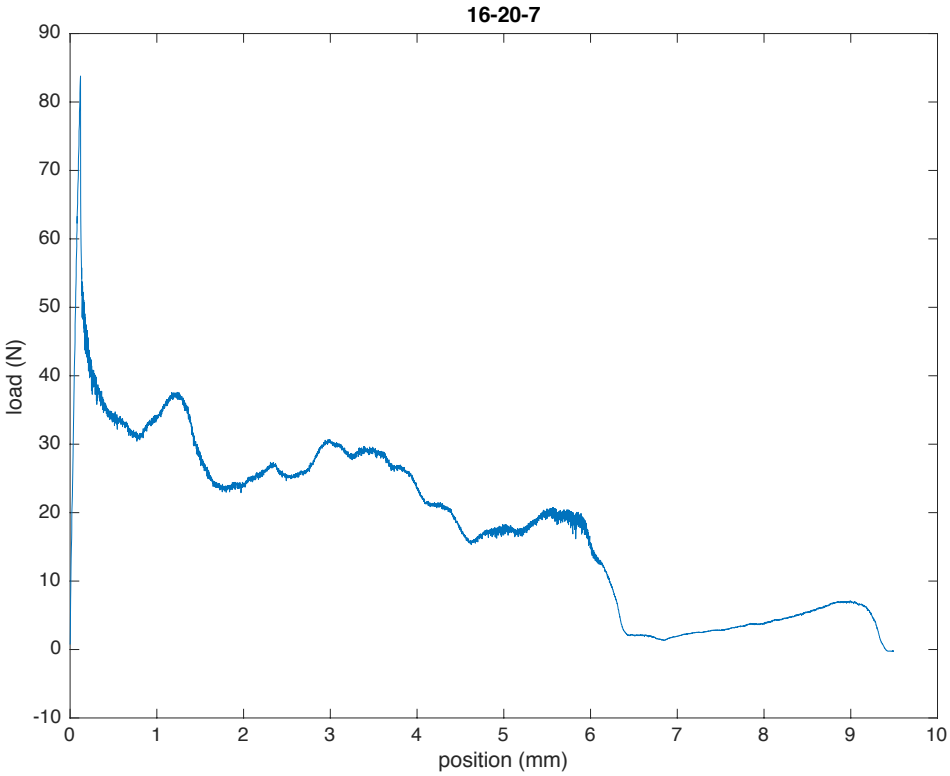

Figure 30. Specimen 16-20-7

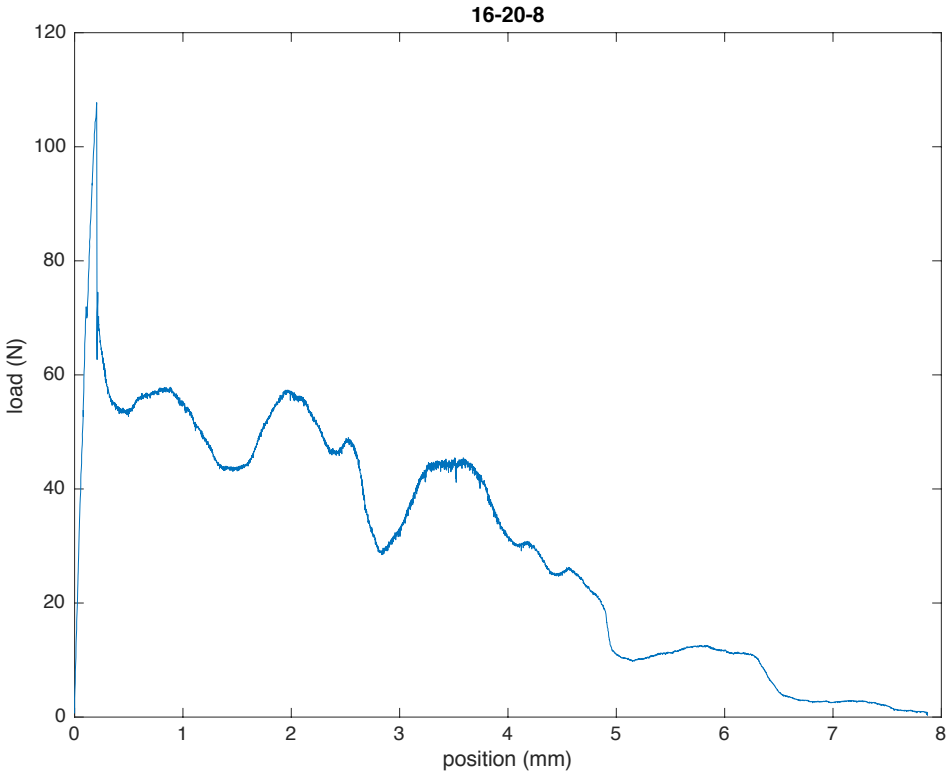

Figure 31. Specimen 16-20-8

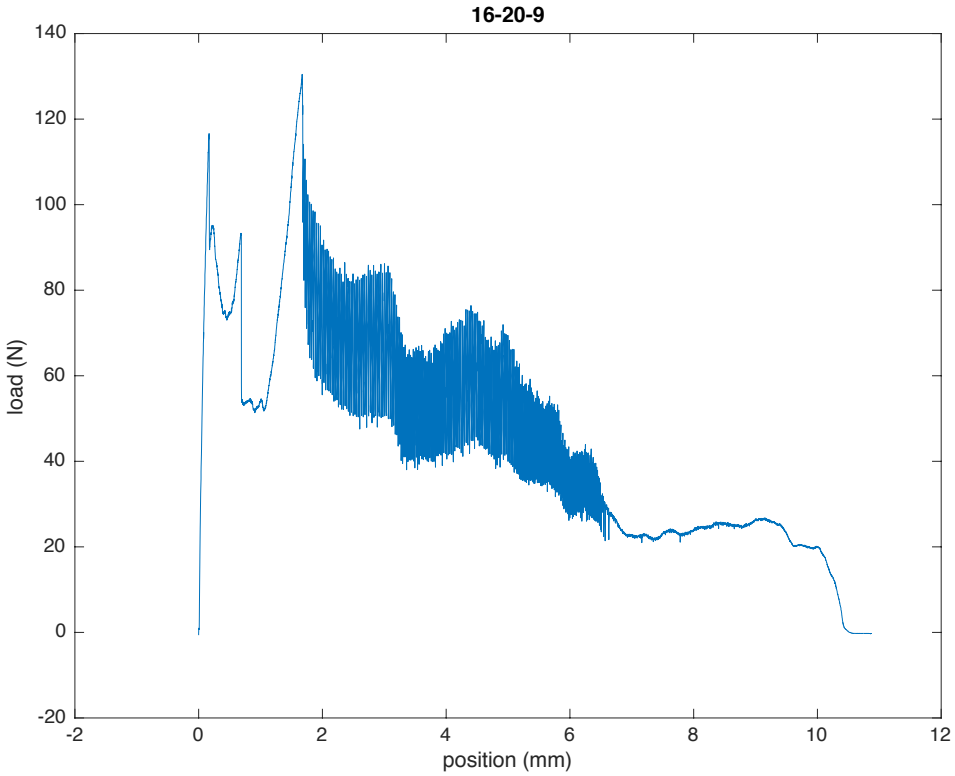

Figure 32. Specimen 16-20-9

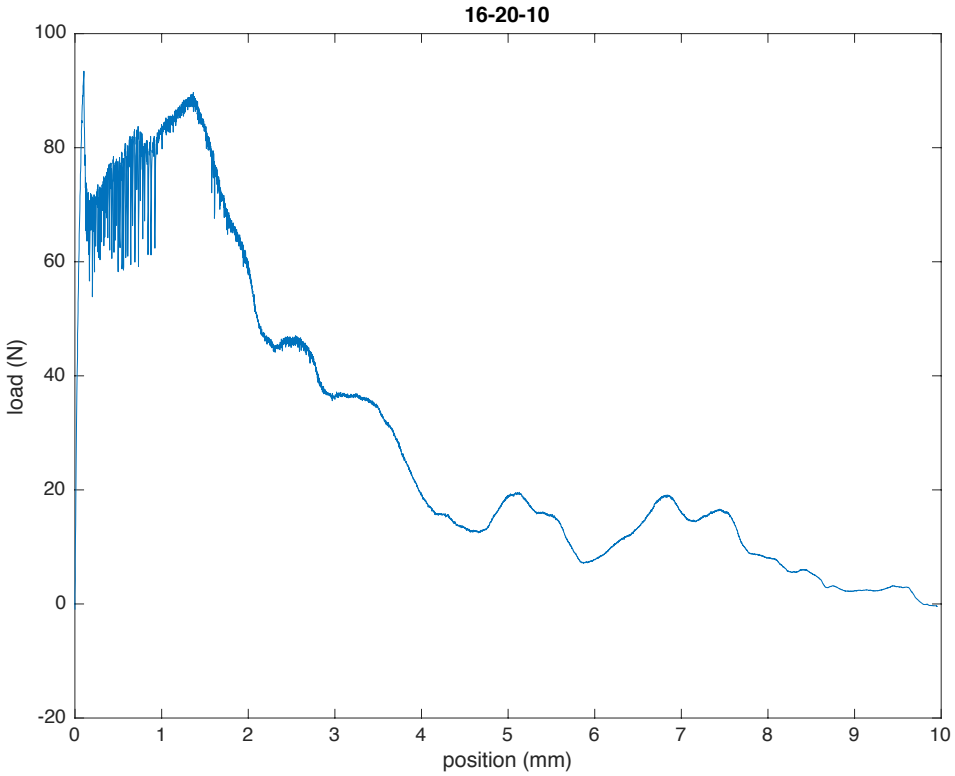

Figure 33. Specimen 16-20-10

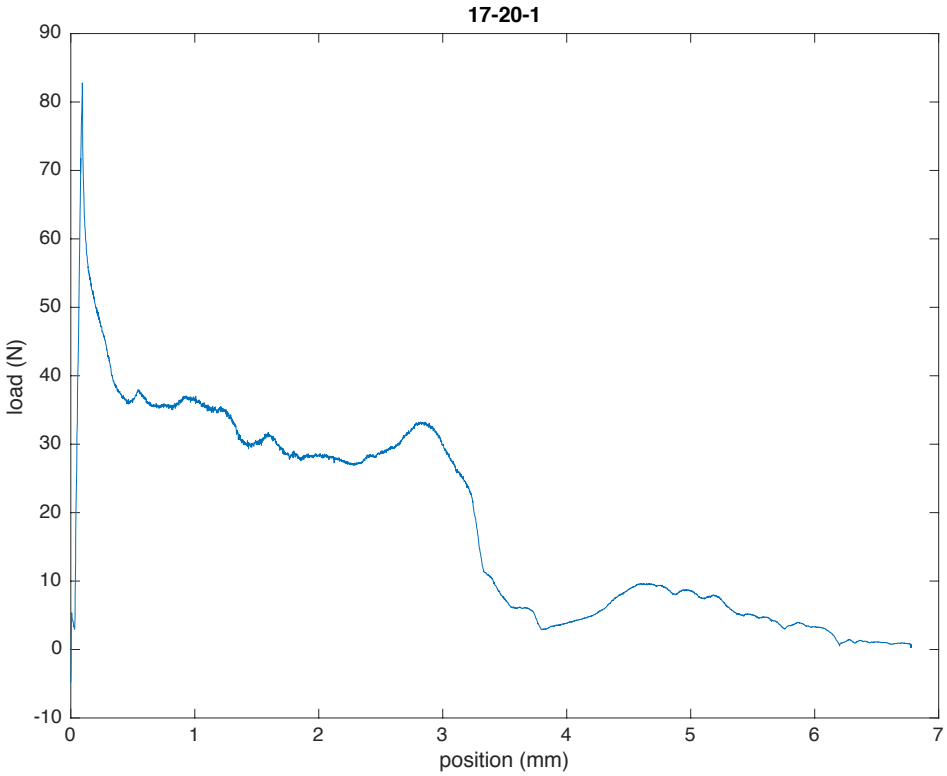

Figure 34. Specimen 17-20-1

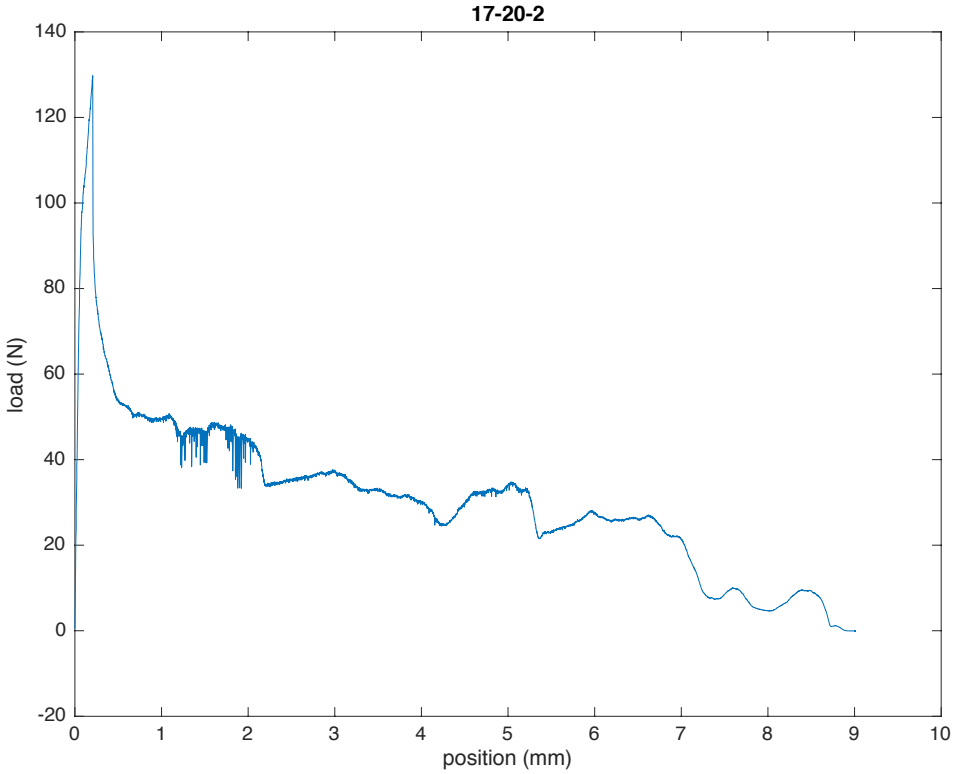

Figure 35. Specimen 17-20-2

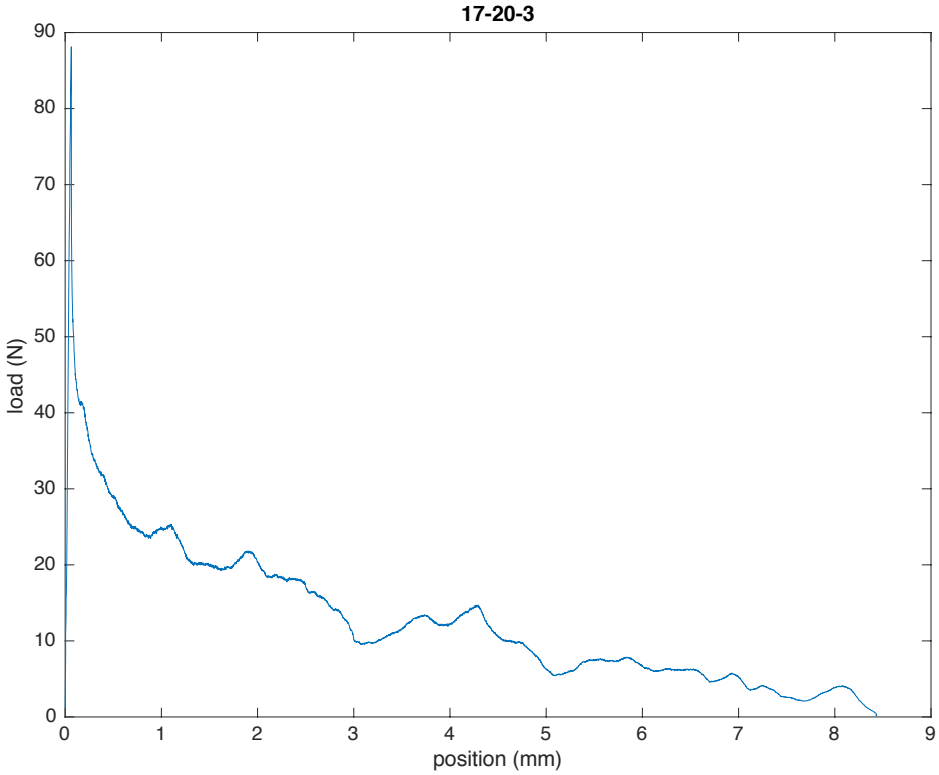

Figure 36. Specimen 17-20-3

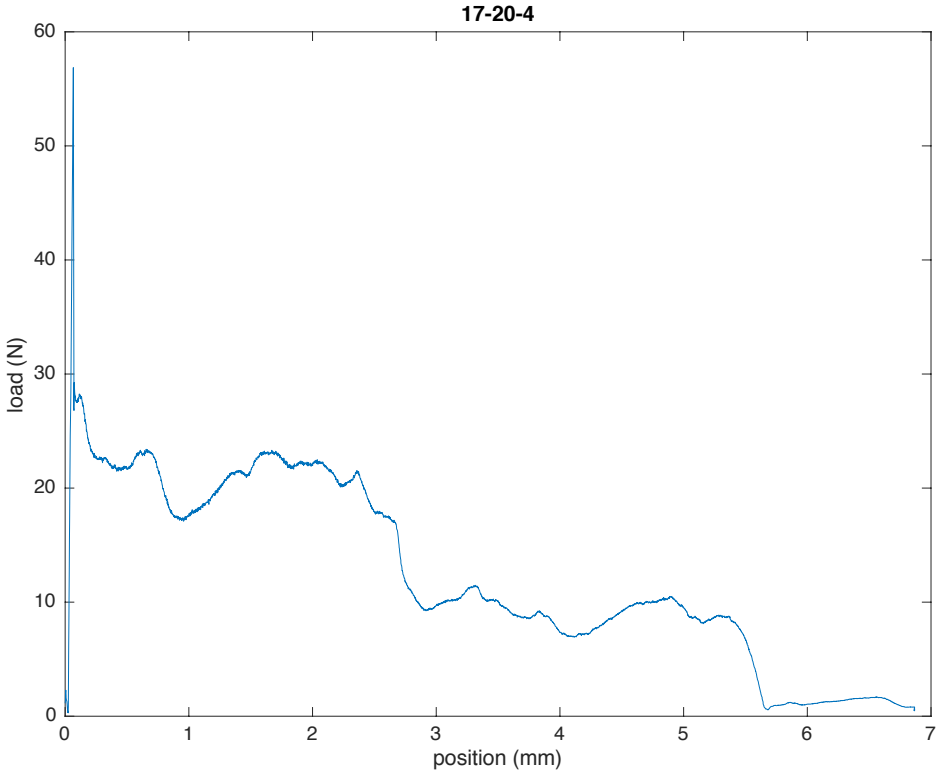

Figure 37. Specimen 17-20-4

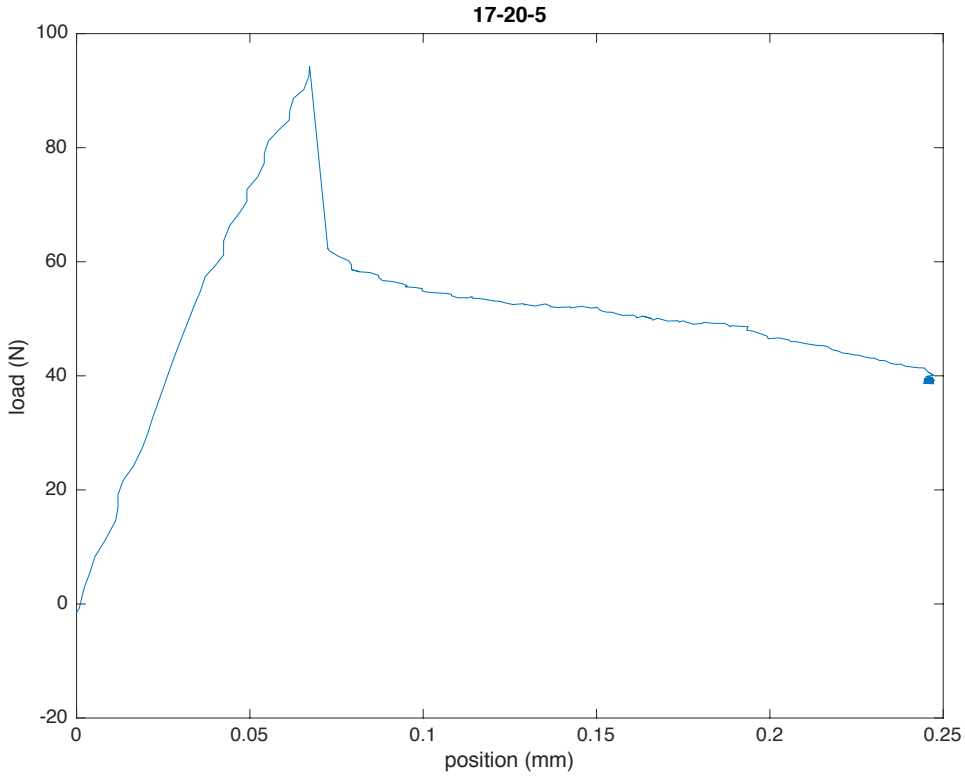

Figure 38. Specimen 17-20-5

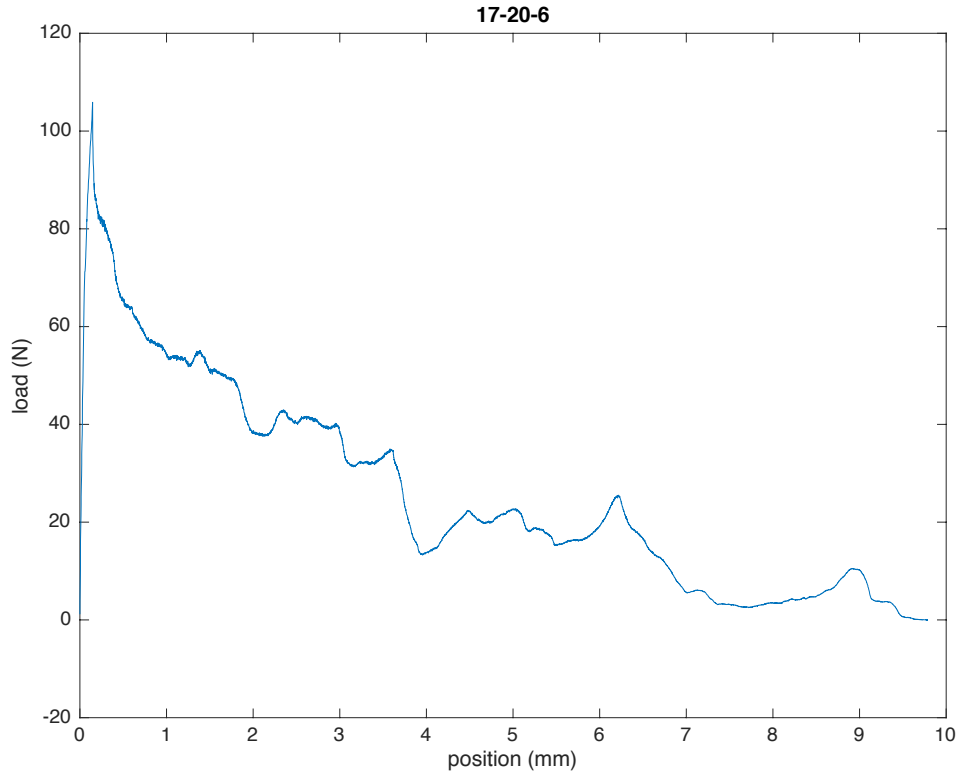

Figure 39. Specimen 17-20-6

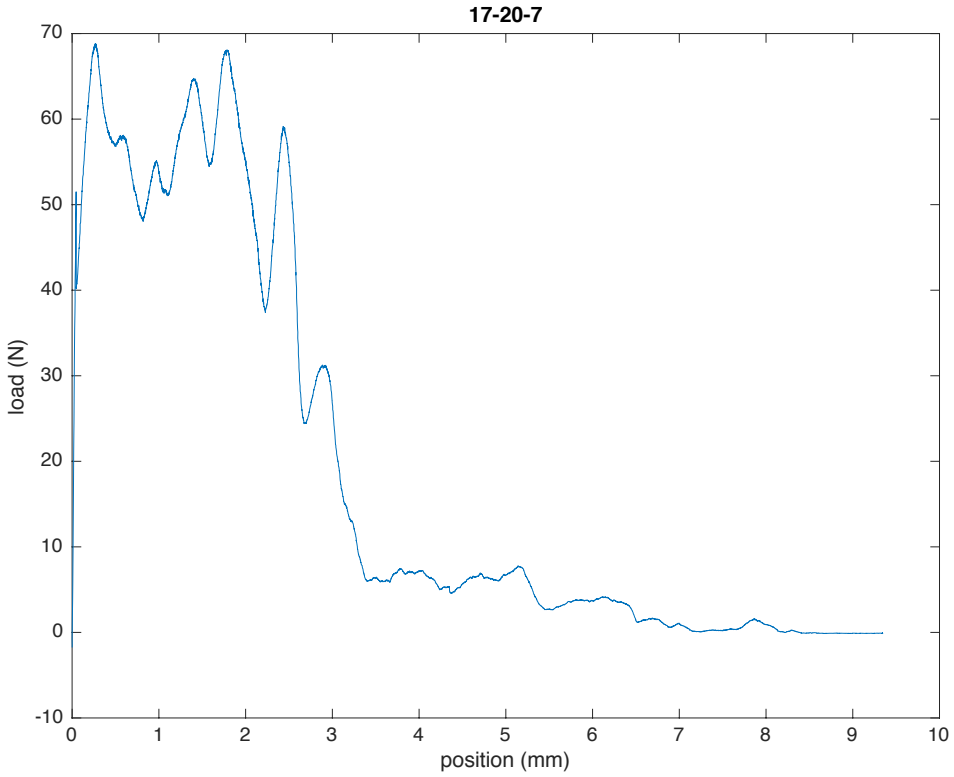

Figure 40. Specimen 17-20-7

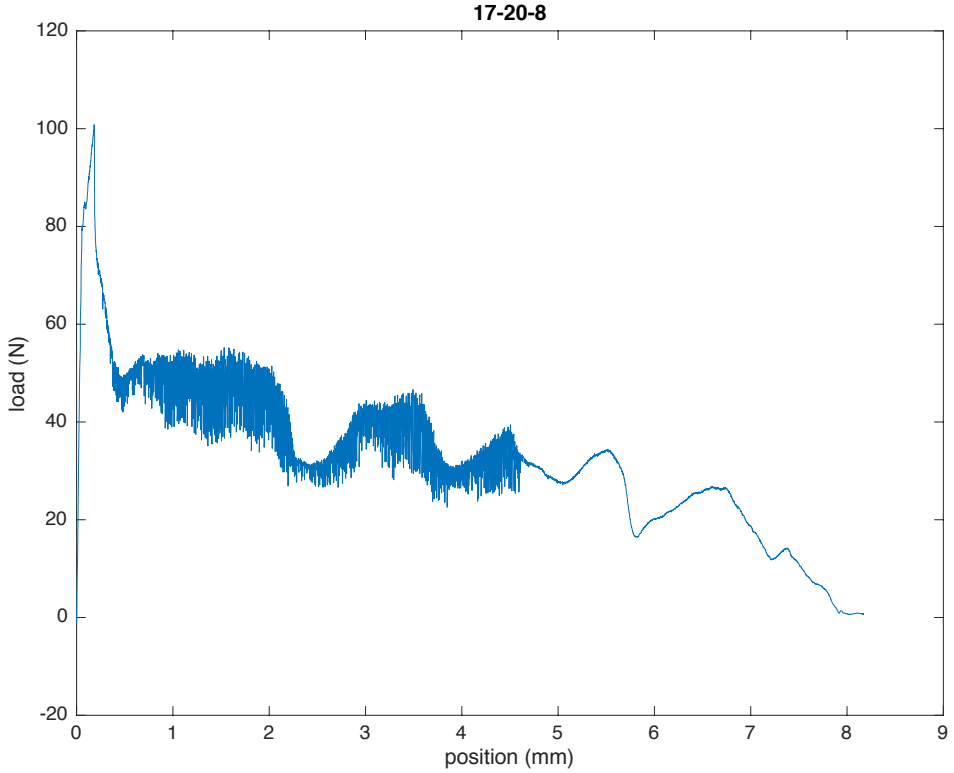

Figure 41. Specimen 17-20-8

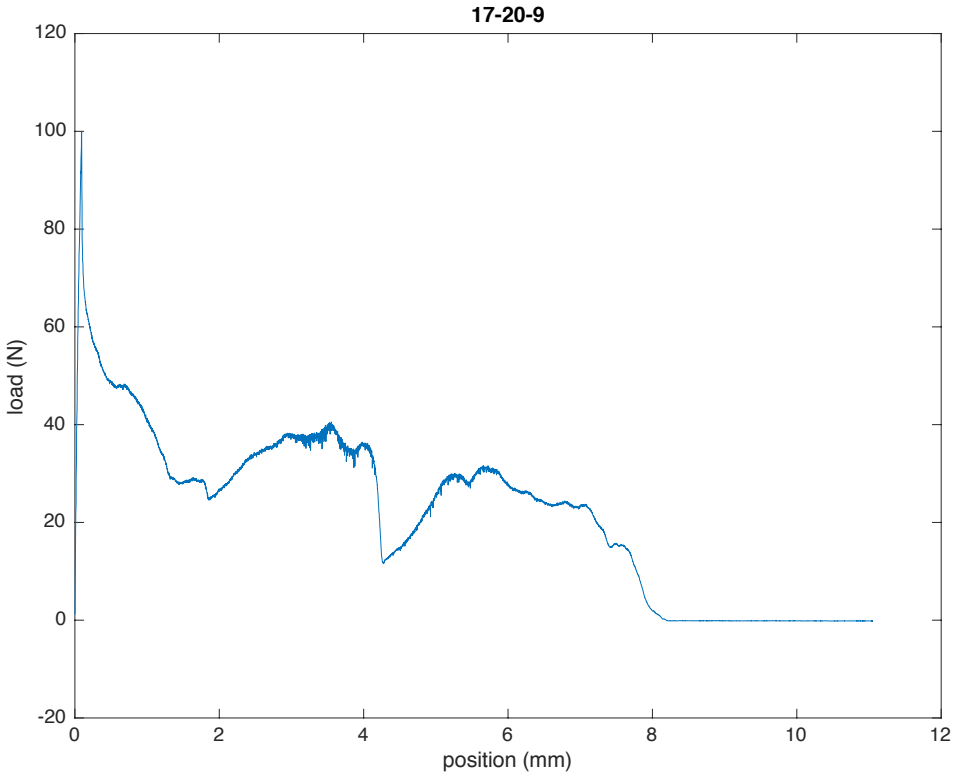

Figure 42. Specimen 17-20-9

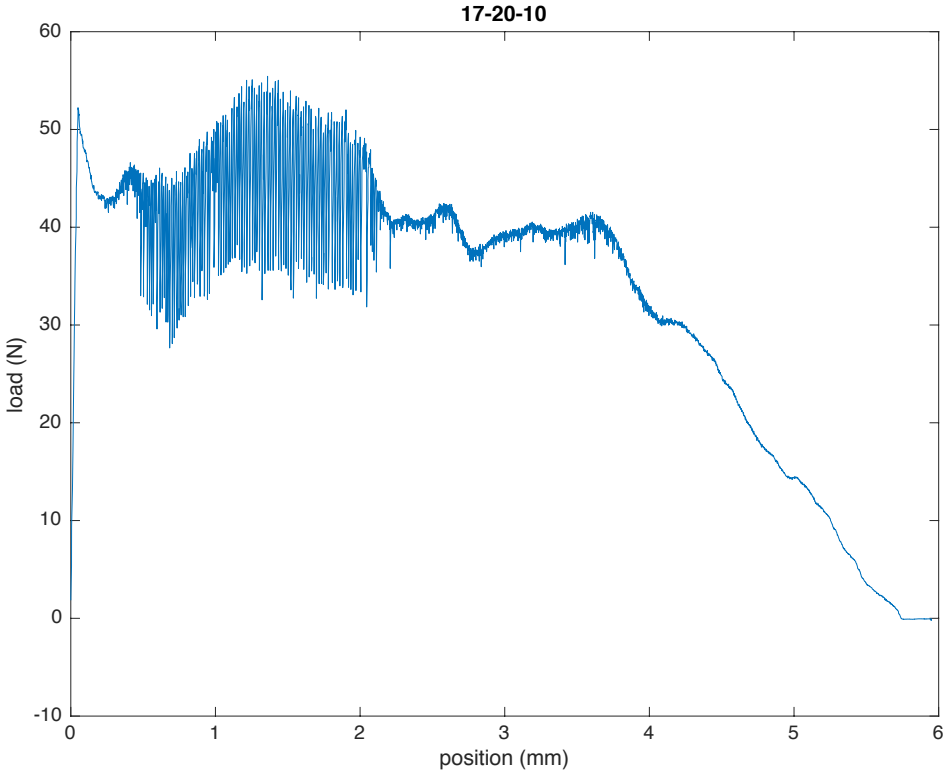

Figure 43. Specimen 17-20-10

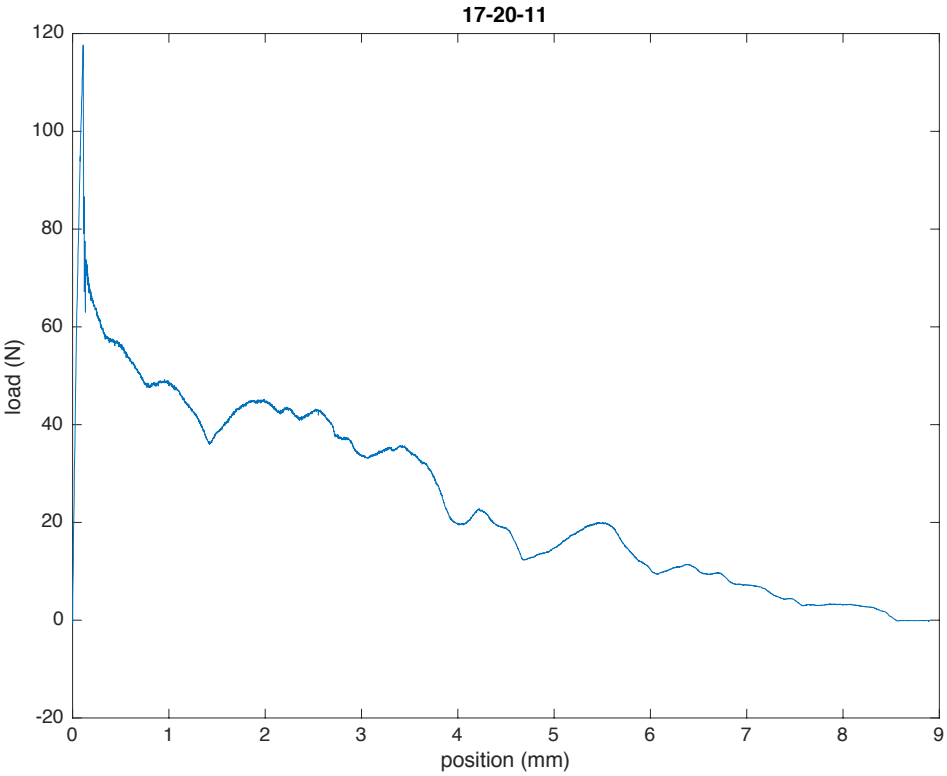

Figure 44. Specimen 17-20-11

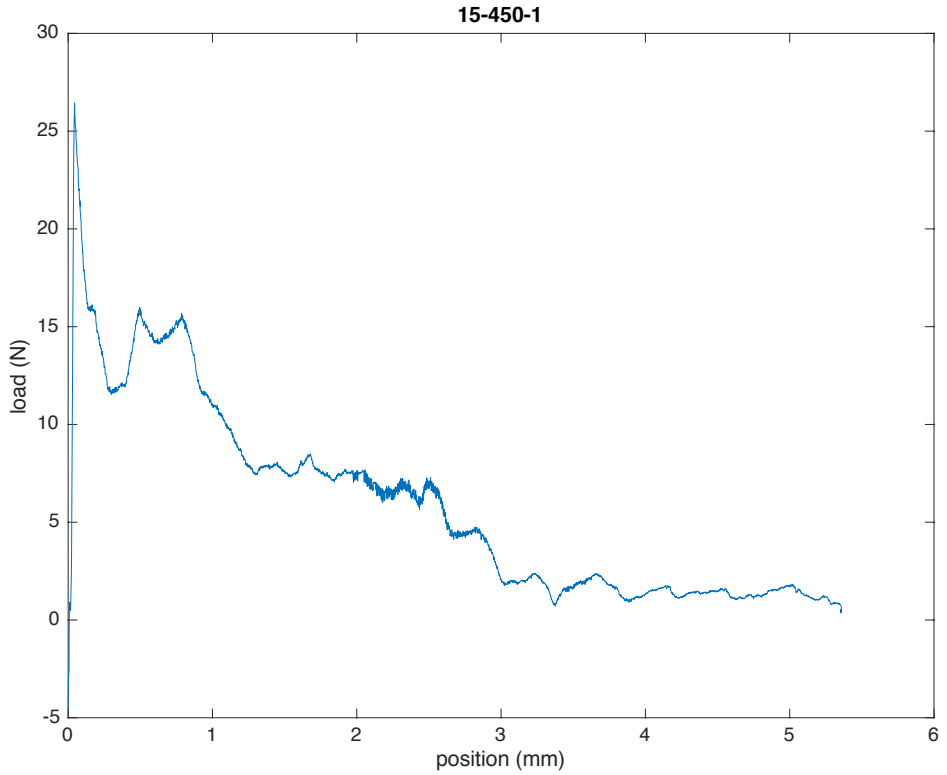

Figure 45. Specimen 15-450-1

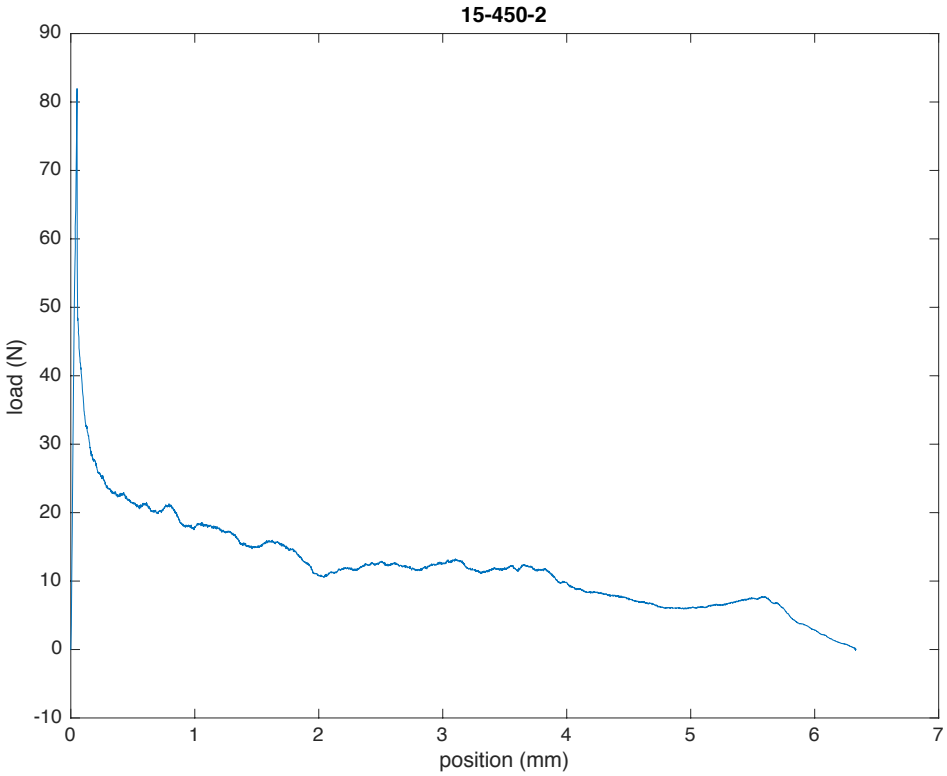

Figure 46. Specimen 15-450-2

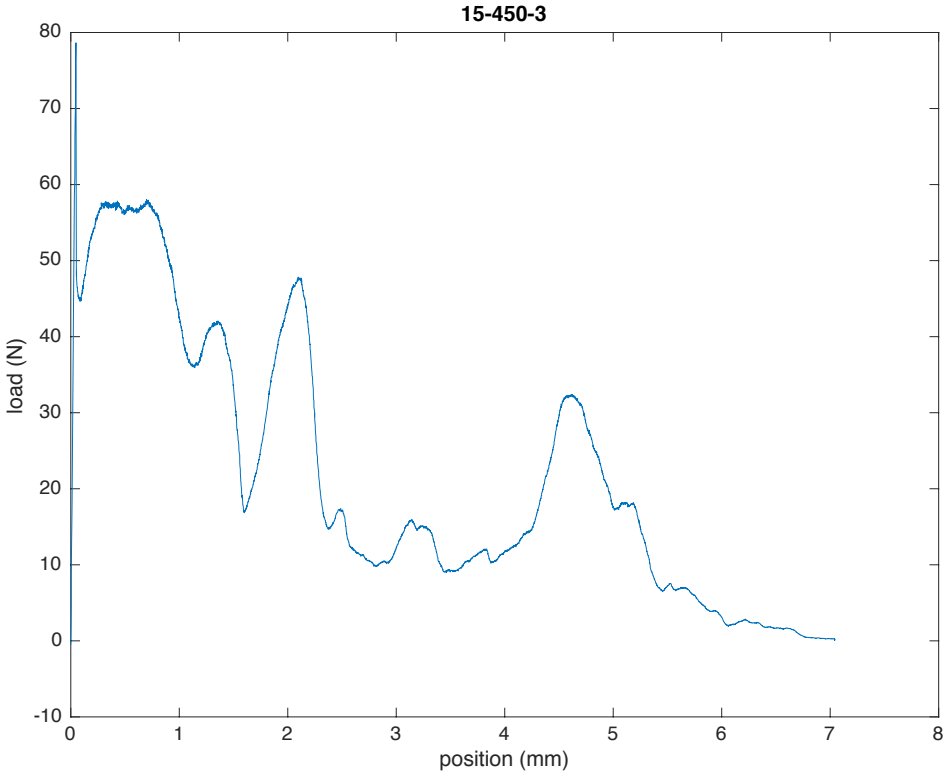

Figure 47. Specimen 15-450-3

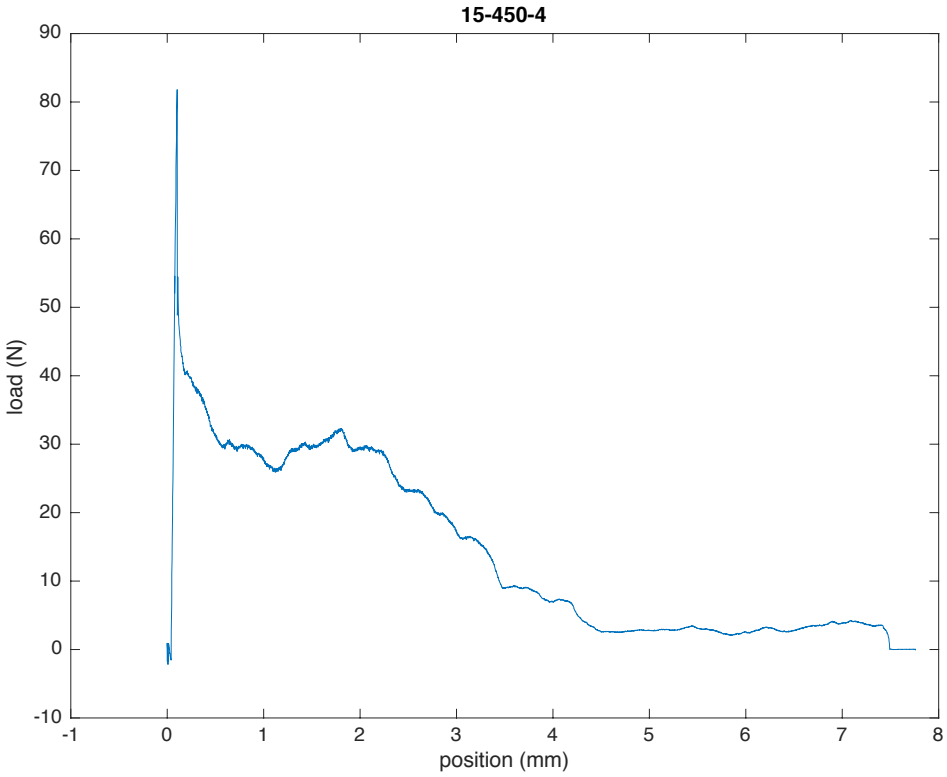

Figure 48. Specimen 15-450-4

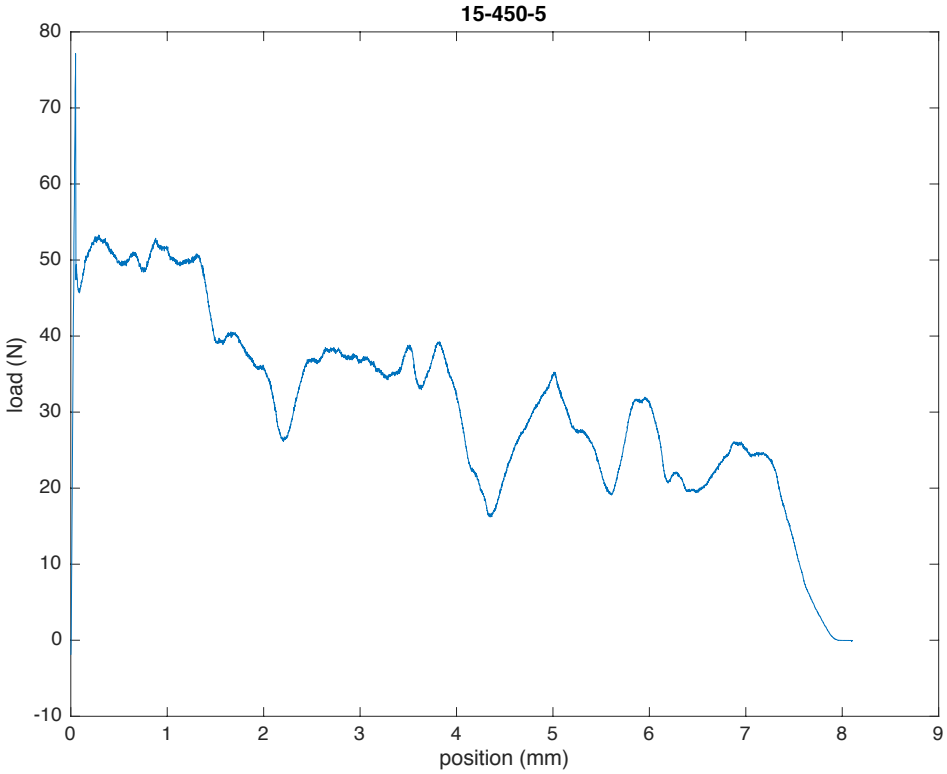

Figure 49. Specimen 15-450-5

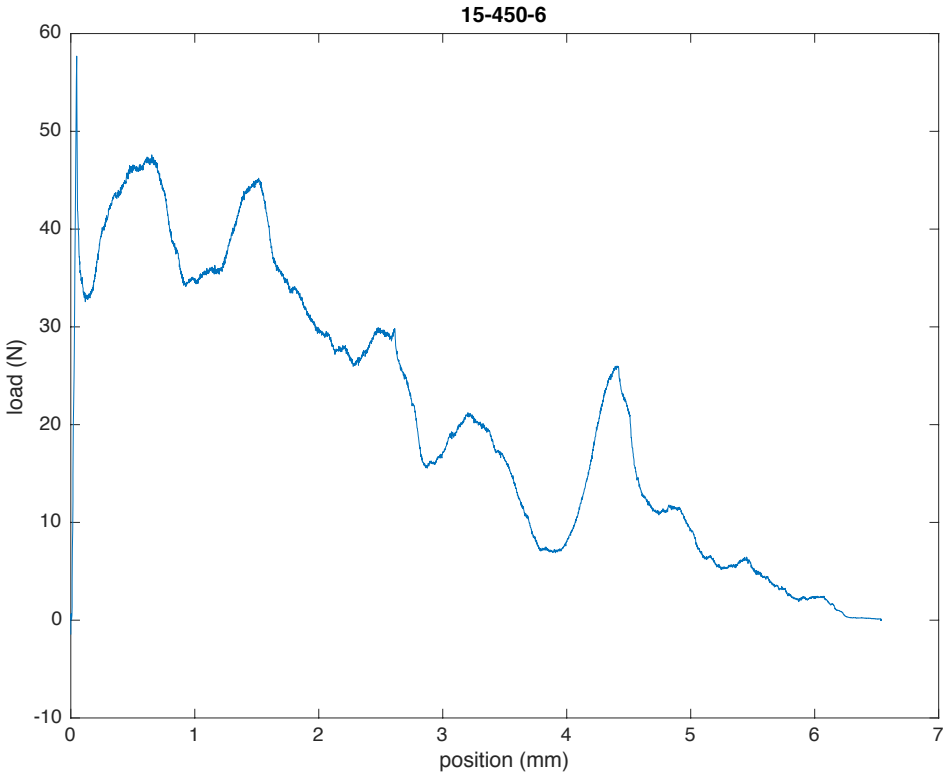

Figure 50. Specimen 15-450-6

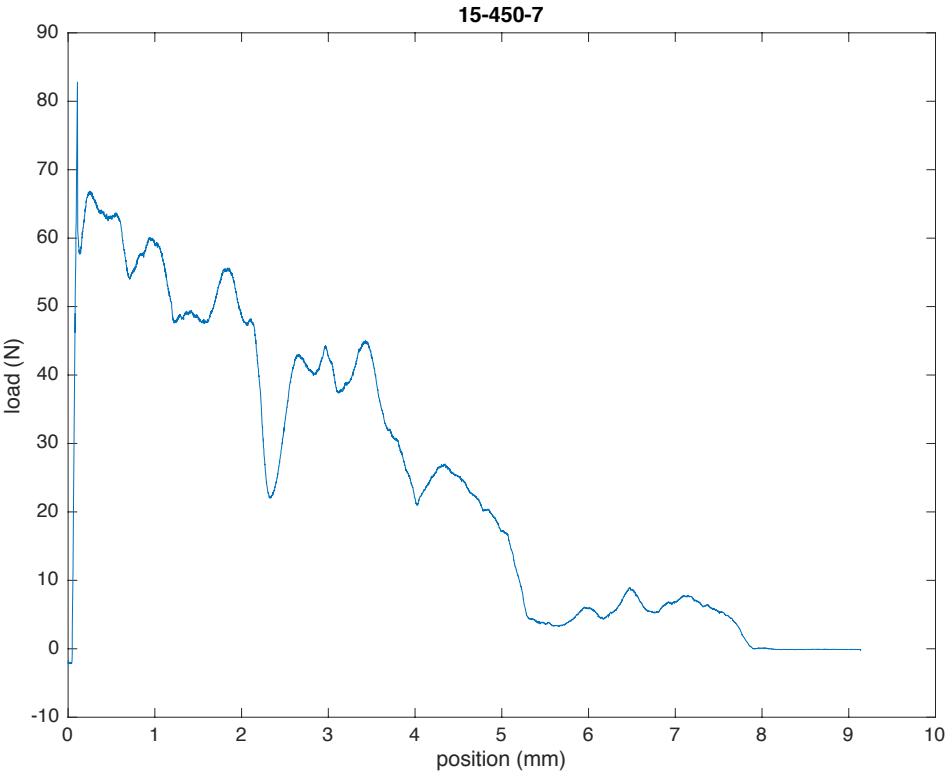

Figure 51. Specimen 15-450-7

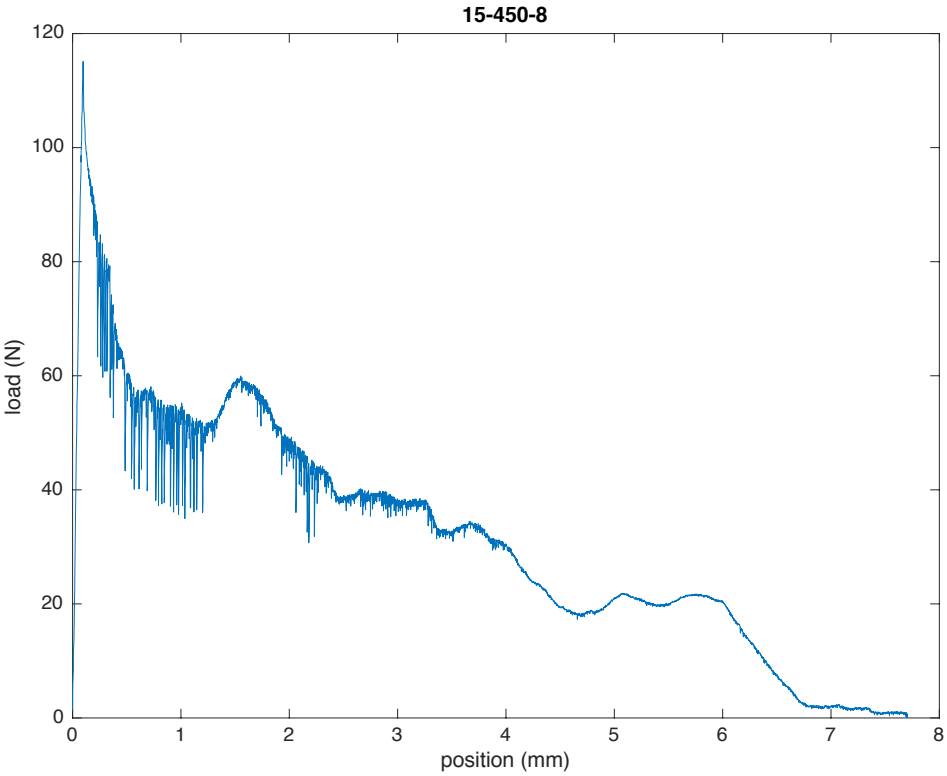

Figure 52. Specimen 15-450-8

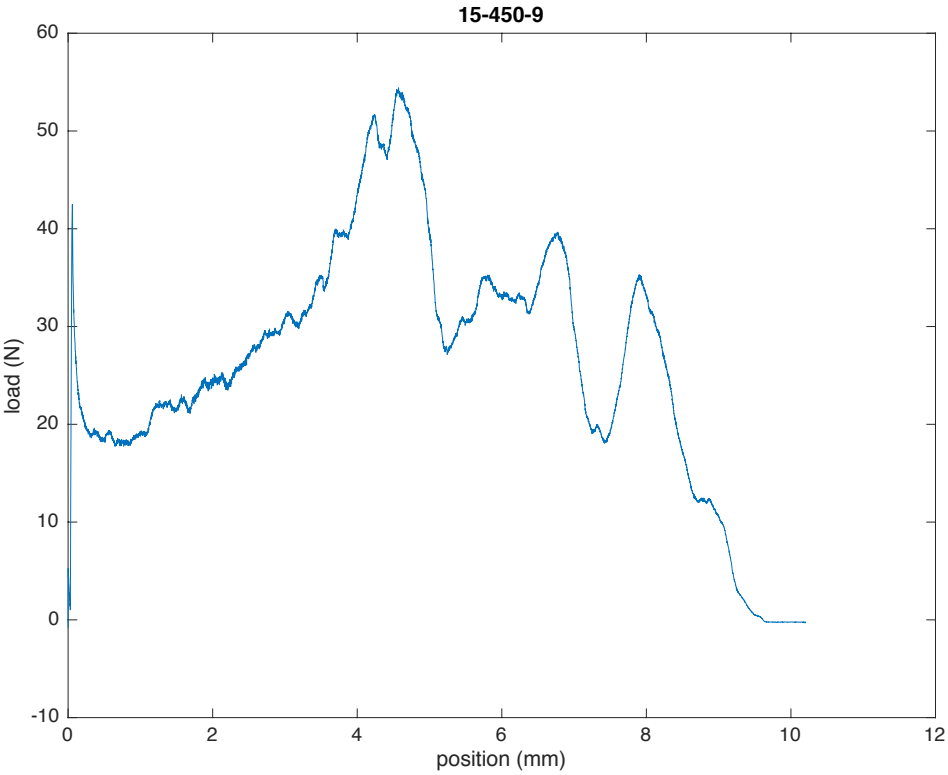

Figure 53. Specimen 15-450-9

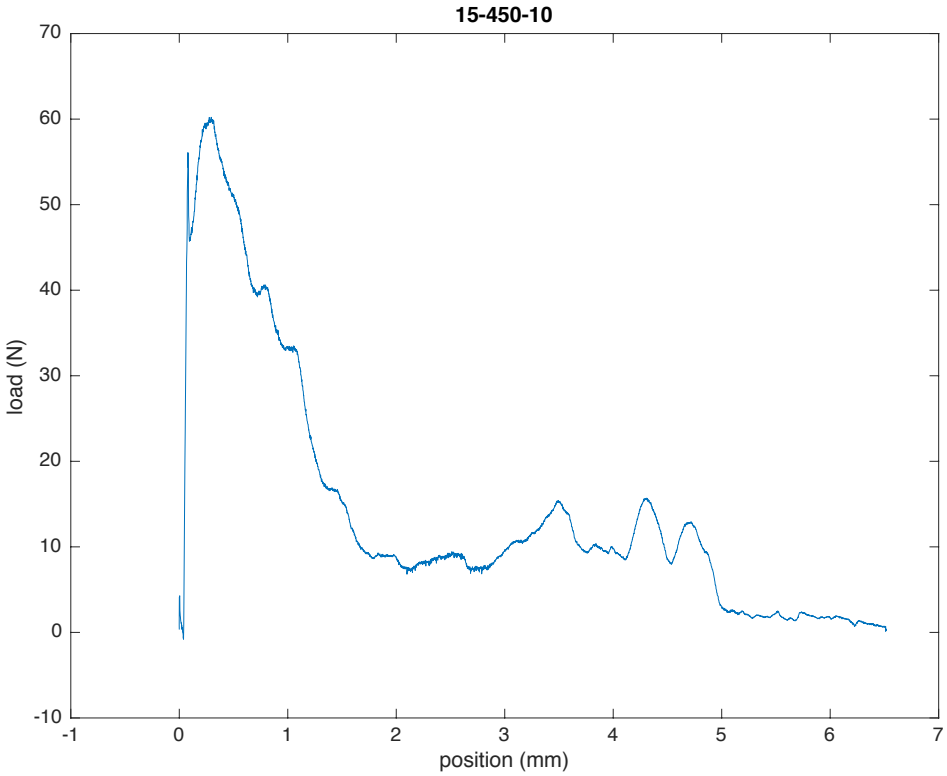

Figure 54. Specimen 15-450-10

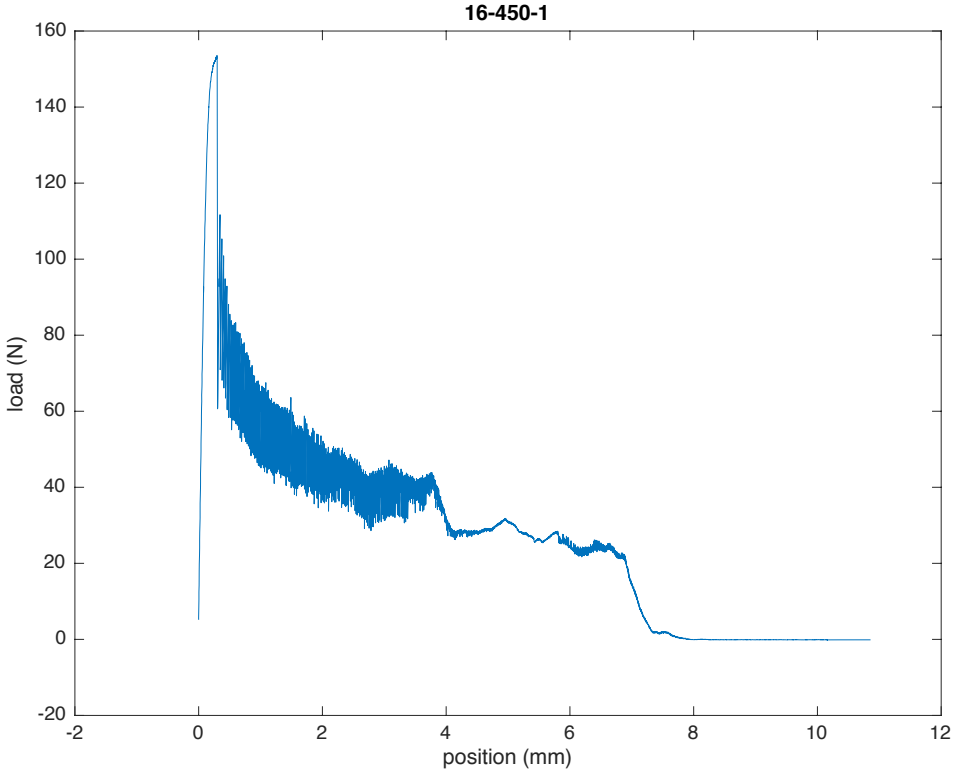

Figure 55. Specimen 16-450-1

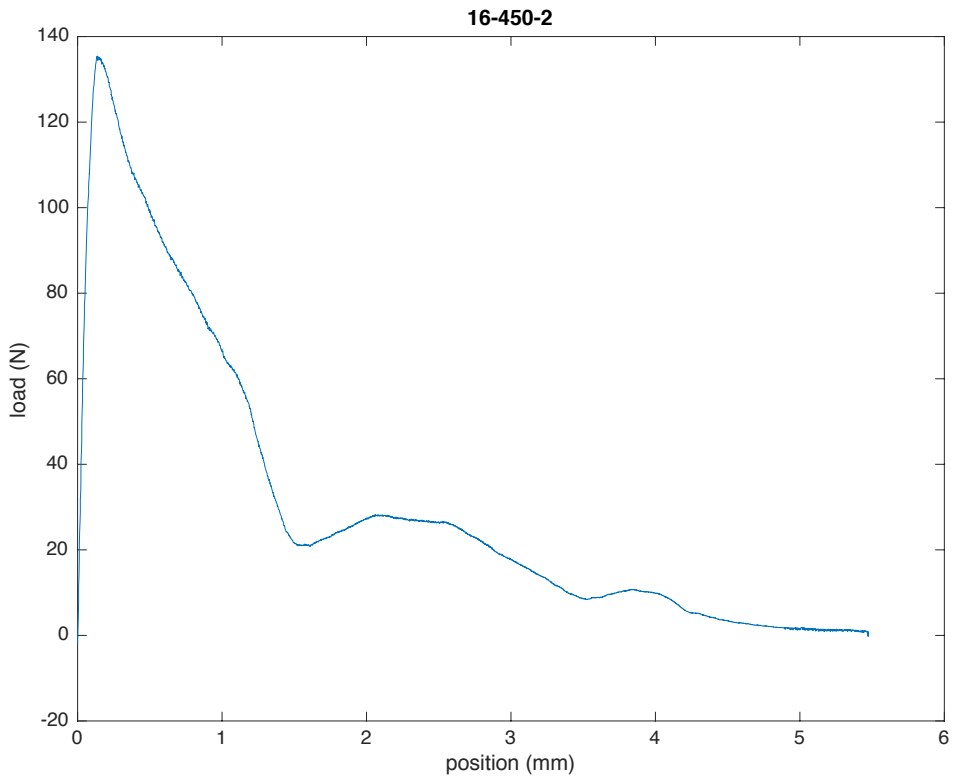

Figure 56. Specimen 16-450-2

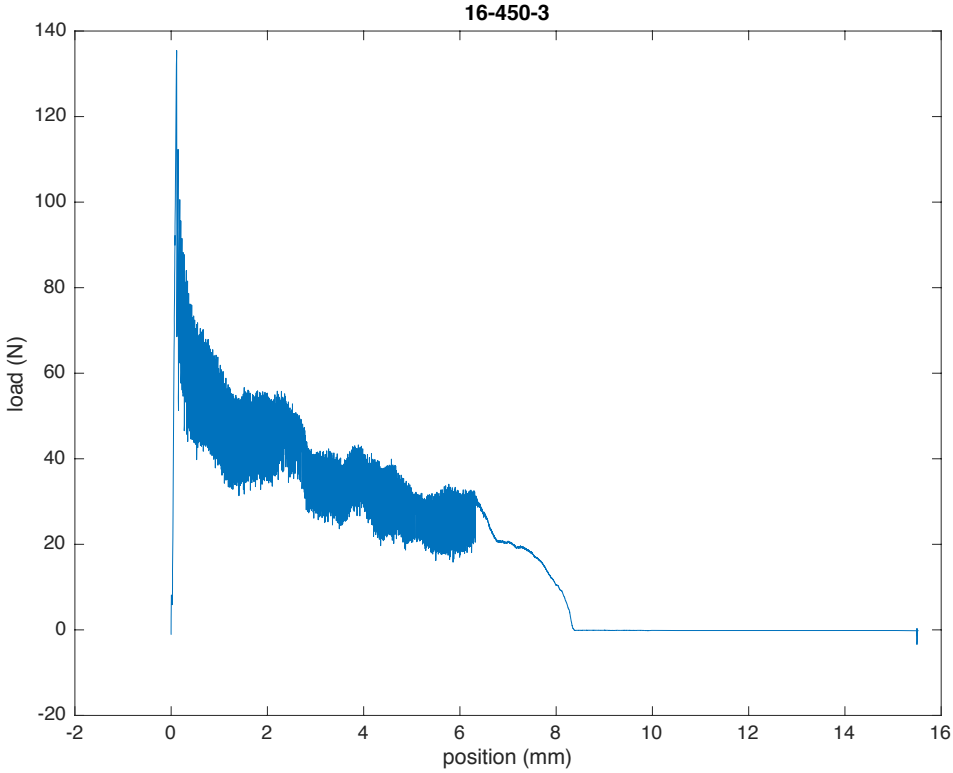

Figure 57. Specimen 16-450-3

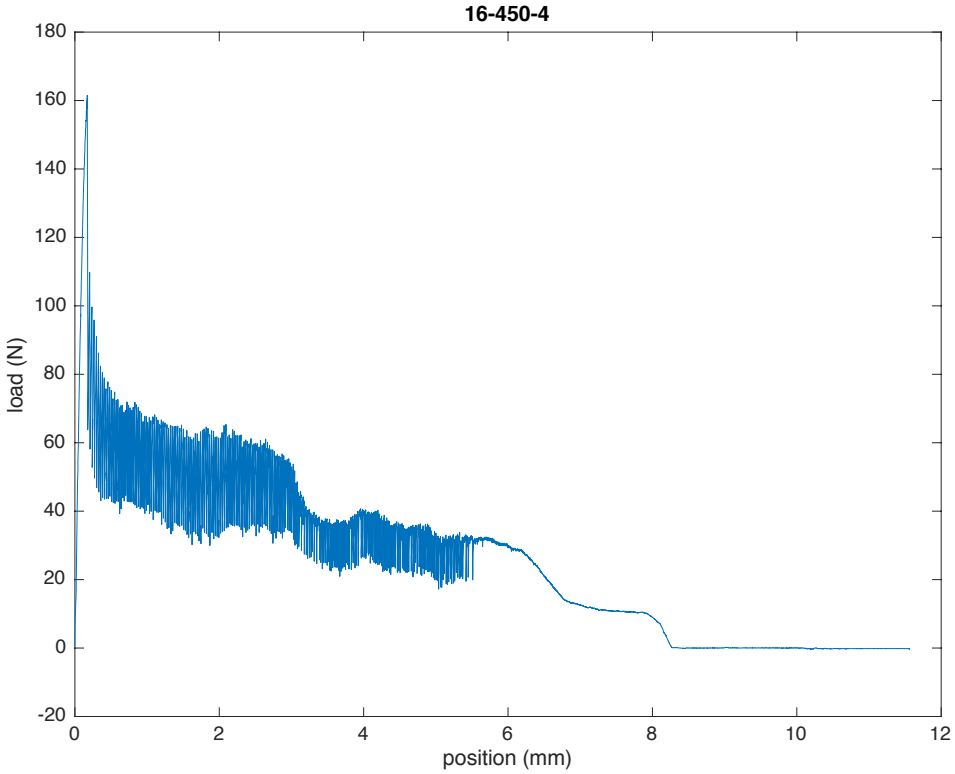

Figure 58. Specimen 16-450-4

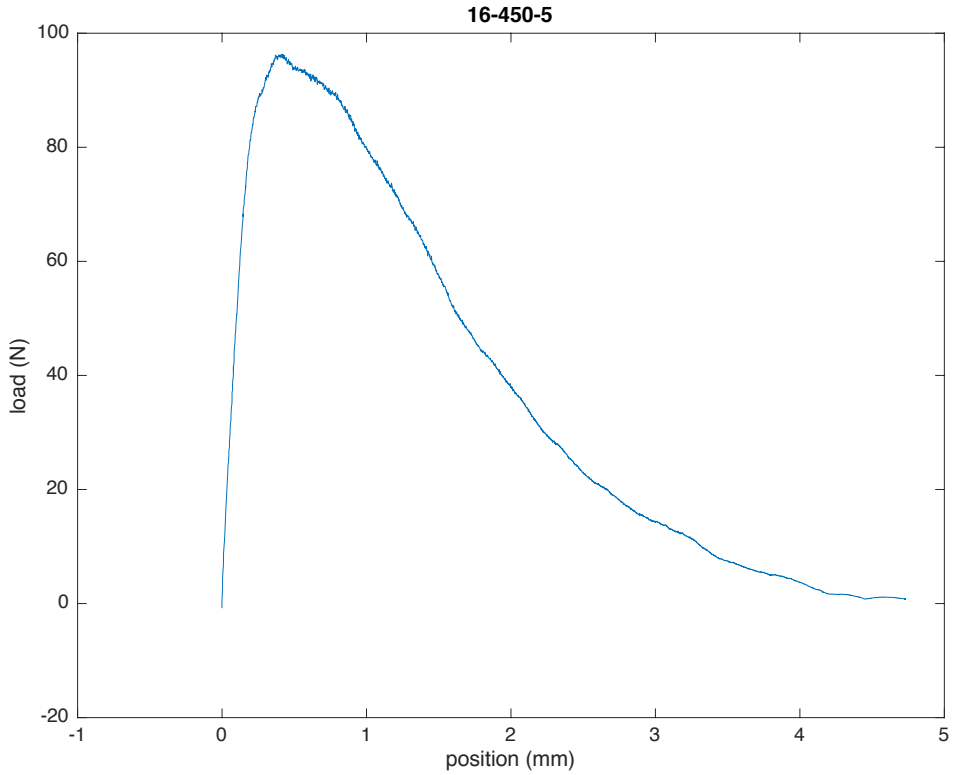

Figure 59. Specimen 16-450-5

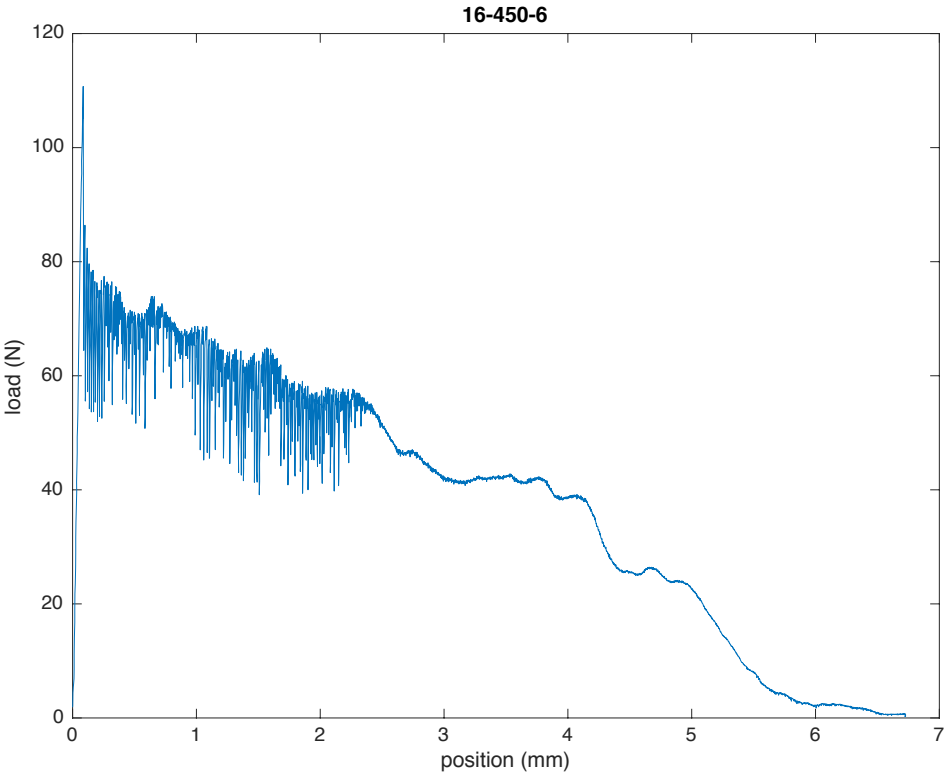

Figure 60. Specimen 16-450-6

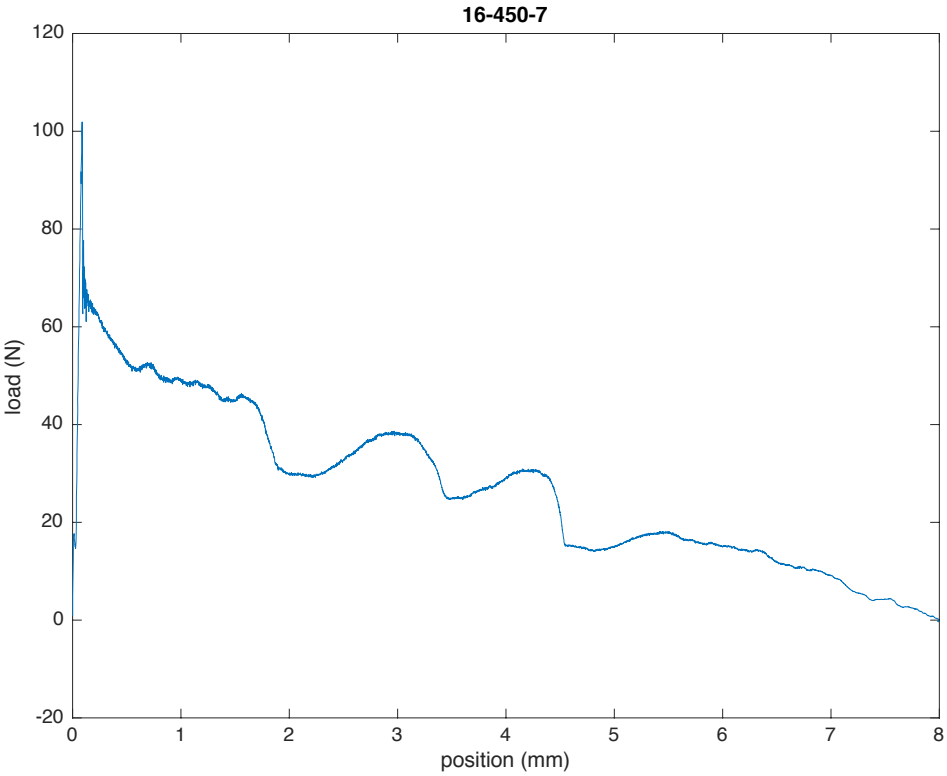

Figure 61. Specimen 16-450-7

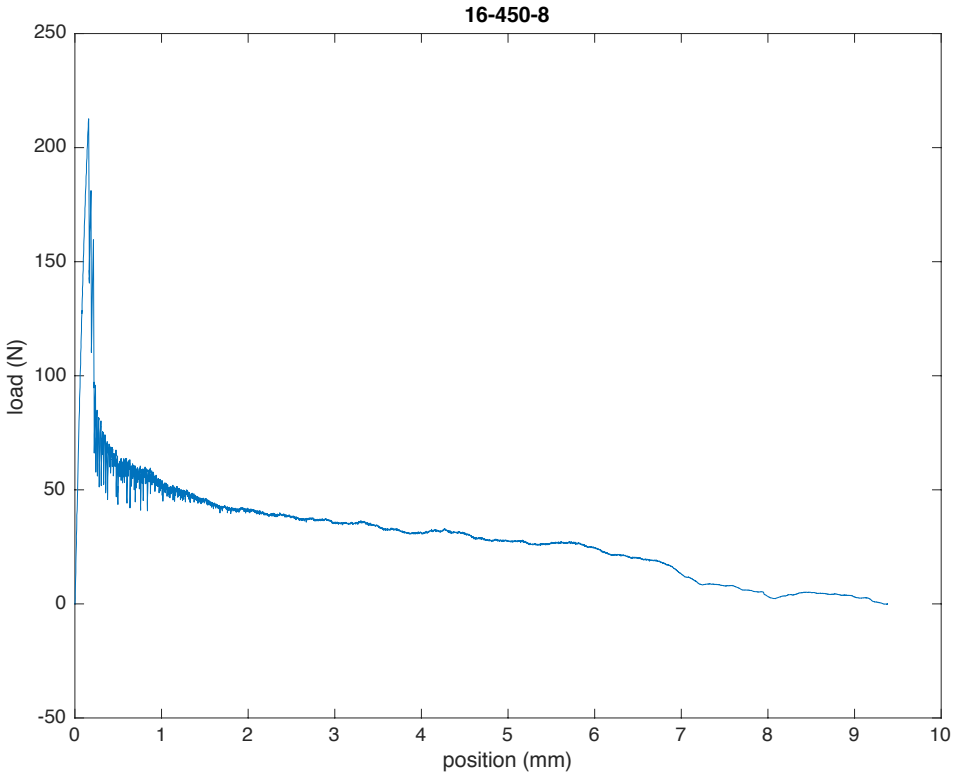

Figure 62. Specimen 16-450-8

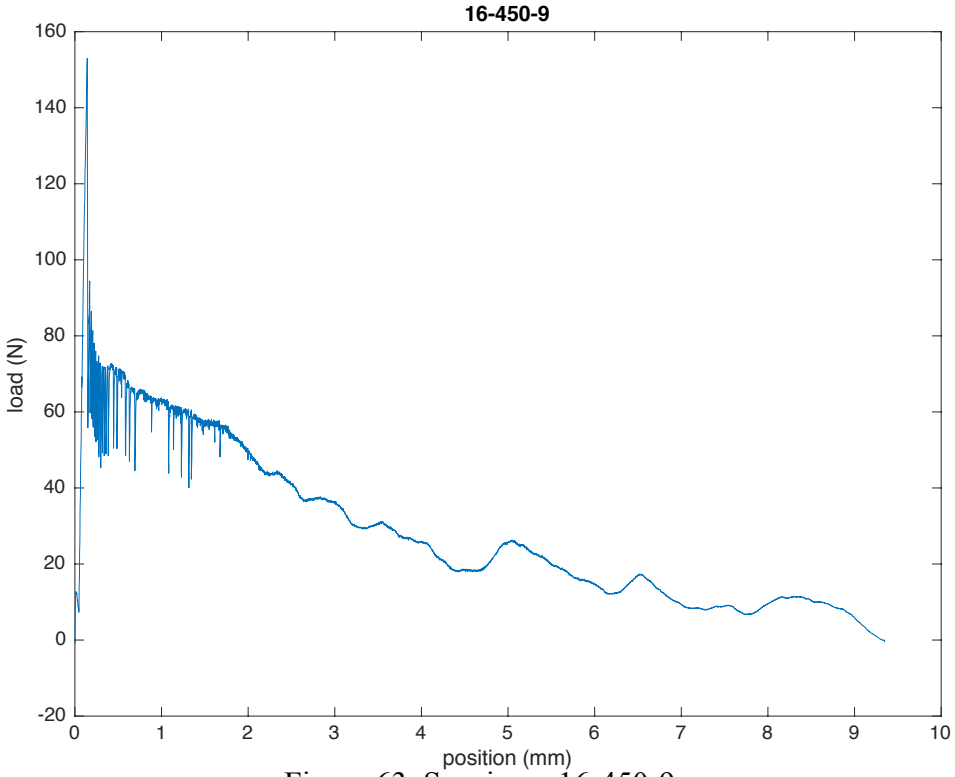

Figure 63. Specimen 16-450-9

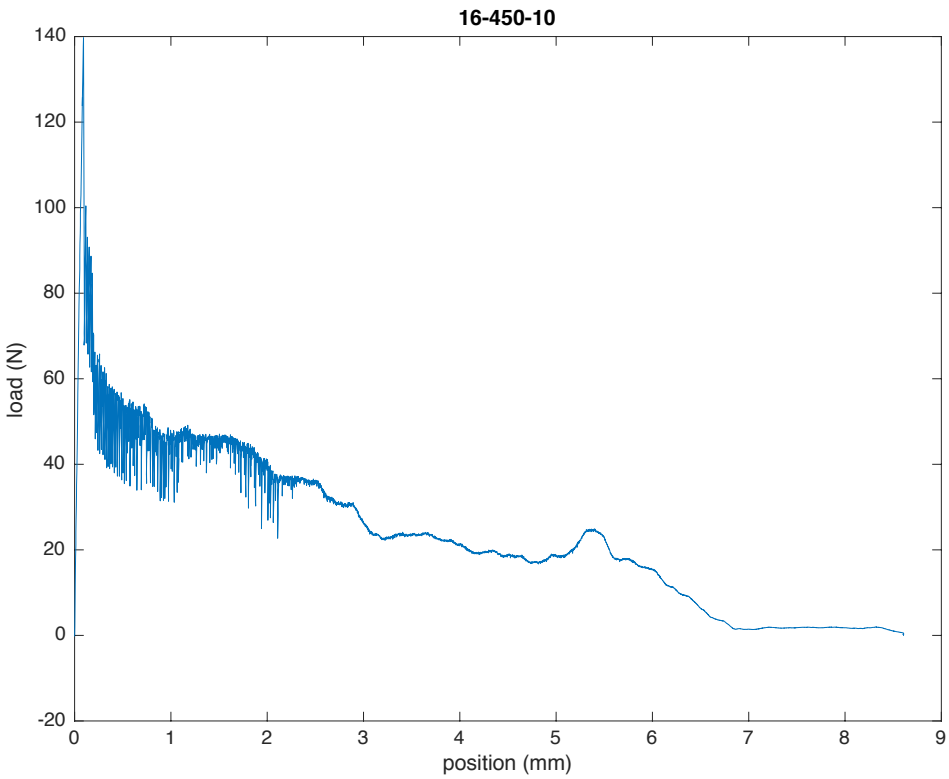

Figure 64. Specimen 16-450-10

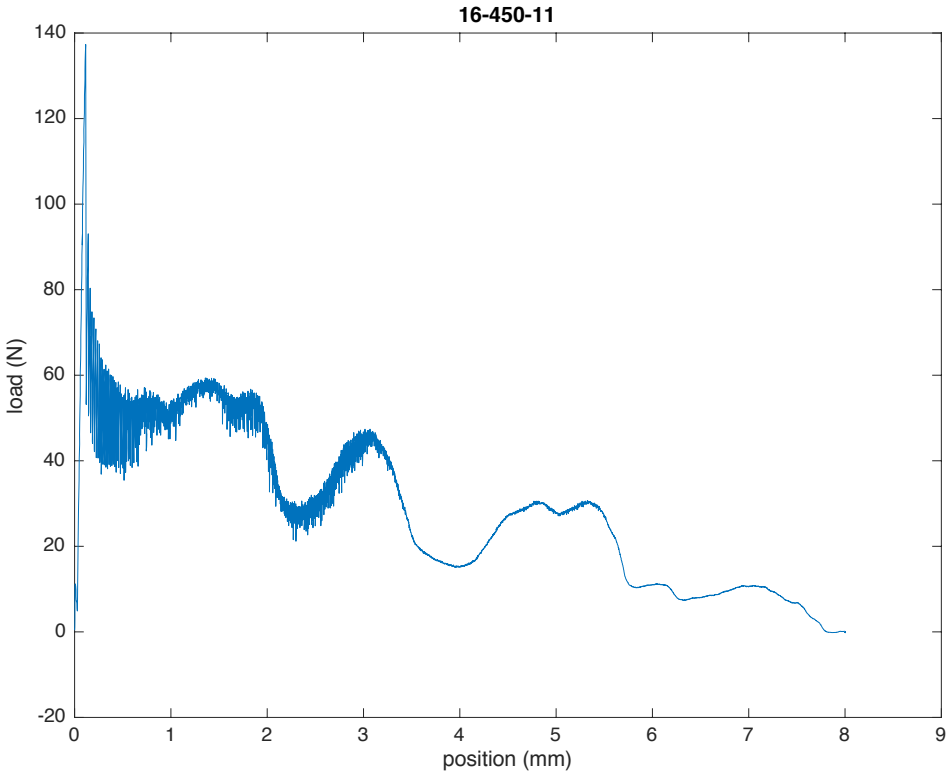

Figure 65. Specimen 16-450-11

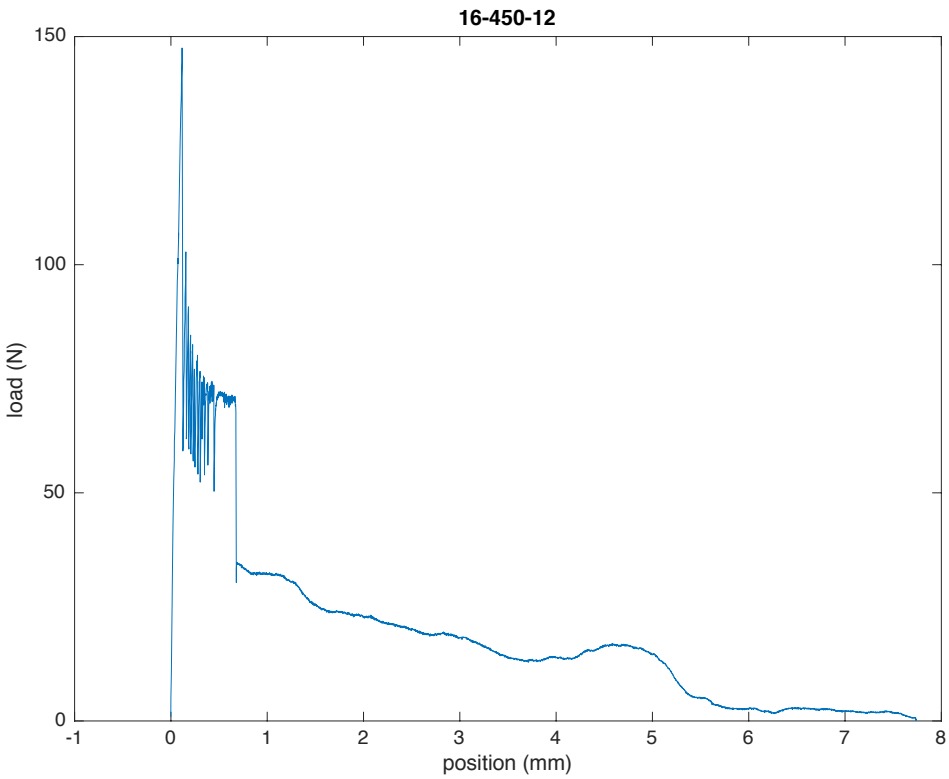

Figure 66. Specimen 16-450-12

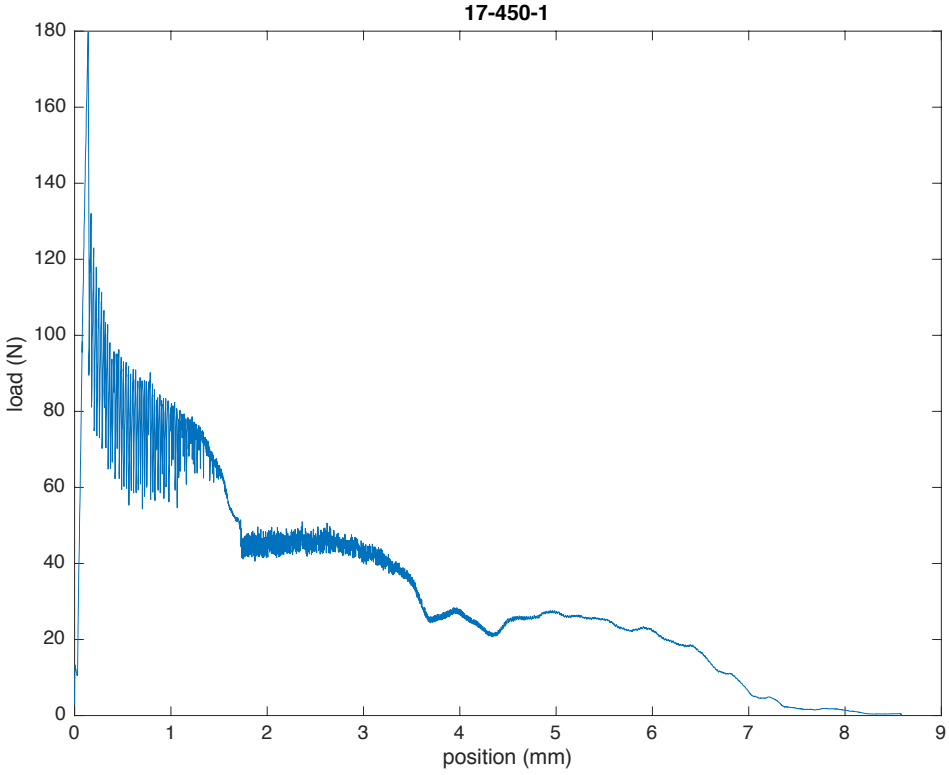

Figure 67. Specimen 17-450-1

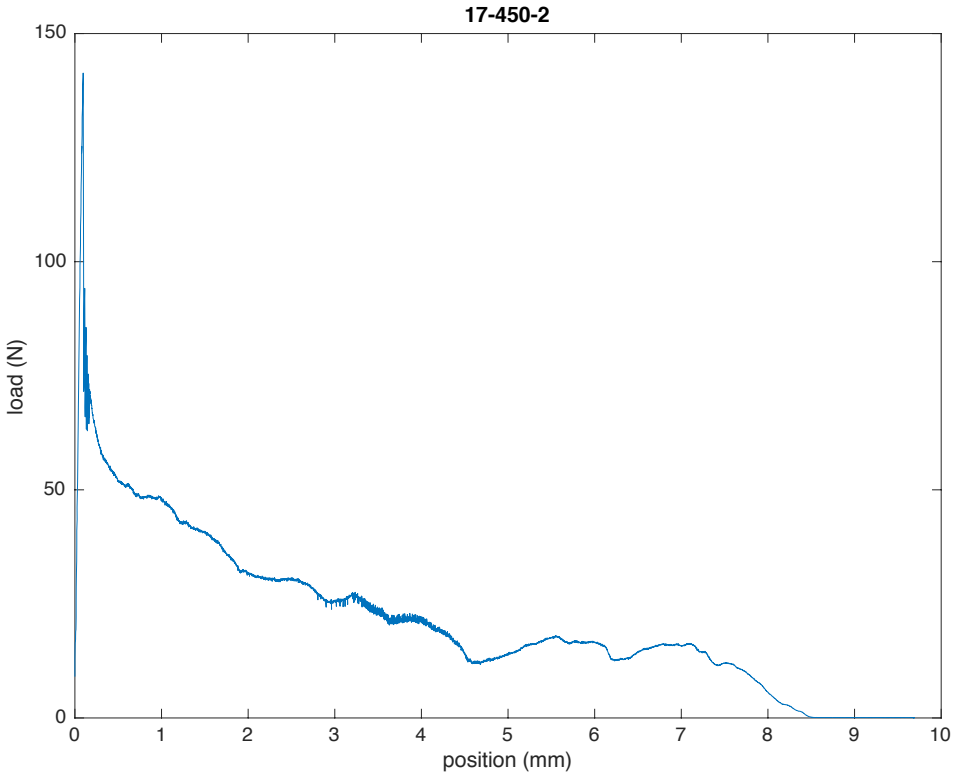

Figure 68. Specimen 17-450-2

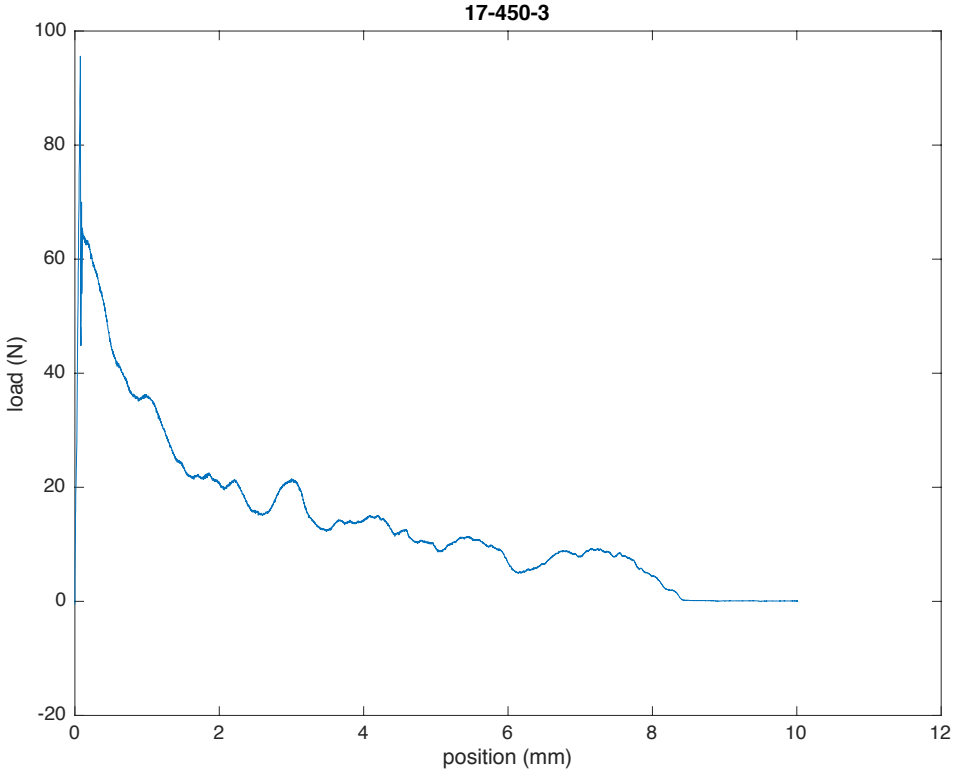

Figure 69. Specimen 17-450-3

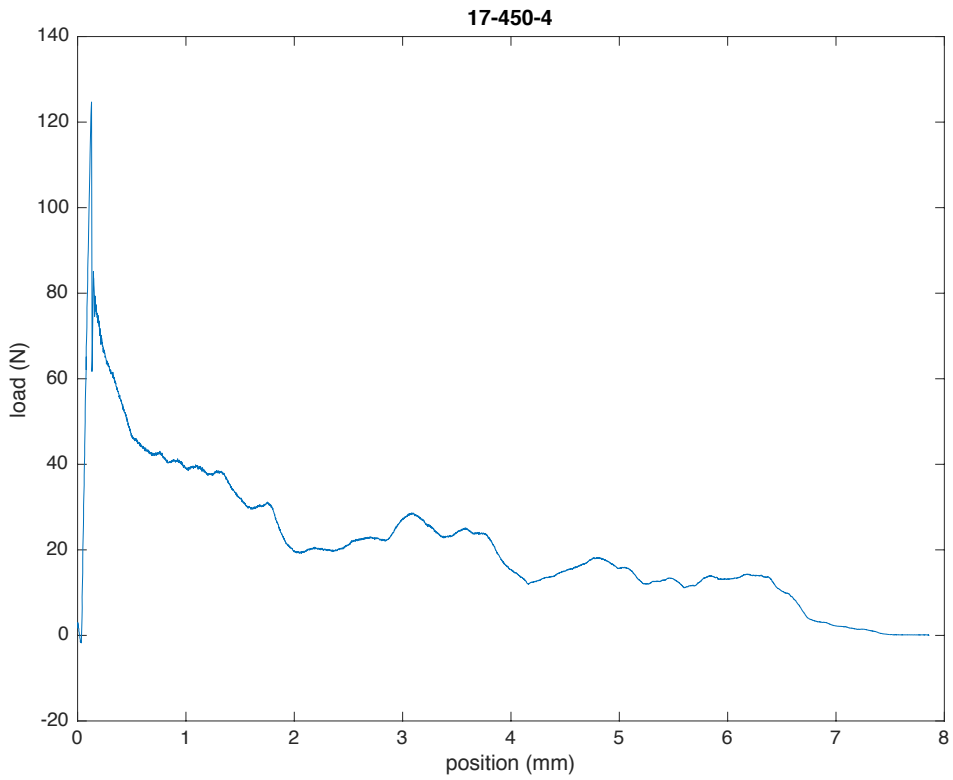

Figure 70. Specimen 17-450-4

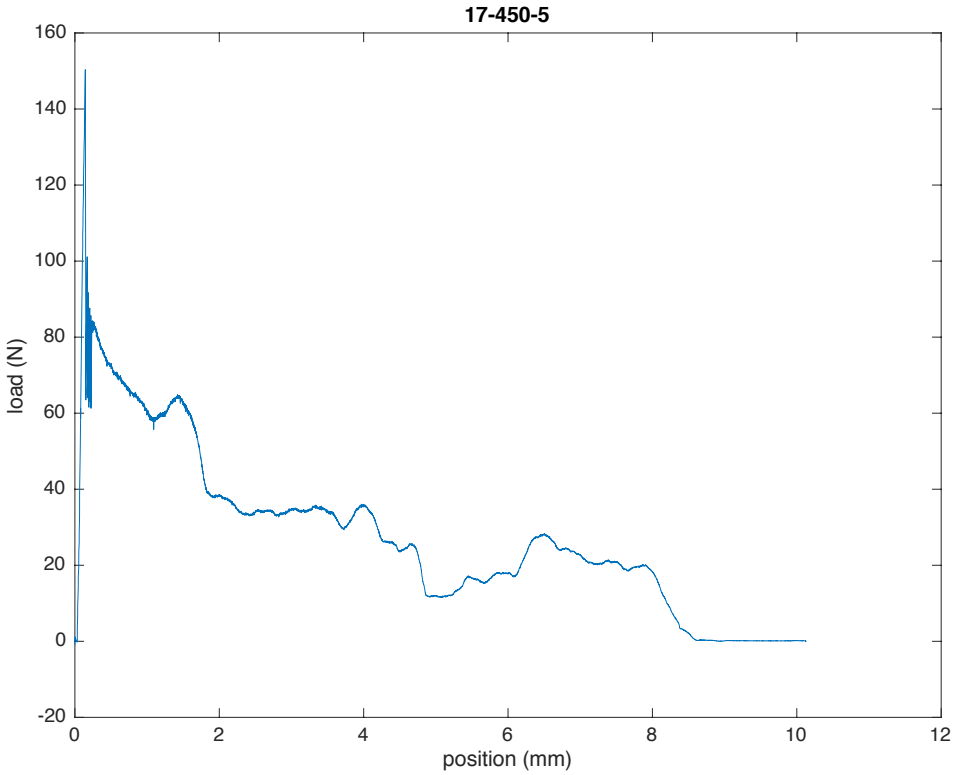

Figure 71. Specimen 17-450-5

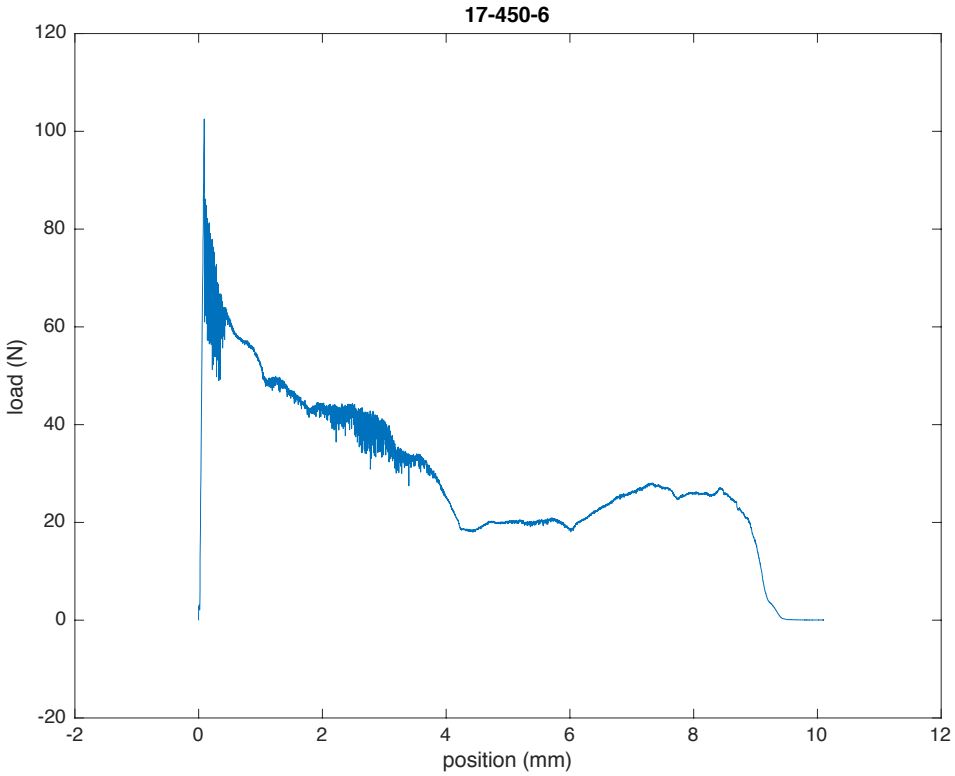

Figure 72. Specimen 17-450-6

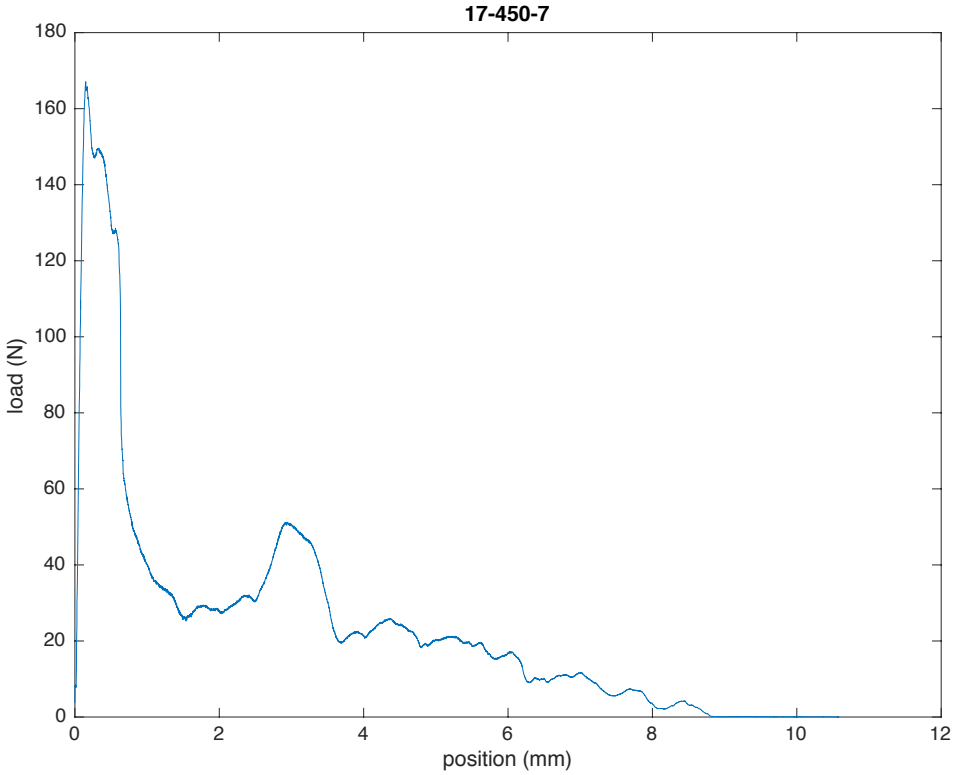

Figure 73. Specimen 17-450-7

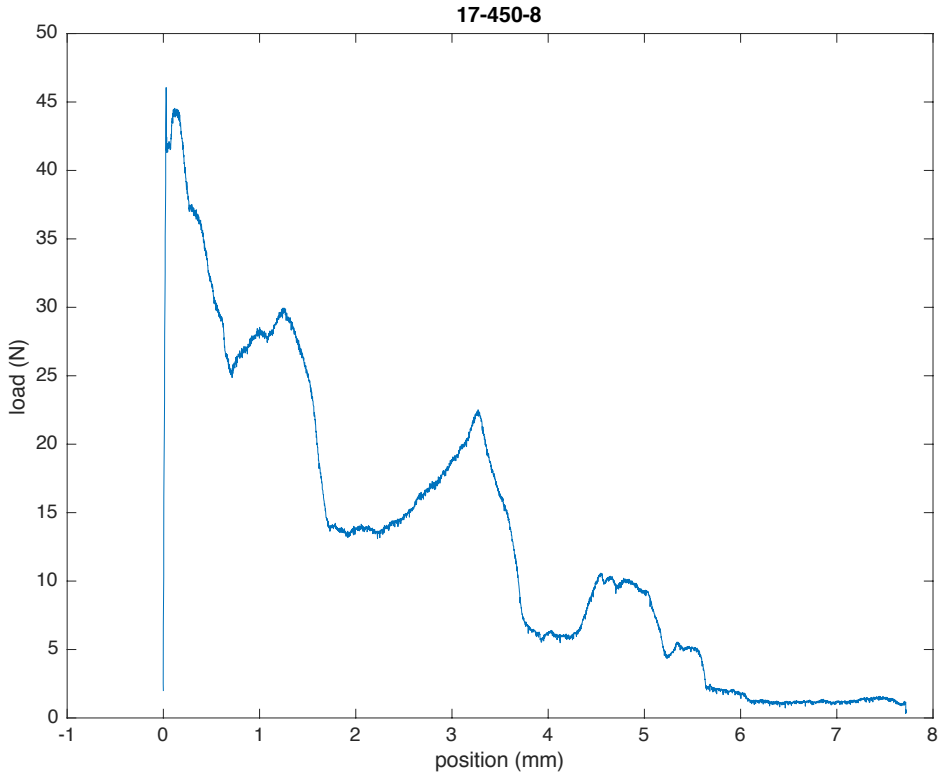

Figure 74. Specimen 17-450-8

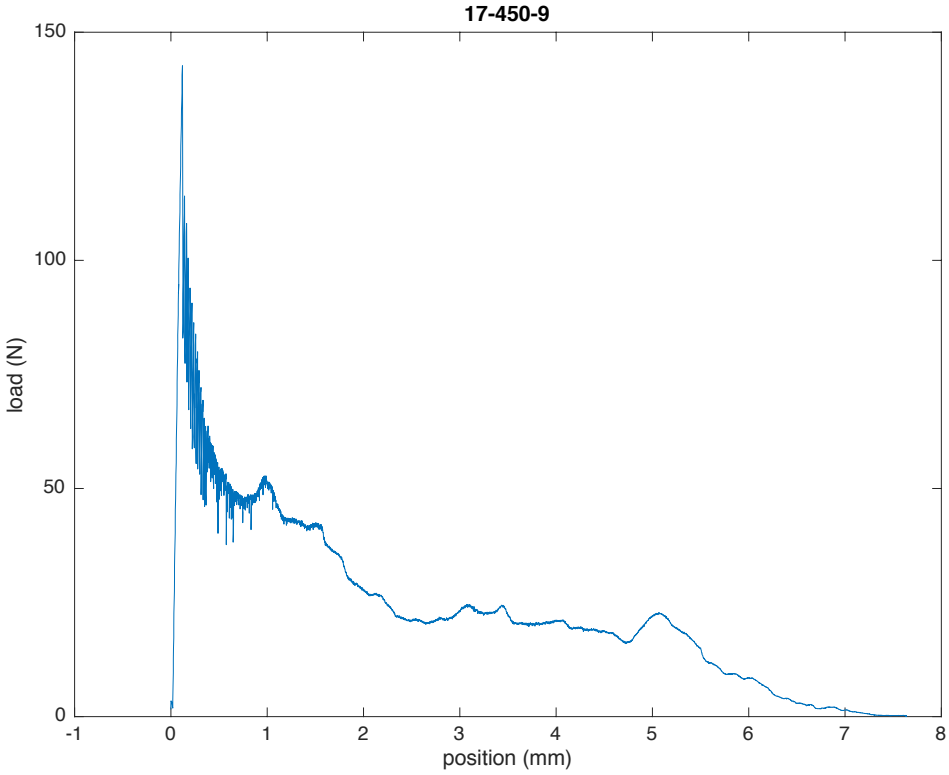

Figure 75. Specimen 17-450-9

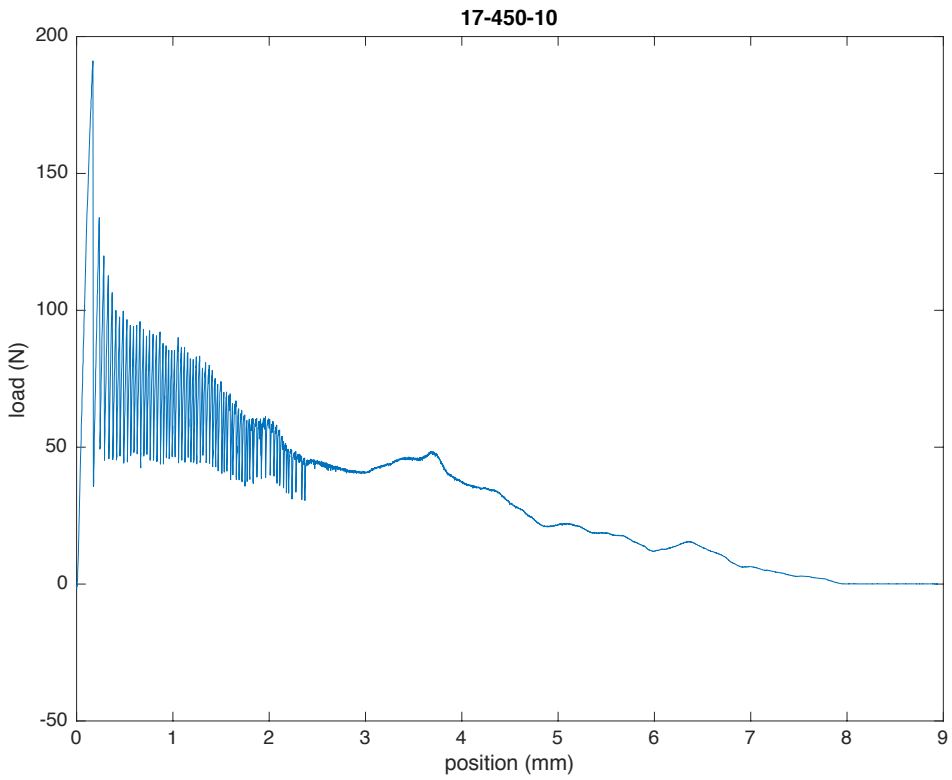

Figure 76. Specimen 17-450-10

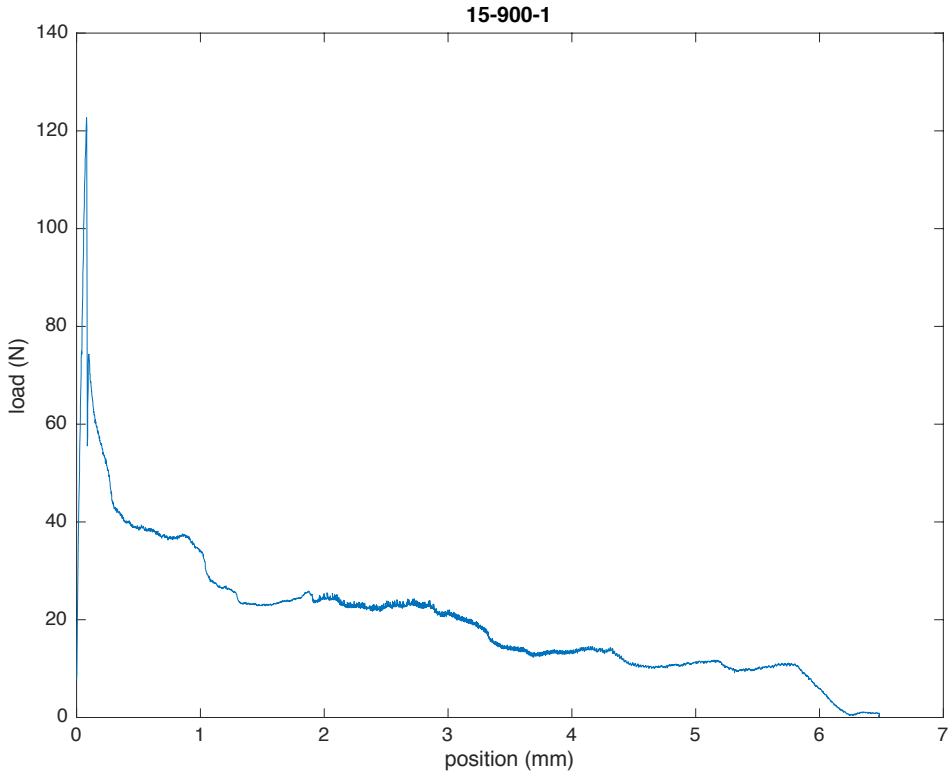

Figure 77. Specimen 15-900-1

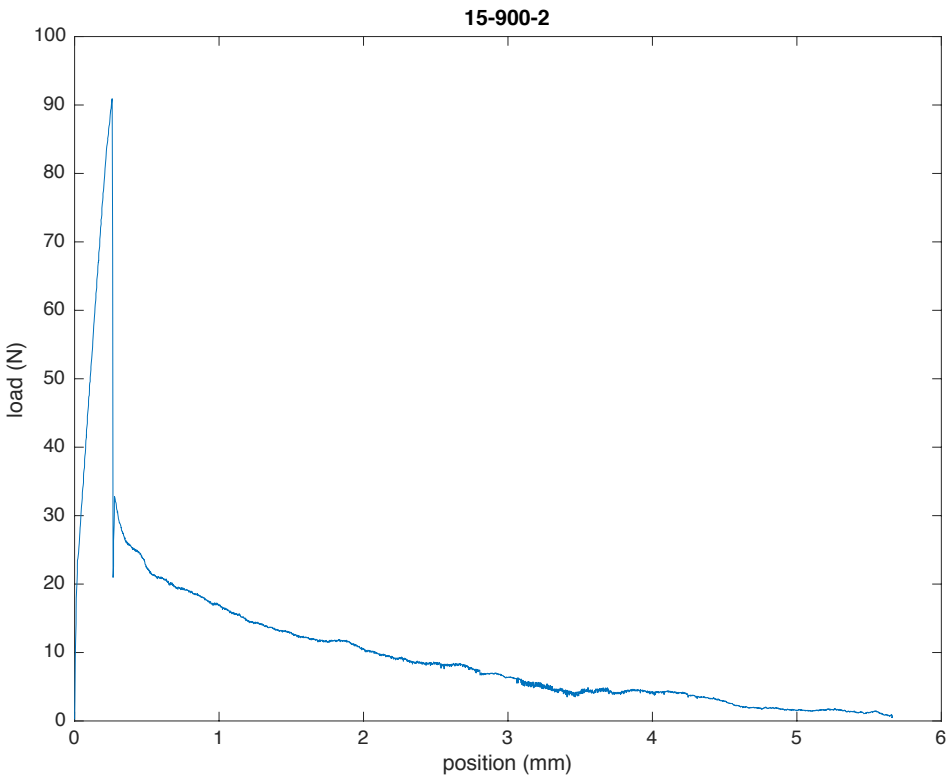

Figure 78. Specimen 15-900-2

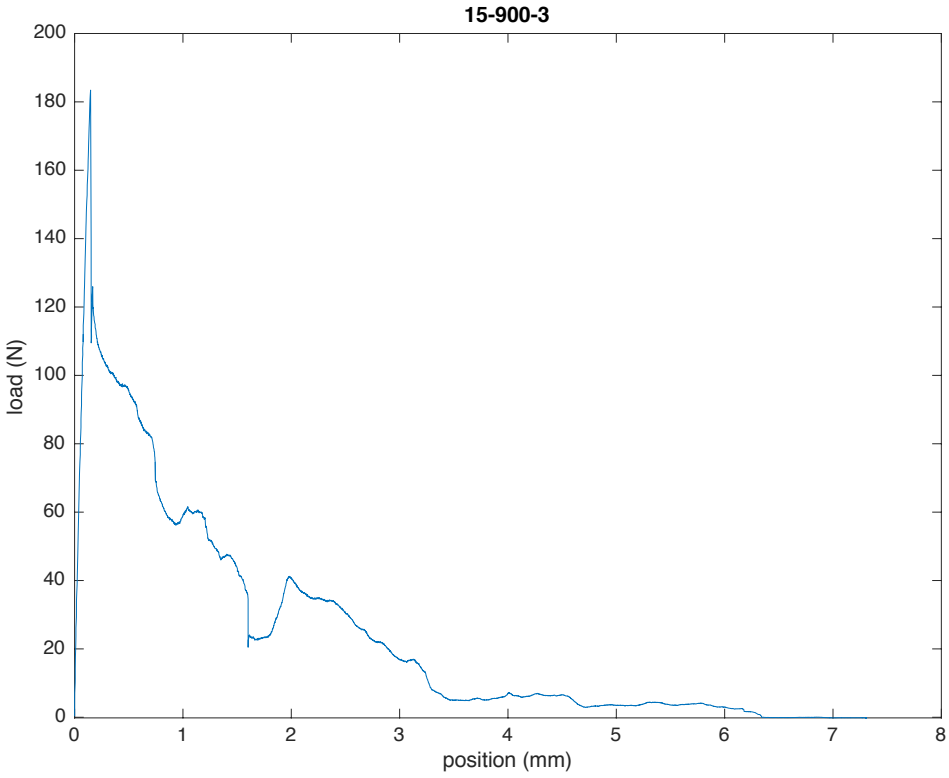

Figure 79. Specimen 15-900-3

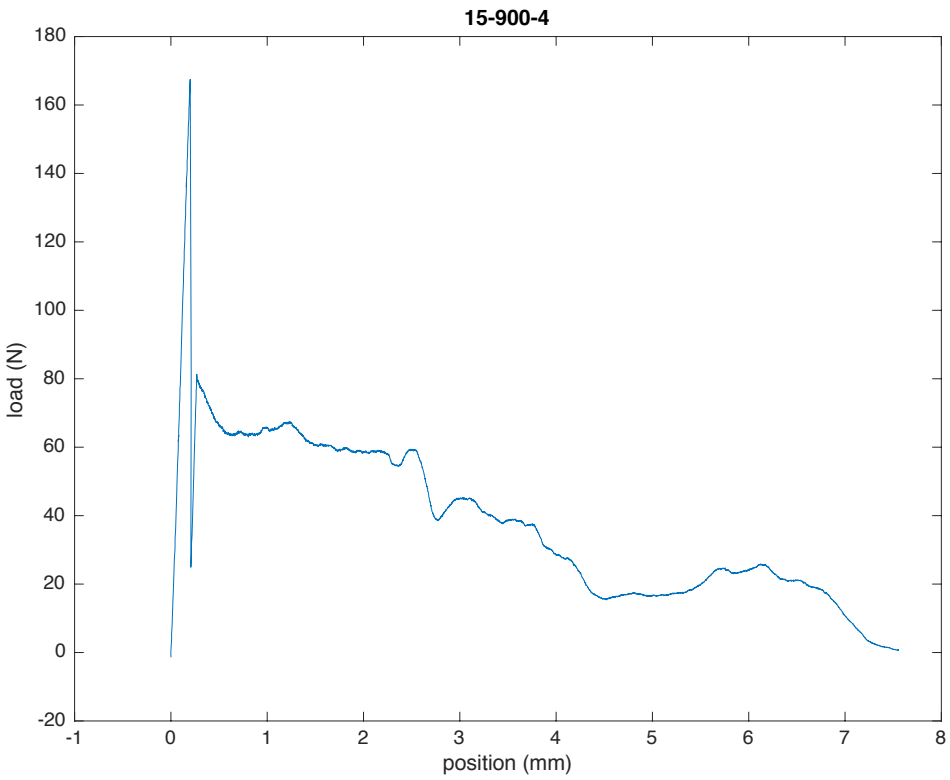

Figure 80. Specimen 15-900-4

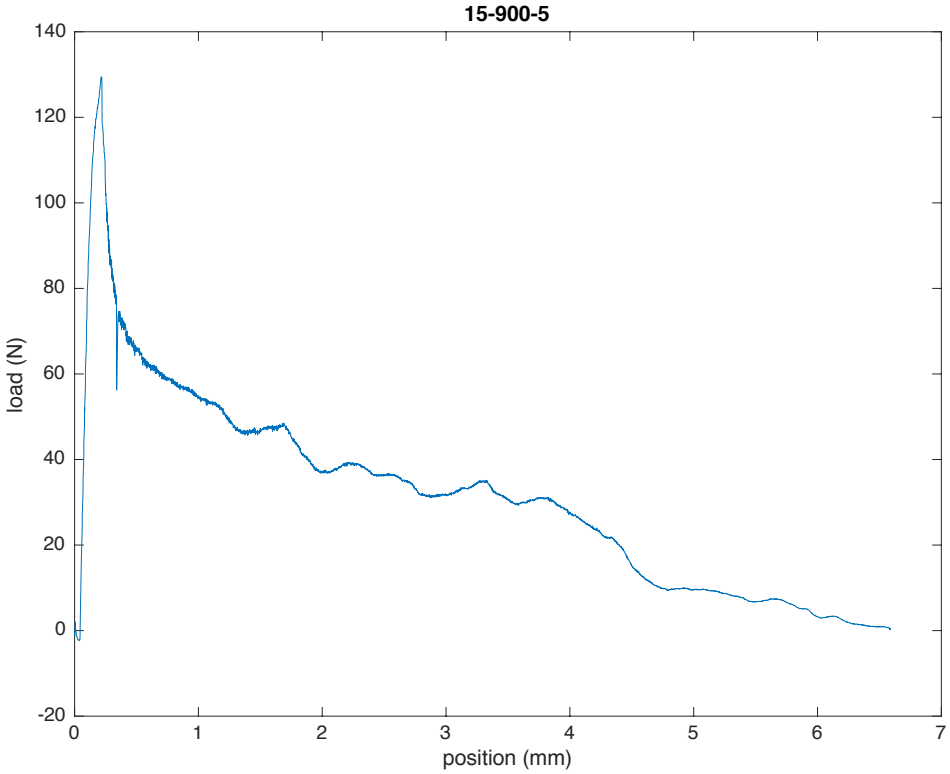

Figure 81. Specimen 15-900-5

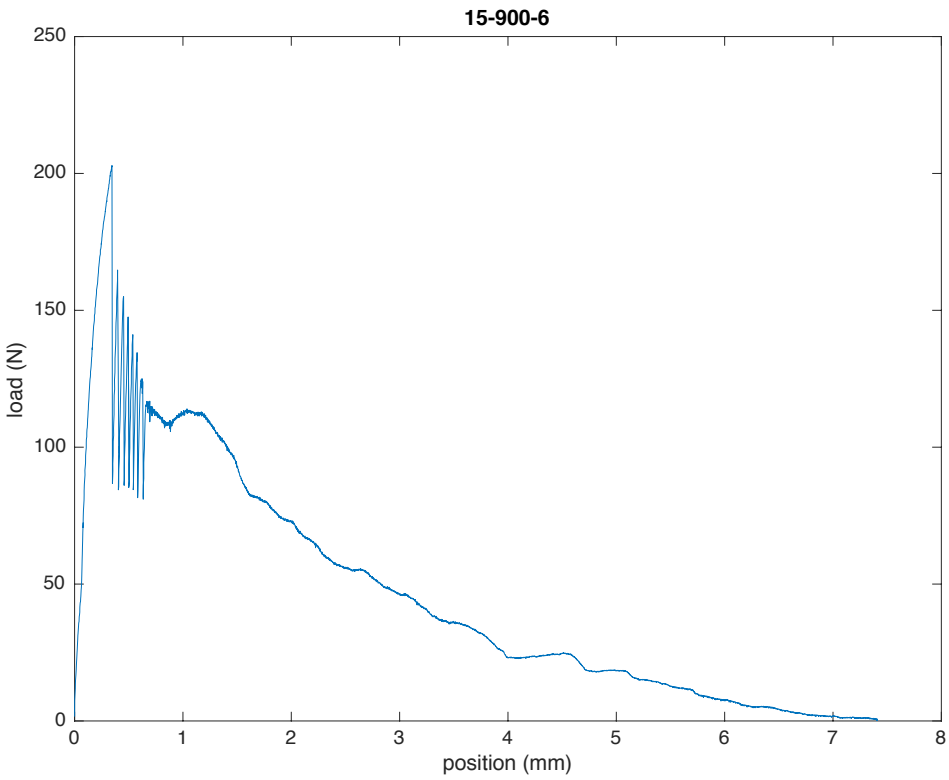

Figure 82. Specimen 15-900-6

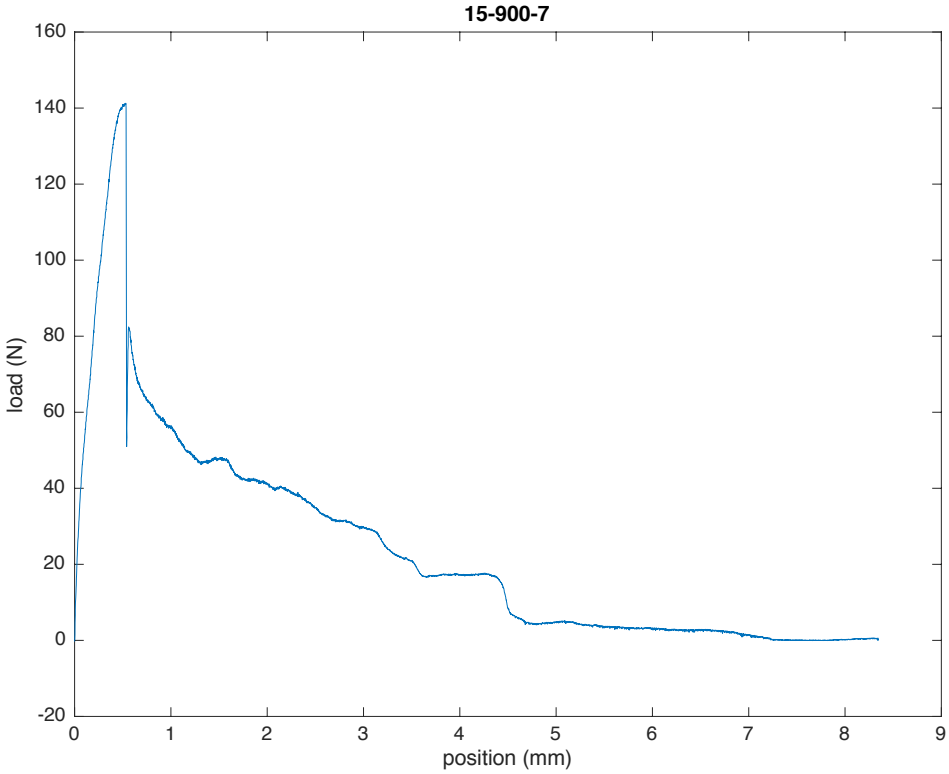

Figure 83. Specimen 15-900-7

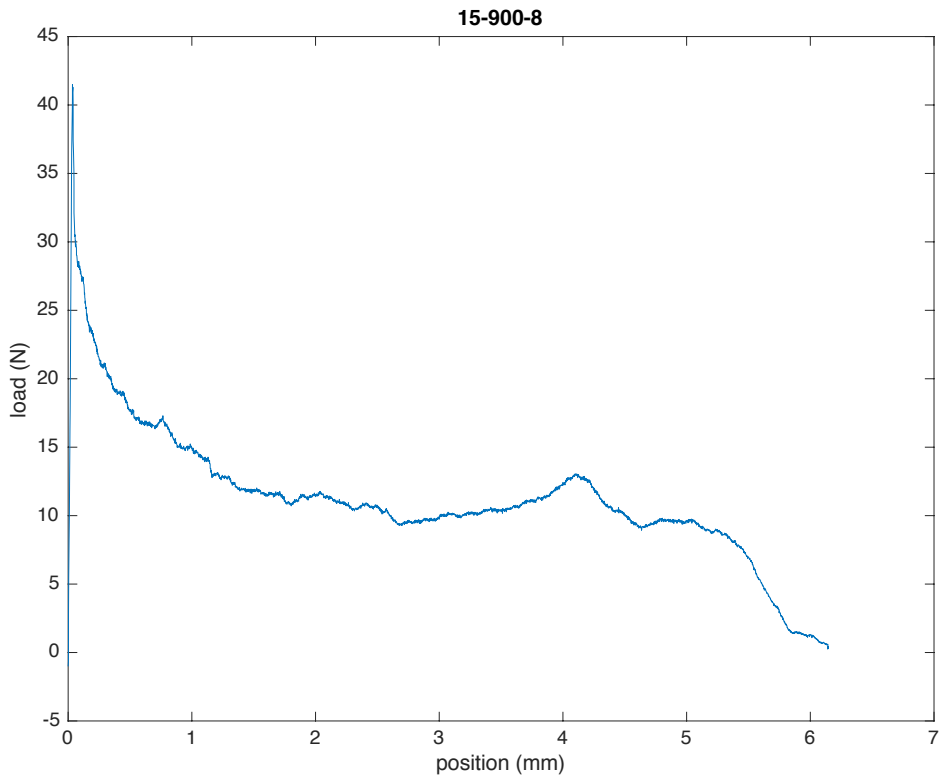

Figure 84. Specimen 15-900-8

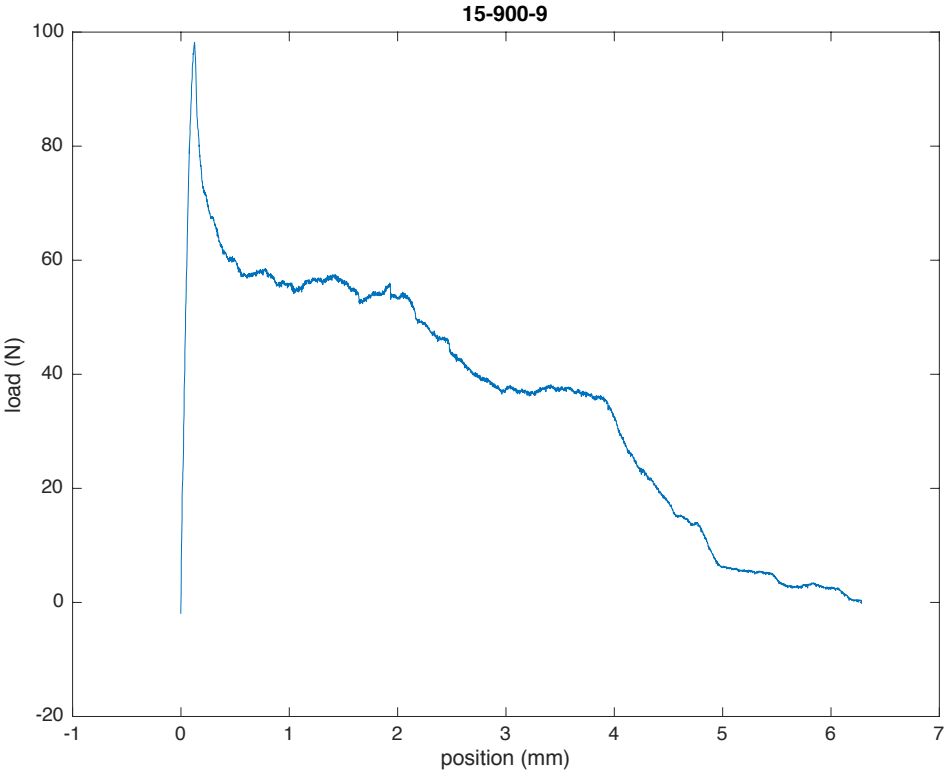

Figure 85. Specimen 15-900-9

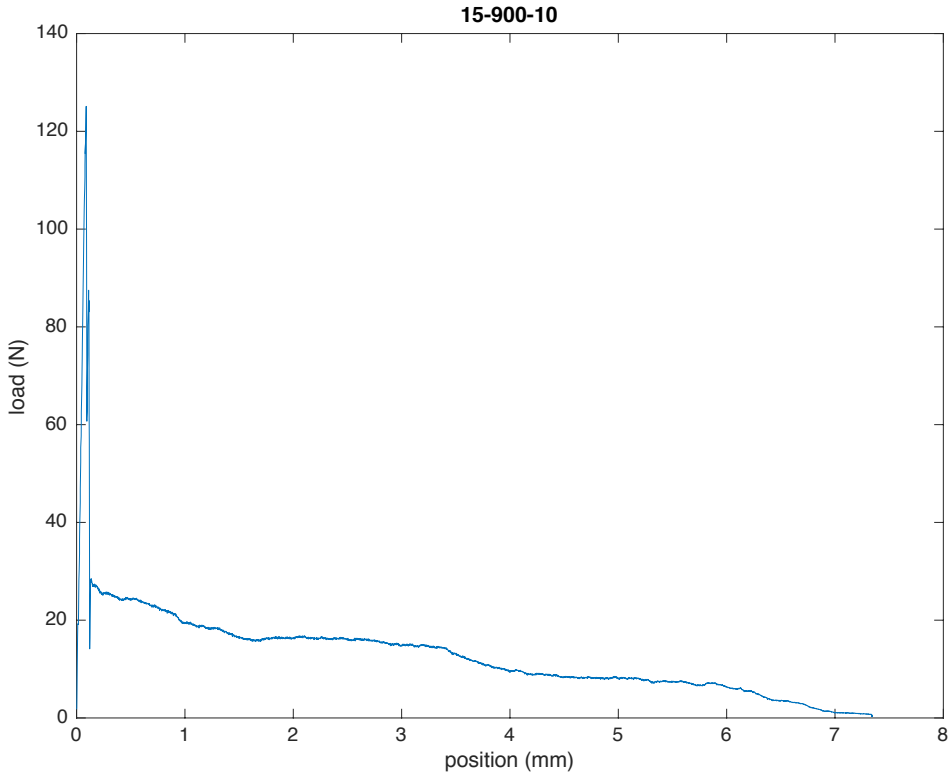

Figure 86. Specimen 15-900-10

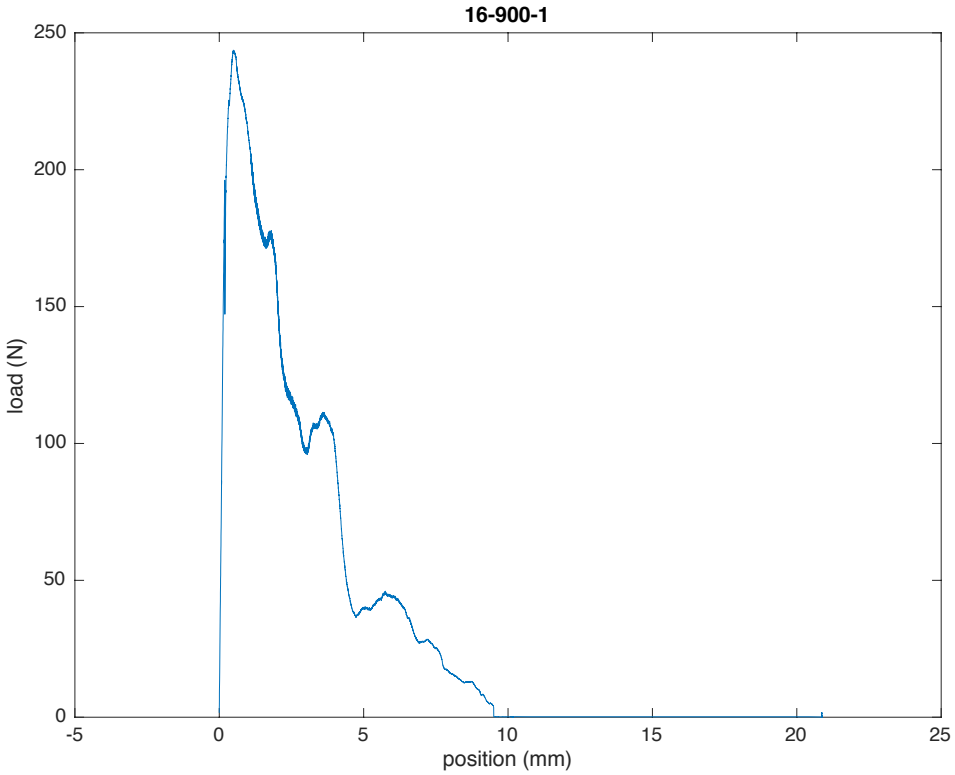

Figure 87. Specimen 16-900-1

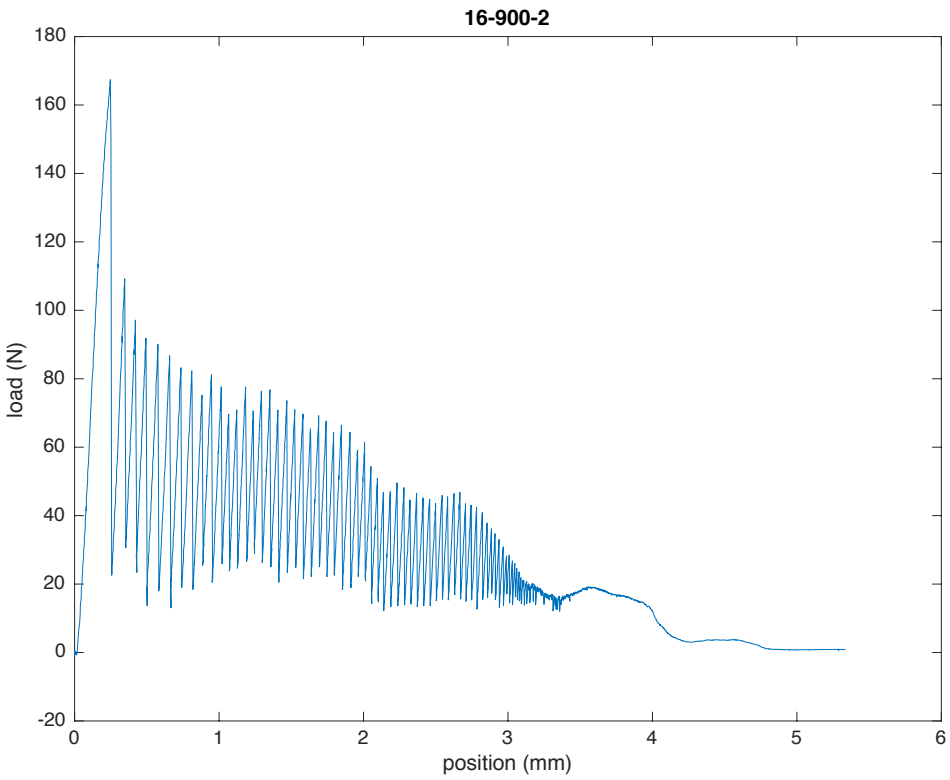

Figure 88. Specimen 16-900-2

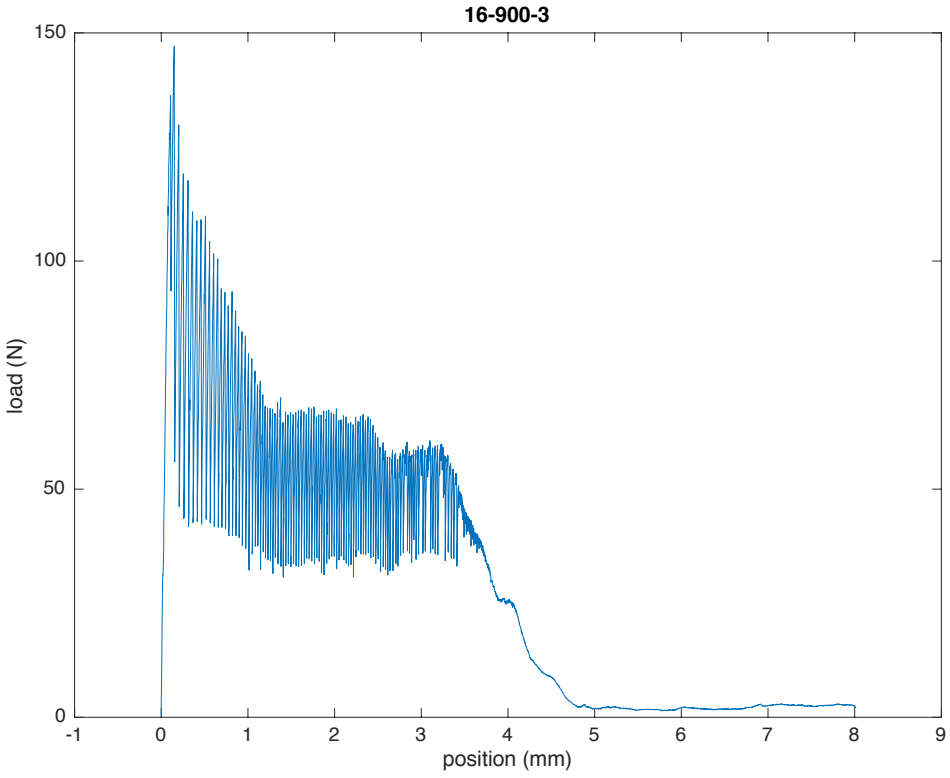

Figure 89. Specimen 16-900-3

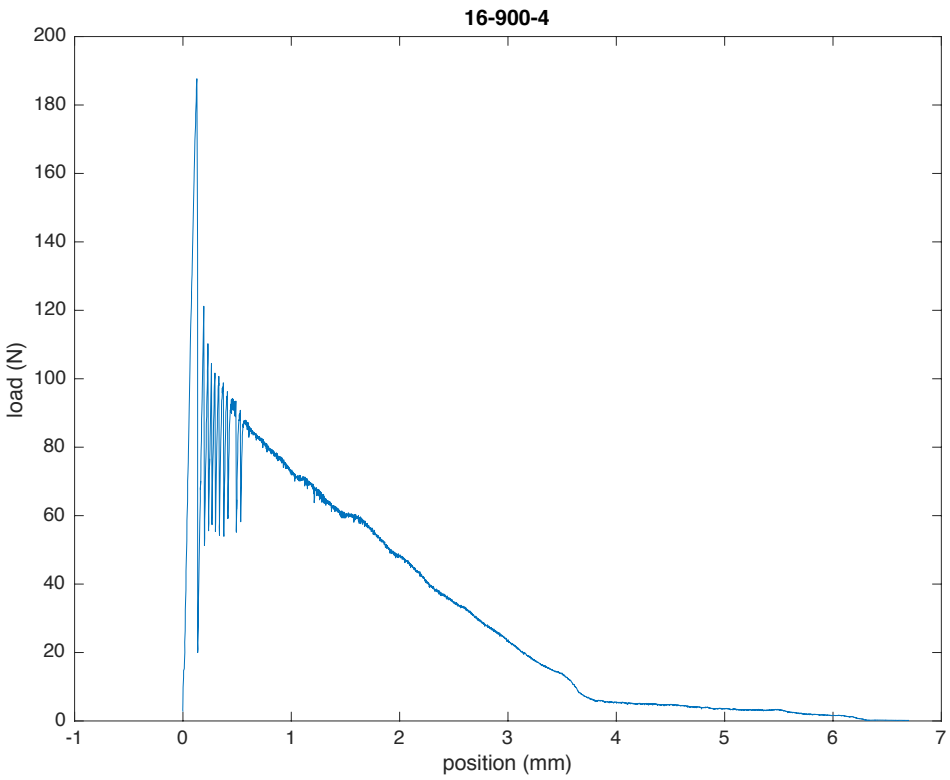

Figure 90. Specimen 16-900-4

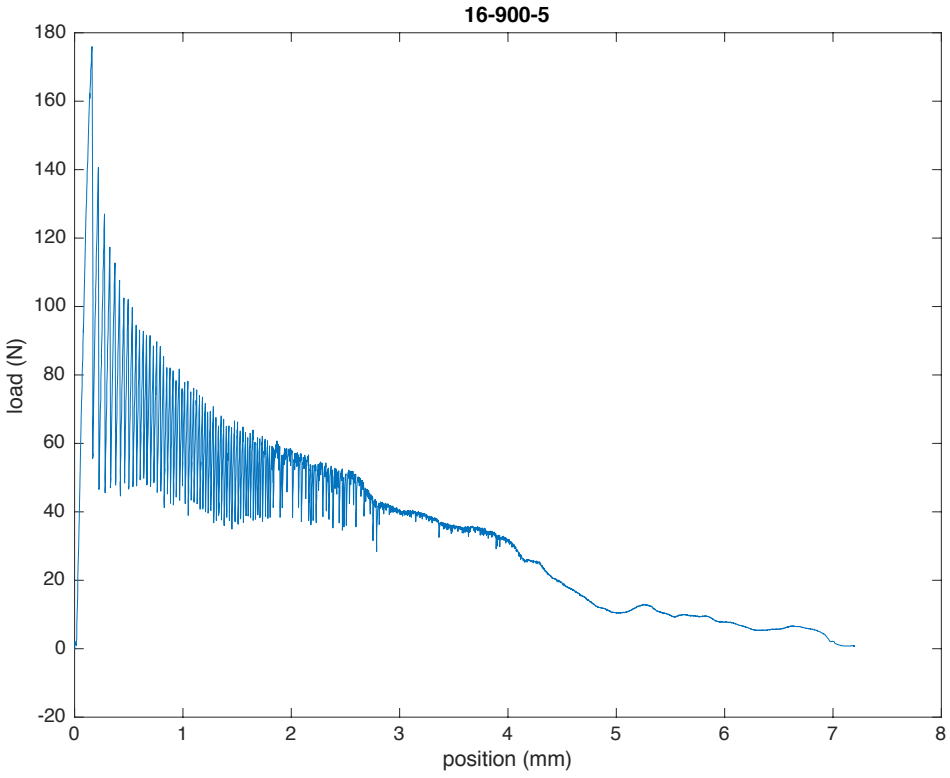

Figure 91. Specimen 16-900-5

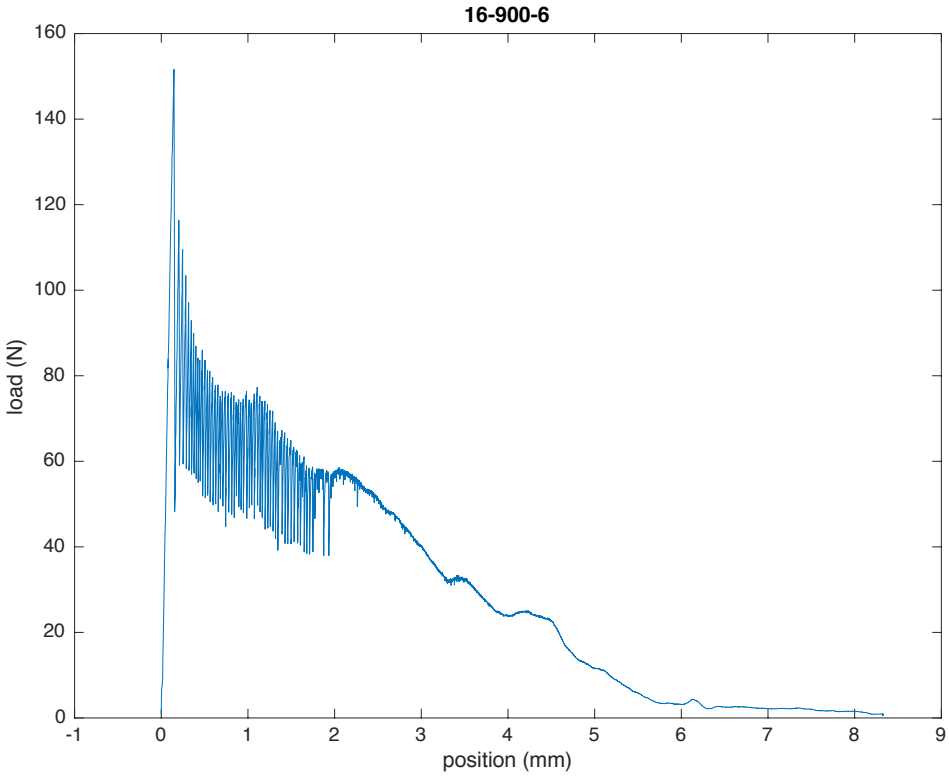

Figure 92. Specimen 16-900-6

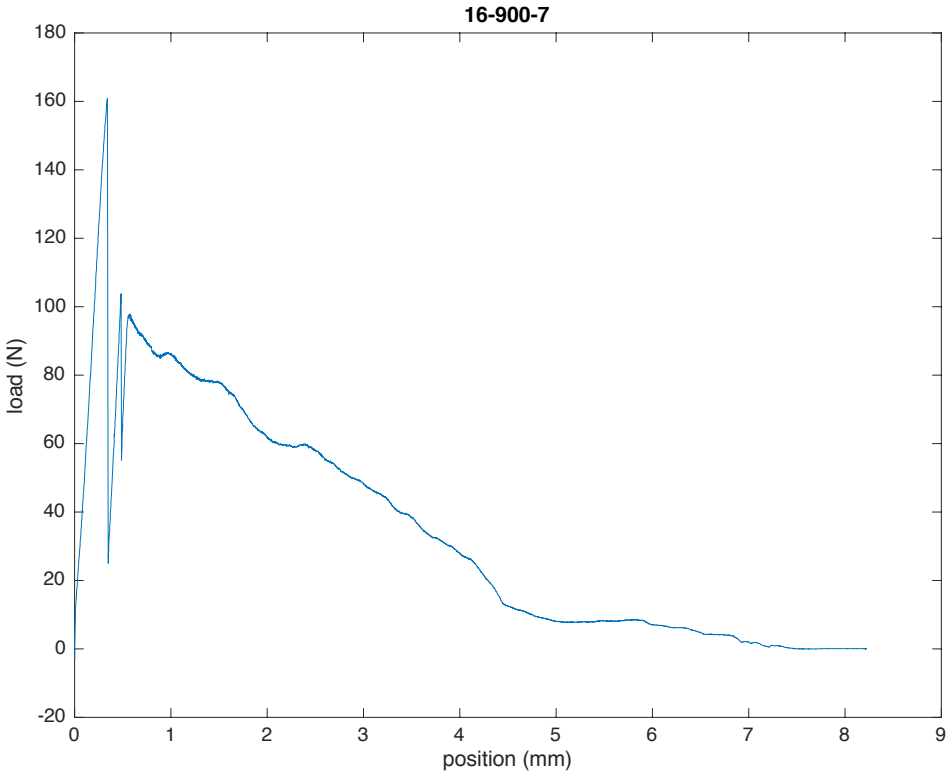

Figure 93. Specimen 16-900-7

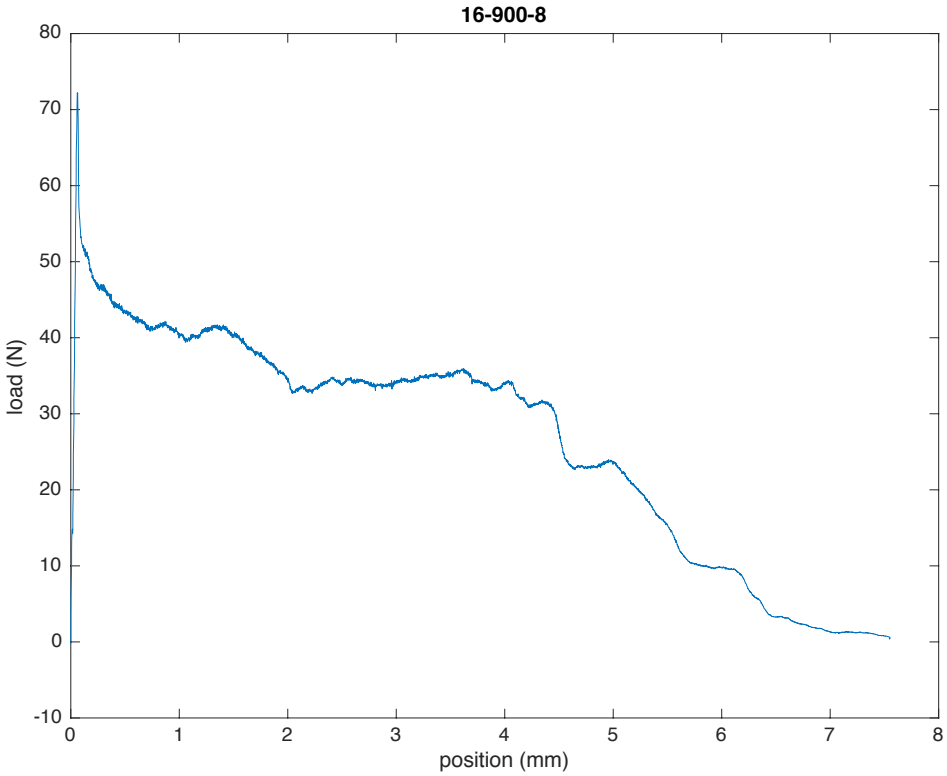

Figure 94. Specimen 16-900-8

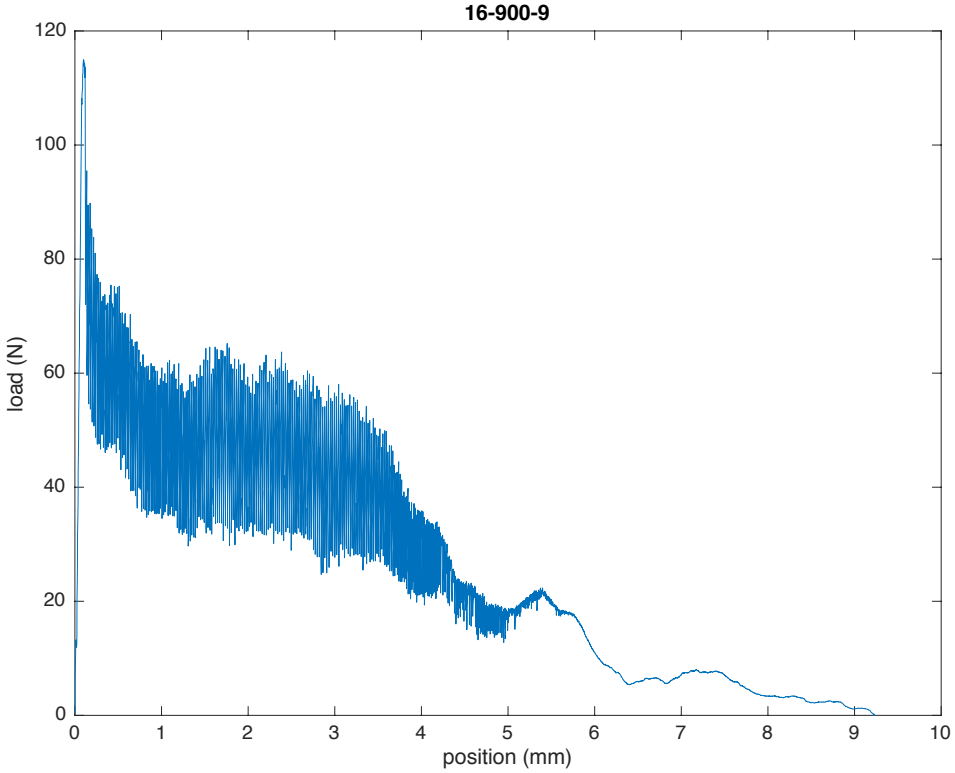

Figure 95. Specimen 16-900-9

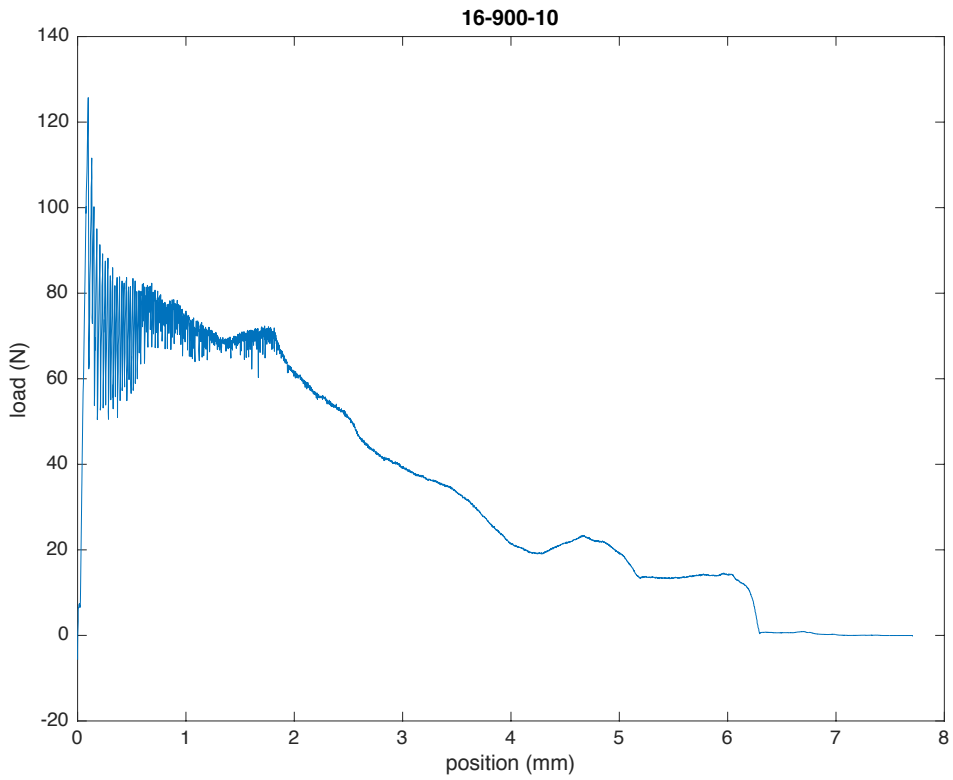

Figure 96. Specimen 16-900-10

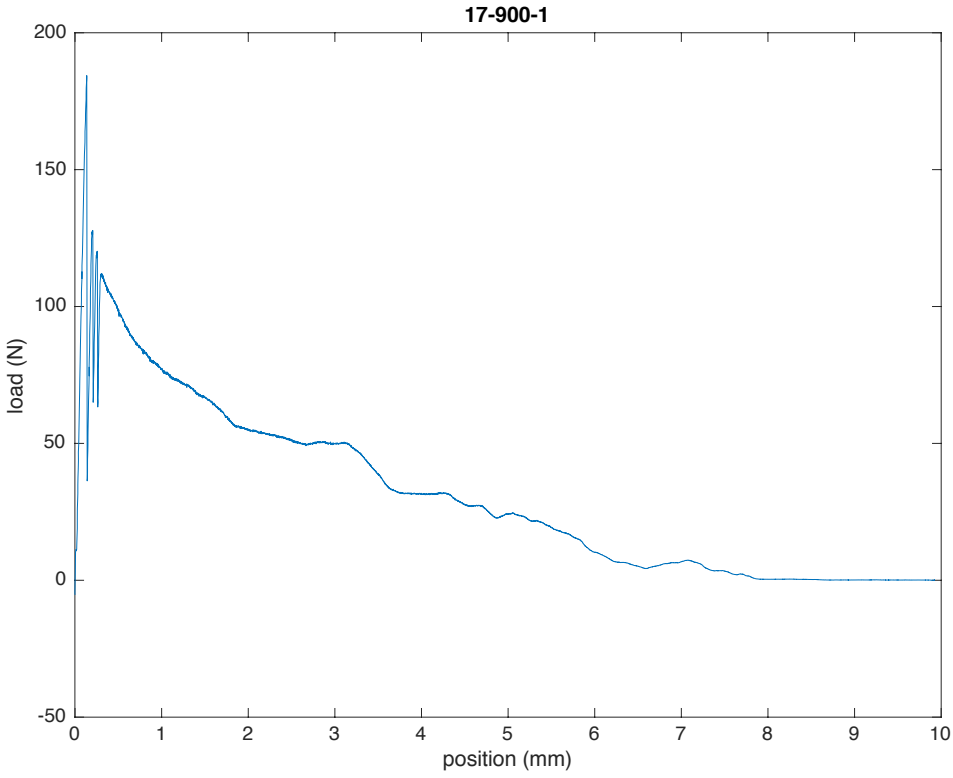

Figure 97. Specimen 17-900-1

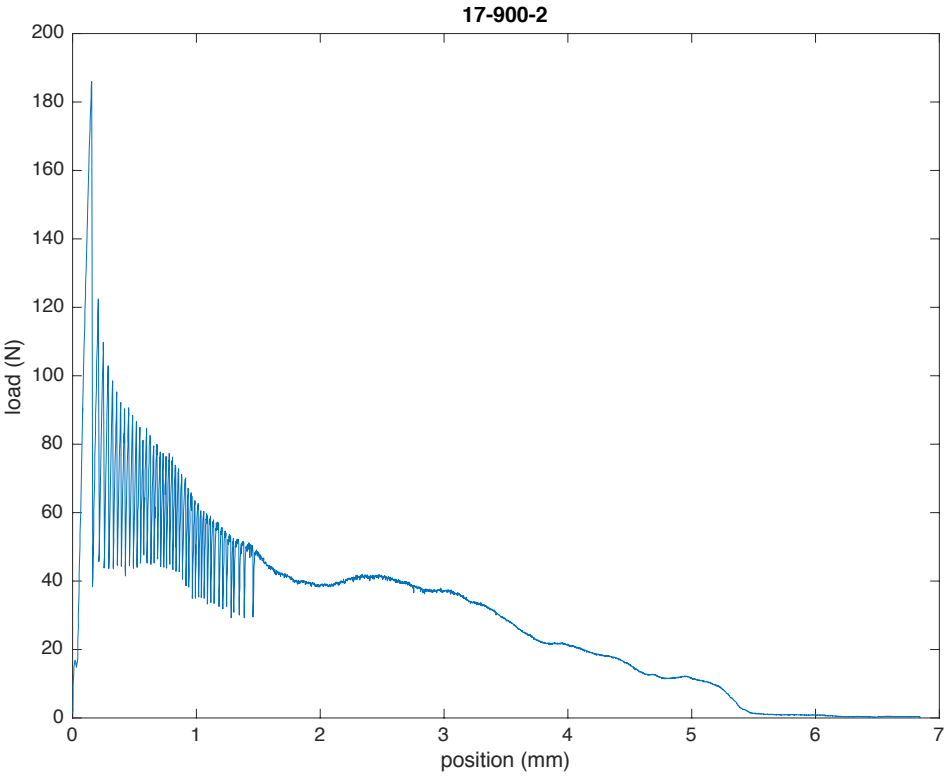

Figure 98. Specimen 17-900-2

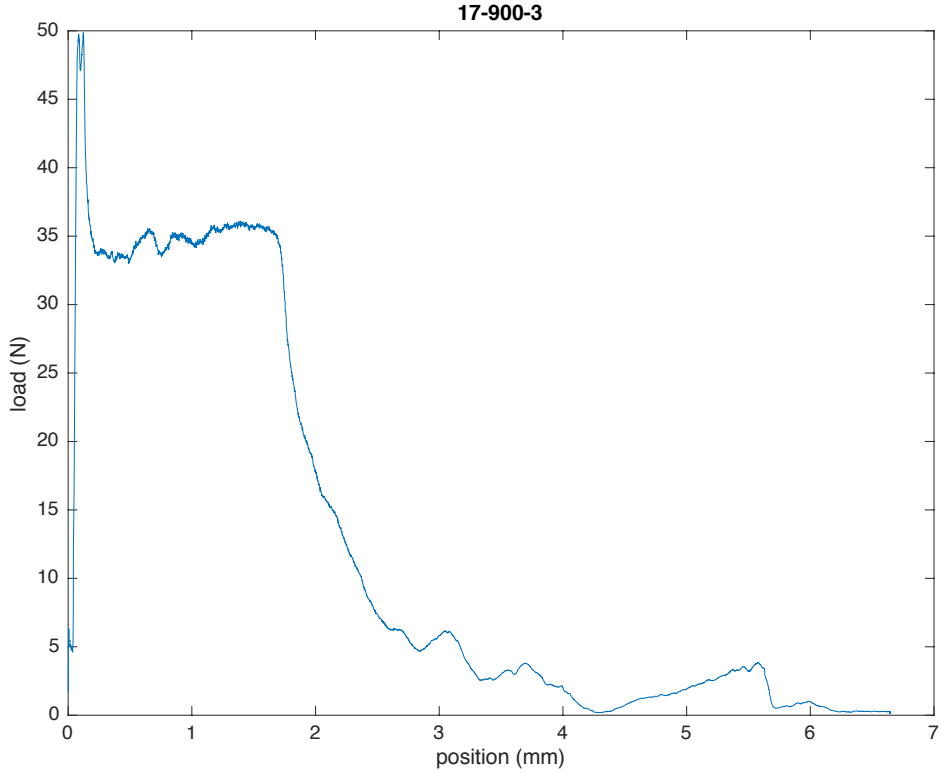

Figure 99. Specimen 17-900-3

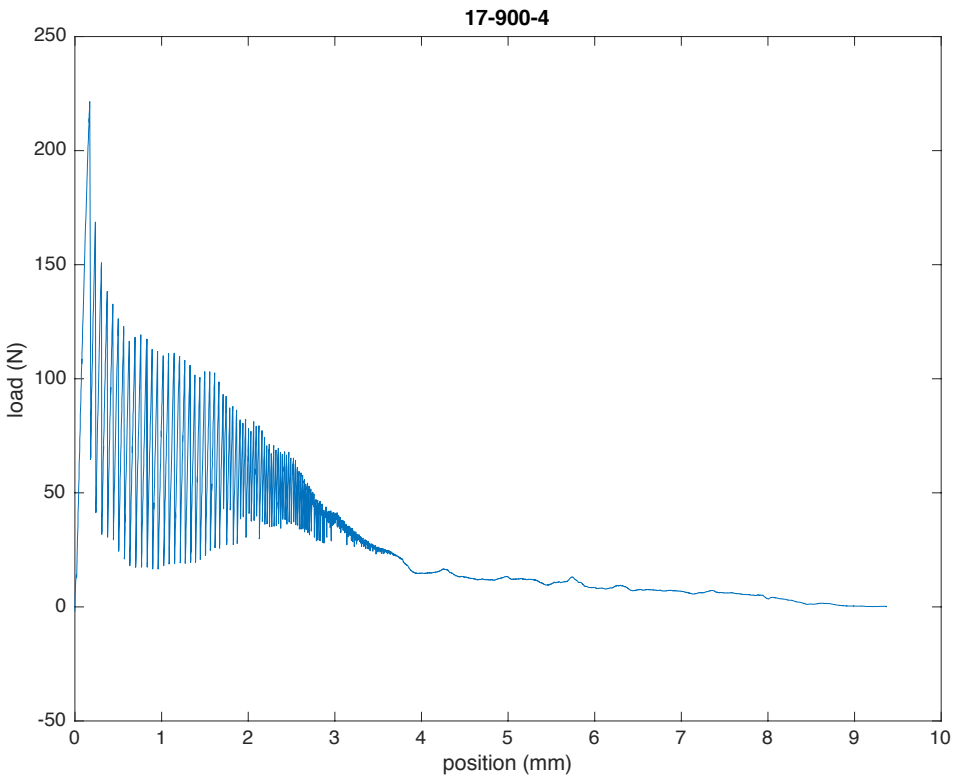

Figure 100. Specimen 17-900-4

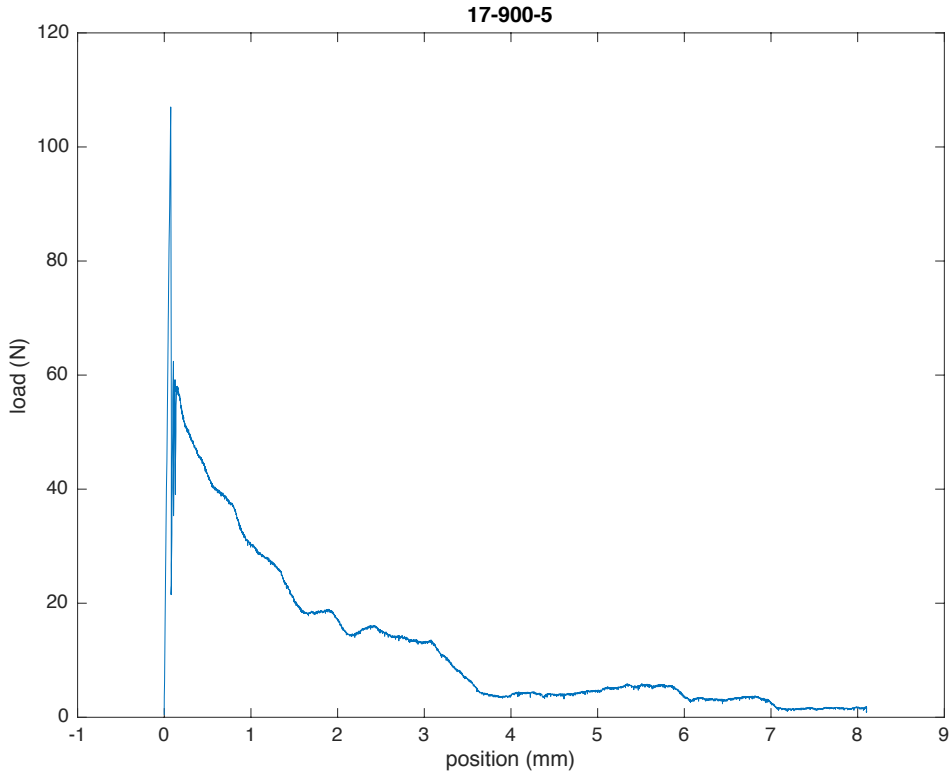

Figure 101. Specimen 17-900-5

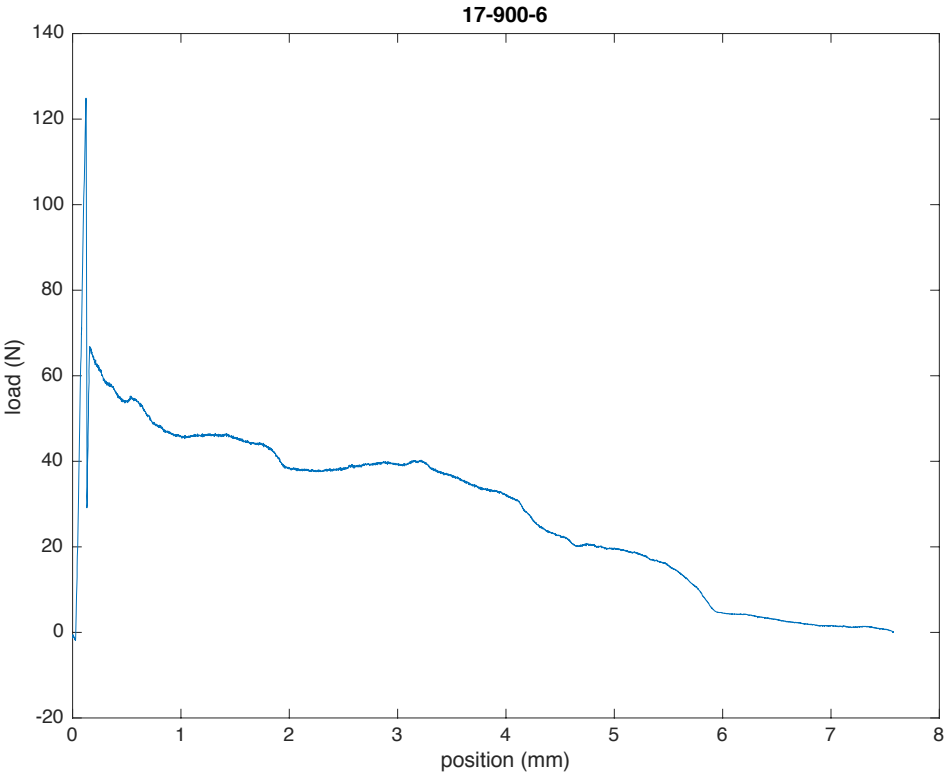

Figure 102. Specimen 17-900-6

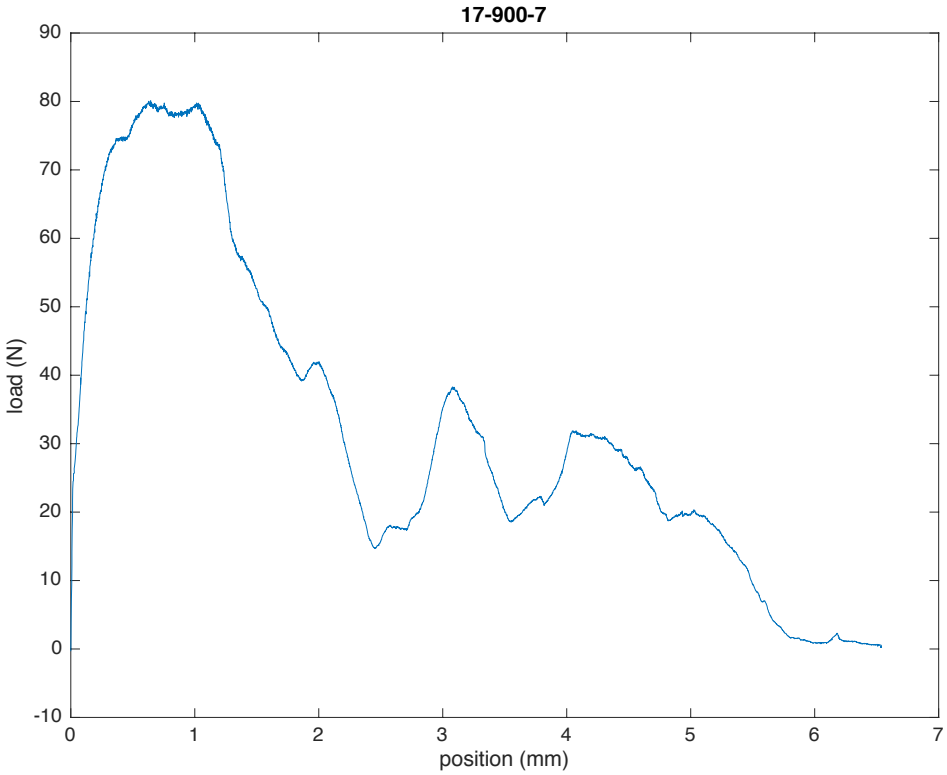

Figure 103. Specimen 17-900-7

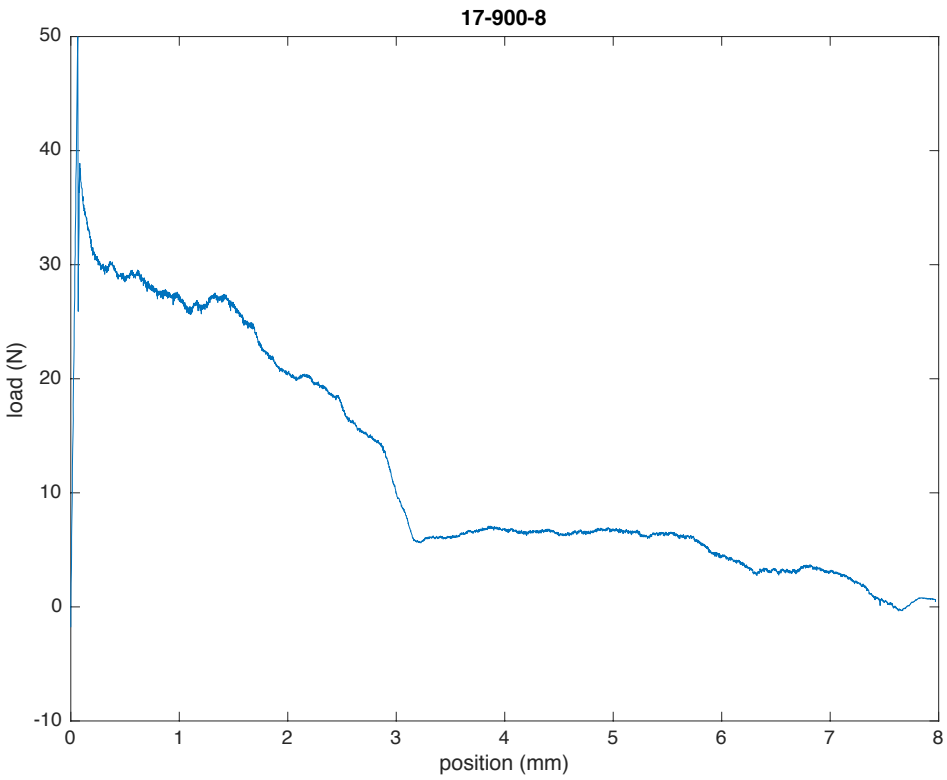

Figure 104. Specimen 17-900-8

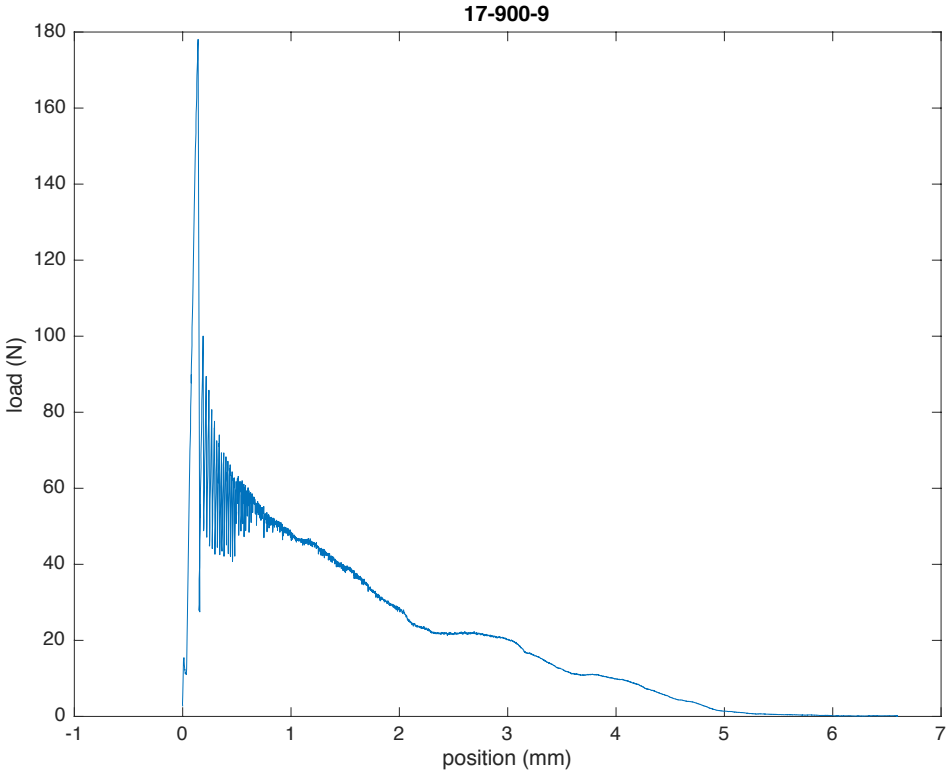

Figure 105. Specimen 17-900-9

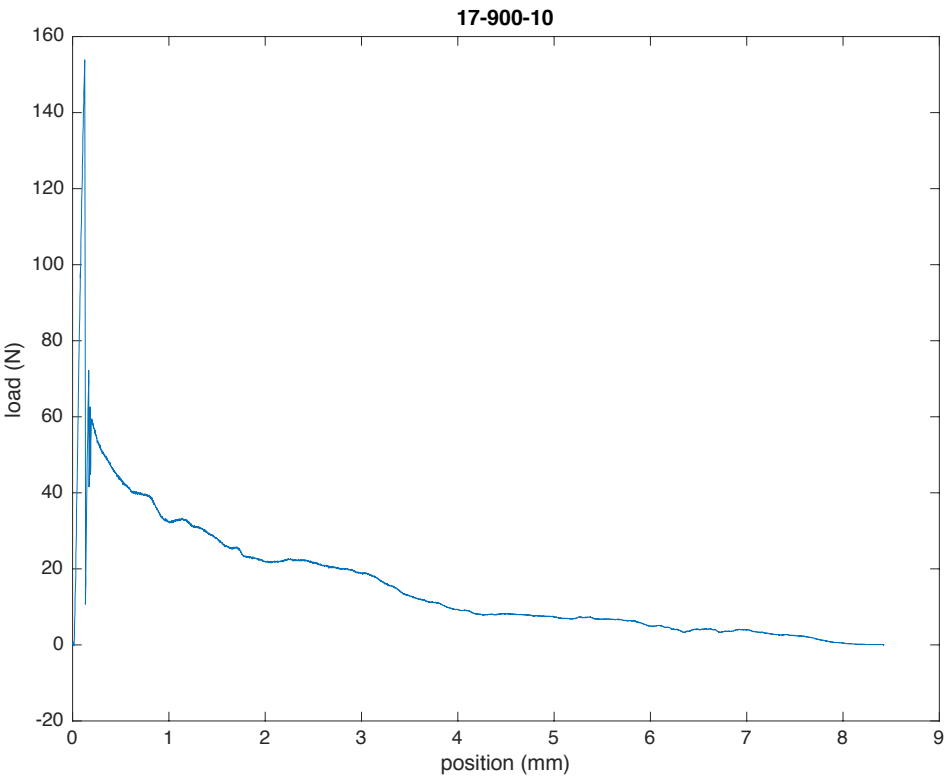

Figure 106. Specimen 17-900-10

Author's Biography

Arden C. McSwain was born in Damariscotta, Maine on January 23rd, 1995. She grew up in Edgecomb, Maine with her five older siblings, mother and father. Arden graduated from Boothbay Region High School in 2013. She is a civil engineering major with a minor in mathematics. She is a member of Tau Beta Pi, Chi Epsilon, Alpha Lambda Delta as well as the University of Maine club field hockey team. Upon graduation, Arden will begin working with Colby Company Engineering in Portland, Maine as a Structural Engineer.